

RECLAMATION

Managing Water in the West

Technical Report No. SRH-2008-7

Two-Dimensional Numerical Model Study of Sediment Movement at the Robles Diversion Dam on the Ventura River, California



U.S. Department of the Interior
Bureau of Reclamation
Technical Service Center
Denver, Colorado

April, 2008

Mission Statements

The mission of the Department of the Interior is to protect and provide access to our Nation's natural and cultural heritage and honor our trust responsibilities to Indian Tribes and our commitments to island communities.

The mission of the Bureau of Reclamation is to manage, develop, and protect water and related resources in an environmentally and economically sound manner in the interest of the American public.

Cover Photo: Looking upstream at the Robles Diversion Dam.

Technical Report No. SRH-2008-7

Two-Dimensional Numerical Model Study of Sediment Movement at the Robles Diversion Dam on the Ventura River, California

Report Prepared by:

Yong G. Lai, Ph.D., Hydraulic Engineer
Sedimentation and River Hydraulics Group, Technical Service Center

Blair P. Greimann, P.E., Ph.D., Hydraulic Engineer
Sedimentation and River Hydraulics Group, Technical Service Center

Report Peer Reviewed by:

Robert Hilldale, Hydraulic Engineer
Sedimentation and River Hydraulics Group, Technical Service Center



U.S. Department of the Interior
Bureau of Reclamation
Technical Service Center
Denver, Colorado

April, 2008

Acknowledgements

Technical assistance, discussion, and review by Robert Hildale (Technical Service Center, Bureau of Reclamation) considerably improved the study and the report. Great appreciation is expressed to them for their efforts.

Table of Contents

	Page
Executive Summary	vi
1.0 Project Background	1
2.0 Numerical Model Study Benefits	2
3.0 Field Data	4
3.1 Topographic and Bathymetric Data	4
3.2 Hydrologic Data	5
3.3 Sediment Data	6
4.0 Methods of Analysis	8
4.1. SRH-2D model	8
4.2. Modeling Scenarios	9
4.3. Numerical Model Details	11
4.3.1. Solution Domain and Mesh Generation	11
4.3.2. Representation of Flow Roughness and Bed Gradation	14
4.4. Sedimentation Analysis Method	15
4.4.1. Sediment Transport Equations	15
4.4.2. Boundary Conditions and Other Input Data	17
5.0 Physical Model Scenarios	19
5.1. Discussion of Physical Model Scenarios	19
5.2. Calibration Using the Measured Flow Data	22
5.3. Mobile-Bed Simulation with the Existing Condition	26
5.4. Mobile-Bed Simulation with the Right HFB	34
5.5. Sediment Results with the Left HFB Gate	43
6.0 Field Model Scenarios	50
6.1. Calibration with Field Flow Cases	50
6.1.1. 2005 Flood Flow	50
6.1.2. 100 Year Flood	51
6.2. Flow Simulation Results at Other Discharges	52
6.3. Mobile-Bed Model Inputs	57
6.4. Qualitative Comparison of Results under the Existing Condition	63
6.5. Results with the 1991 Hydrograph	66
6.6. Results with the 1998 Hydrograph	72
7.0 Discussion and Uncertainty	79
7.1. Discussion and Summary	79
7.2. Model Uncertainties and Limitations	82
8.0 References	83

Index of Figures

	Page
Figure 1. Aerial view of Robles Diversion taken in 2005.	2
Figure 2. Topography near the Robles Diversion Dam based on the LiDAR data in March 2005	4
Figure 3. The 1991 and 1998 hydrographs used for the sediment modeling.....	5
Figure 4. Total sediment load (input) at RM 14.8674 computed from the SRH-1D model.....	6
Figure 5. Size distribution of the bed materials at a location about 0.4 mile upstream of the Robles Diversion Dam (d_{50} is about 154 mm).....	7
Figure 6. Solution domain (red) of the 2D numerical model for the field simulation.....	12
Figure 7. Mesh generated for the calibration study of field flows discussed in Chapter 5.0.....	13
Figure 8. 3D perspective view of the topography for the existing condition scenario based on March 2005 LiDAR survey data	13
Figure 9. Three zones were used to represent the bed properties on the solution domain: the main channel, light vegetation and heavy vegetation	14
Figure 10. Layouts of three physical model scenarios (looking upstream)	19
Figure 11. Flow hydrograph and total sediment load at the inlet with the 1991 hydrograph	20
Figure 12. Flow hydrograph and total sediment load at the inlet with the 1998 hydrograph	21
Figure 13. Size distribution of the base sediment mixture used for the physical model test ($d_{50}=1.75$ mm)	21
Figure 14. Layout of the right HFB case	22
Figure 15. Mesh and bathymetry of the RHFB numerical model used for the calibration study.....	23
Figure 16. Perspective view of the bathymetry of the RHFB case in the physical model used for the calibration study.....	24
Figure 17. Comparison of measured (red) and computed (black) depth-averaged velocity for case PM-FLOW-1	25
Figure 18. Comparison of measured (red) and computed (black) depth-averaged velocity for case PM-FLOW-2	25
Figure 19. Mesh for the existing condition scenario mobile-bed simulation (physical model).....	26
Figure 20. Bed elevation of the existing condition scenario for the mobile-bed simulation (Physical model)	26
Figure 21. Gate operation curve (flow capacity versus time) of the existing radial gates for the existing condition modeling.....	27
Figure 22. Comparison of bed topography at the end of the hydrograph (6 hours) between the physical model and the simulation for PM-SED-EX-91	28
Figure 23. Simulated bed form evolution at different times for case PM-SED-EX-91 (1:4 vertical distortion)	29

Figure 24. Comparison of bed topography at time 8 hours between the physical model and the simulation for PM-SED-EX-98.....	31
Figure 25. Comparison of bed topography near the right bank between the physical and numerical models for PM-SED-EX-98 at the end of the hydrograph (8 hours).....	32
Figure 26. Simulated bed form evolution with time for case PM-SED-EX-98 (1:4 vertical distortion).....	33
Figure 27. Mesh used for the RHFB scenario for the mobile-bed simulation of the physical model cases.....	34
Figure 28. Bed elevation of the RHFB scenario for the mobile-bed simulation of the physical model cases.....	34
Figure 29. Gate operation capacity of the high flow bypass gates for the right HFB scenario for case PM-SED-RHFB-91 (1991 hydrograph).....	35
Figure 30. Gate operation capacity of the existing gates and the HFB gates for the right HFB scenario for case PM-SED-RHFB-98 (1998 hydrograph)	36
Figure 31. Comparison of bed topography at the end of the hydrograph (6 hours) between the physical and numerical models for PM-SED-RHFB-91	37
Figure 32. Comparison of bed topography at the end of the hydrograph (6 hours) between the physical and numerical models PM-SED-RHFB-91	38
Figure 33. Simulated bed form evolution in time for case PM-SED-RHFB-91 (1:4 vertical distortion).....	39
Figure 34. Comparison of bed topography at the end of the hydrograph (8 hours) between the physical and numerical models for PM-SED-RHFB-98	41
Figure 35. Simulated bed form evolution in time for case PM-SED-RHFB-98 (1:4 vertical distortion).....	42
Figure 36. Mesh used for the LHFB scenario mobile-bed simulation of the physical model cases.....	43
Figure 37. Bed elevation of the LHFB scenario for the mobile-bed simulation of the physical model cases.....	43
Figure 38. Gate operation capacity of the high flow bypass gates for case PM-SED-LHFB-91 (1991 hydrograph).....	44
Figure 39. Gate operation capacity of the existing gates and the HFB gates for case PM-SED-LHFB-98 (1998 hydrograph).....	45
Figure 40. Comparison of bed topography at the end of the hydrograph (6 hours) between the physical and numerical models for PM-SED-LHFB-91	46
Figure 41. Simulated bed evolution in time for case PM-SED-LHFB-91 (1:4 vertical distortion).....	47
Figure 42. Comparison of bed topography at the end of hydrograph (8 hours) between the physical and numerical models for PM-SED-LHFB-98	48
Figure 43. Simulated bed evolution in time for case PM-SED-LHFB-98 (1:4 vertical distortion).....	49
Figure 44. Comparison of the water surface elevation (WSE) from SRH-2D and HEC-RAS; SRH-2D represents the WSE along the channel thalweg, and HRC-RAS is cross section averaged WSE.....	51
Figure 45. Simulated water depth for the 24,000 cfs flow discharge in the Robles dam area.....	53

Figure 46. Simulated water depth for the 15,000 cfs flow discharge in the Robles dam area.....	54
Figure 47. Simulated water depth for the 6,000 cfs flow discharge in the Robles dam area.....	55
Figure 48. Simulated water surface elevation at cross section 14.2045 for three discharges; Distance is measured from the middle of road on the left side of the river (looking downstream).....	56
Figure 49. Simulated water surface elevation at cross section 13.9205 for three discharges; Distance is measured from the middle of road on the left side of the river (looking downstream).....	56
Figure 50. Computed velocity distribution at cross section 14.1089 RM.	57
Figure 51. Excavation area, shown in red box, for the mobile-bed simulation	58
Figure 52. Perspective view of the three topographic scenarios.....	60
Figure 53. Zoom-in view of the meshes for the three topographical scenarios....	61
Figure 54. Gate capacity versus time for the existing and HFB gates for the field modeling; the 1998 hydrograph is also shown as a reference	63
Figure 55. A comparison of the deposition depth after 200 hours between the 1991 hydrograph and 1998 hydrograph for the existing condition with the before-dam removal sediment input.....	64
Figure 56. Simulated flow velocity and pattern for the 1998 hydrograph before-dam removal scenario at 200 hours	66
Figure 57. Simulated bed elevation and deposited depth for the existing condition with the 1991 hydrograph and after-dam removal sediment input.....	68
Figure 58. Simulated bed elevation and deposited depth for the RHFB scenario with the 1991 hydrograph and after-dam removal sediment input.....	69
Figure 59. Simulated bed elevation and deposited depth for the LHFB scenario with the 1991 hydrograph and after-dam removal sediment input.....	70
Figure 60. Comparison of deposition depth between before-dam and after-dam removal for the 1991 hydrograph and existing condition scenario.....	71
Figure 61. Comparison of bed elevation between before-dam and after-dam removal for the 1991 hydrograph and existing condition scenario.....	71
Figure 62. Comparison of deposition depth between the right and left HFB cases for the 1991 hydrograph and after dam removal	72
Figure 63. Simulated bed elevation and deposited depth for the existing condition with the 1998 hydrograph and after-dam removal sediment input.....	74
Figure 64. Simulated bed elevation and deposited depth for the RHFB scenario with the 1998 hydrograph and after-dam removal sediment input.....	75
Figure 65. Simulated bed elevation and deposited depth for the LHFB scenario with the 1998 hydrograph and after-dam removal sediment input.....	76
Figure 66. Comparison of deposited depth between before-dam and after-dam removal for the 1998 hydrograph and existing condition scenario.....	77
Figure 67. Comparison of bed elevation between before-dam and after-dam removal for the 1998 hydrograph and existing condition scenario.....	77
Figure 68. Comparison of deposited depth between the right and left HFB cases for the 1998 hydrograph and after dam removal	78

Index of Tables

	Page
Table 1. Peak flows downstream of the confluence with N. Fork Matilija Creek and the water elevation at RM 12.7841	5
Table 2. Total sediment volume (yd ³) moving through RM 14.8674 over the 200-hour period (volume is without voids).....	6
Table 3. List of model simulation cases and associated conditions.....	10
Table 4. Size ranges of each sediment size class	18
Table 5. The lower (d _{low}) and upper (d _{upp}) diameter of each sediment size class used for the numerical modeling of the physical model scenarios	22
Table 6. Comparison of simulated and surveyed water elevation at two points...	51
Table 7. Flow parameters for the three simulations.....	52
Table 8. Record of sediment removal at Robles Diversion Dam	65
Table 9. Total amount of sediments moving into and stored in the area between RM 14.1098 and the weir based on model (volume excluding voids)	73
Table 10. Cumulative volume (excluding voids) deposited upstream of the weir during the period of test hydrograph.....	80
Table 11. Average deposition depth (with voids) and total deposition volume (without voids) under the existing condition scenario.....	81

Executive Summary

Summary

This report presents the results of a Bureau of Reclamation numerical model study of the proposed high flow bypass (HFB) spillway for Robles Diversion Dam. Robles Diversion Dam is located on the Ventura River approximately 14 river miles from the ocean. A two-dimensional flow and sediment transport model (SRH-2D) was used to determine the interaction of flows and bed load sediments near the facility following decommissioning and removal of Matilija Dam located about two river miles upstream. The HFB spillway was proposed to enhance sediment movement through the diversion pool thereby reducing the impacts of elevated bed load levels resulting from the upstream dam removal.

Major Findings

Three diversion gate scenarios were modeled, similar to the physical model tests: Existing Condition, Right High Flow Bypass (RHFB), and Left High Flow Bypass (LHFB). Layouts of the three scenarios are illustrated in Figure E. 1.

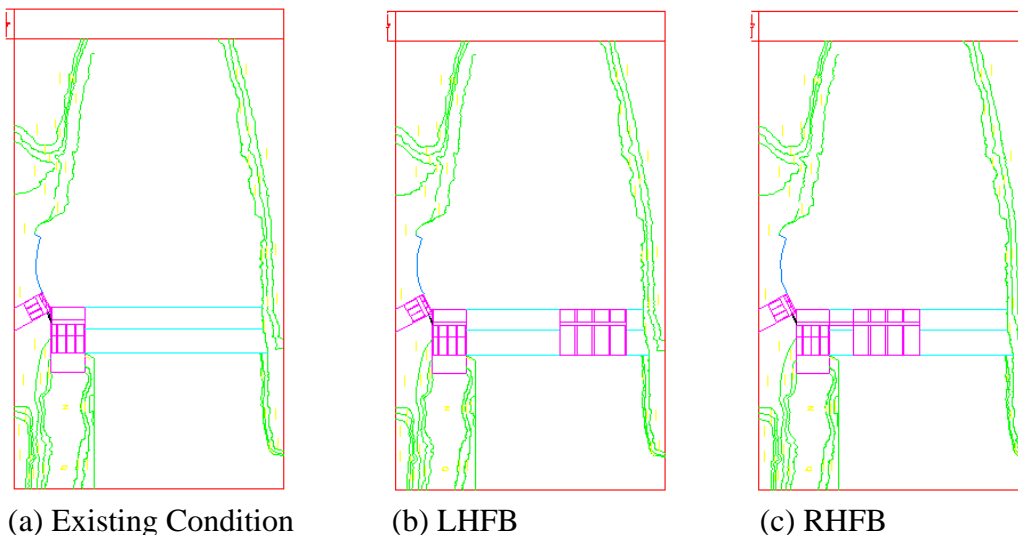


Figure E. 1 Layout of three diversion gate scenarios

Numerical modeling was carried out under both the physical model condition and the prototype field condition scenarios. Major findings based on the model results may be summarized as follows:

Physical Model Scenario

Numerical modeling of physical model cases presented in Chapter 5.0 show the following:

- (1) Results from both the numerical and physical models are in agreement with each other. This on one hand provides confidence in the numerical model, and on the other hand points to the reliability of the results from both models.
- (2) With the existing radial gates, excessive deposition would occur upstream of the Robles weir. Specifically, the sediment delta would reach the diversion canal gates under both the 6,000 cfs and 14,000 cfs hydrographs. The thickness of the delta is high enough that there is a high likelihood of bedload sediments being transported into the canal.
- (3) With the high flow bypass (HFB) gates added, the model results show that it is less likely that the bedload sediments would enter the diversion canal.
- (4) The total amount of sediment depositions upstream of the weir is tabulated in Table 10 for all simulated physical model cases. It shows that more than 85% of the incoming sediments would be trapped upstream of the weir under the 6,000 cfs hydrograph with or without the HFB gates. The benefit of the HFB gates exists only for flows higher than 6,000 cfs. For example, with the 14,000 cfs hydrograph, about 70% of the input sediments are deposited upstream of the weir for the existing condition scenario while the percentage is reduced to about 53% if the HFB gates are operated. It is interesting to note that the delta deposition remains constant when the flow is increased from 6,000 cfs hydrograph to 14,000 cfs hydrograph.
- (5) No appreciable difference is observed between the left and right HFB options in terms of the ability to move the sediment.
- (6) The final bed topography near the existing and diversion canal gates may be altered through the sluicing ability of the existing radial gates. But not enough study has been carried out to derive a quantitative scheme for sluicing.

Field Scenario

The physical model test cases are limited in several aspects. The 14,000 cfs hydrograph used in the lab is not the same as the 1998 hydrograph in the field

which had a peak of more than 20,000 cfs. Also, the total sediments added for the 14,000 cfs hydrograph may not be high enough, as the computed input based on the transport capacity is more than 10 yd³. Coupled with the potential effects of the limited size of the test box and the scalability, there is a need to model the field cases which would eliminate most of the limitations mentioned above. Major findings from both the physical and numerical models are summarized as follows:

- (1) Major conclusions derived from the physical model cases remain valid when the field model results are examined except for changes in some quantities.
- (2) The field model results were calibrated with the available flow data. A qualitative comparison of the simulated mobile-bed results with field observations under the existing condition scenario showed that the model results were reasonable. The total amount of predicted sediment deposition upstream of the weir was in agreement with the field observation; and the predicted bed form and flow pattern after a major flood were plausible.
- (3) The flow discharge of 1,000 cfs may be taken as the threshold below which no appreciable sediment movement and deposition would occur near the Robles Diversion Dam.
- (4) For all modeled scenarios, sediments would be accumulated behind the Robles Diversion Dam (Weir) quickly. The overall deposition pattern was largely determined during the rising limb of the hydrograph. Only minor deposition and bed form adjustments would occur shortly after the flow peak.
- (5) After dam removal, more sediment is expected to accumulate upstream of the Robles Diversion Dam for the existing condition scenario. The estimated deposition depth (with voids) and volume (without voids) are tabulated in Table 11 under the existing condition scenario.
- (6) Model results showed that the existing radial gates alone are not capable of efficiently moving the additional sediments added after dam removal. Sediment deposition in front of the canal gates would be so high that there is a high likelihood the bedload sediments would be transported into the diversion canal if a flood similar to 1998 (about 15-year flood) would occur.
- (7) If the high flow bypass (HFB) radial gates are in place, the total sediment deposition between RM 14.1098 and Robles Diversion Dam would be reduced by approximately 50% and 40% for the 1991 and 1998 hydrographs, respectively. HFB gates are capable of moving sediments efficiently once the dam is removed and there is less likelihood for the bedload sediments to enter the diversion canal.

(8) Numerical model results showed that the right HFB appeared to have an advantage over the left HFB. Firstly, the average total deposition depth near the weir was lower for the right HFB case: 2.5 ft for the right HFB versus 3.0 ft for the left HFB for the 1991 hydrograph and 5.0 ft versus 6.5 ft for the 1998 hydrograph. Secondly, the total sediment volume deposited between RM 14.1098 and Robles Diversion Dam is also lower for the right HFB. Finally, more deposition occurred in front of the canal diversion gates for the left HFB scenario.

Recommendations

The numerical model results are in qualitative and quantitative agreement with the physical model results and field observations. The existing radial gates at Robles Diversion are not capable of efficiently moving the additional sediments added after dam removal. The HFB gates are capable of moving sediments efficiently once the dam is removed and there is less likelihood for the bedload sediments to enter the diversion canal.

1.0 Project Background

Robles diversion dam is located on the Ventura River near Ventura, California at approximately river mile (RM) 14.16 (figure 1). The diversion supplies water to Lake Casitas by canal. The normal maximum diversion is approximately 500 ft³/s. The existing diversion dam is a low rock weir with a gated spillway, canal diversion headworks and a fish pass located on the right abutment. The diversion weir has a hydraulic height of 13 feet. The fish passage was constructed in 2002 to allow southern California steelhead (*Oncorhynchus mykiss*), a listed species, to migrate upstream of the diversion dam. Matilija Dam is a 160 ft high (originally 190 ft high) concrete arch dam located about 2 miles upstream of Robles diversion dam on Matilija Creek. Decommissioning and removal of Matilija Dam is proposed to address a dam safety risk and re-establish access for endangered steelhead to the upper reaches of Matilija Creek. The storage behind the dam has been significantly reduced by deposition of coarse sediment (Greimann, 2006). The proposed removal of Matilija Dam is expected to result in increased sediment transport to the Ventura River for many years. The focus of this study is the hydraulic design of a new high flow bypass (HFB) spillway for Robles diversion dam. The HFB will improve the movement of bed load sediments past the diversion structure. This report covers numerical modeling of the diversion facility conducted at the Bureau of Reclamation's Technical Service Center (TSC) in Denver, Colorado. The numerical model study provided design support to the Army Corps of Engineers, Los Angeles District, the principle designer for the project.

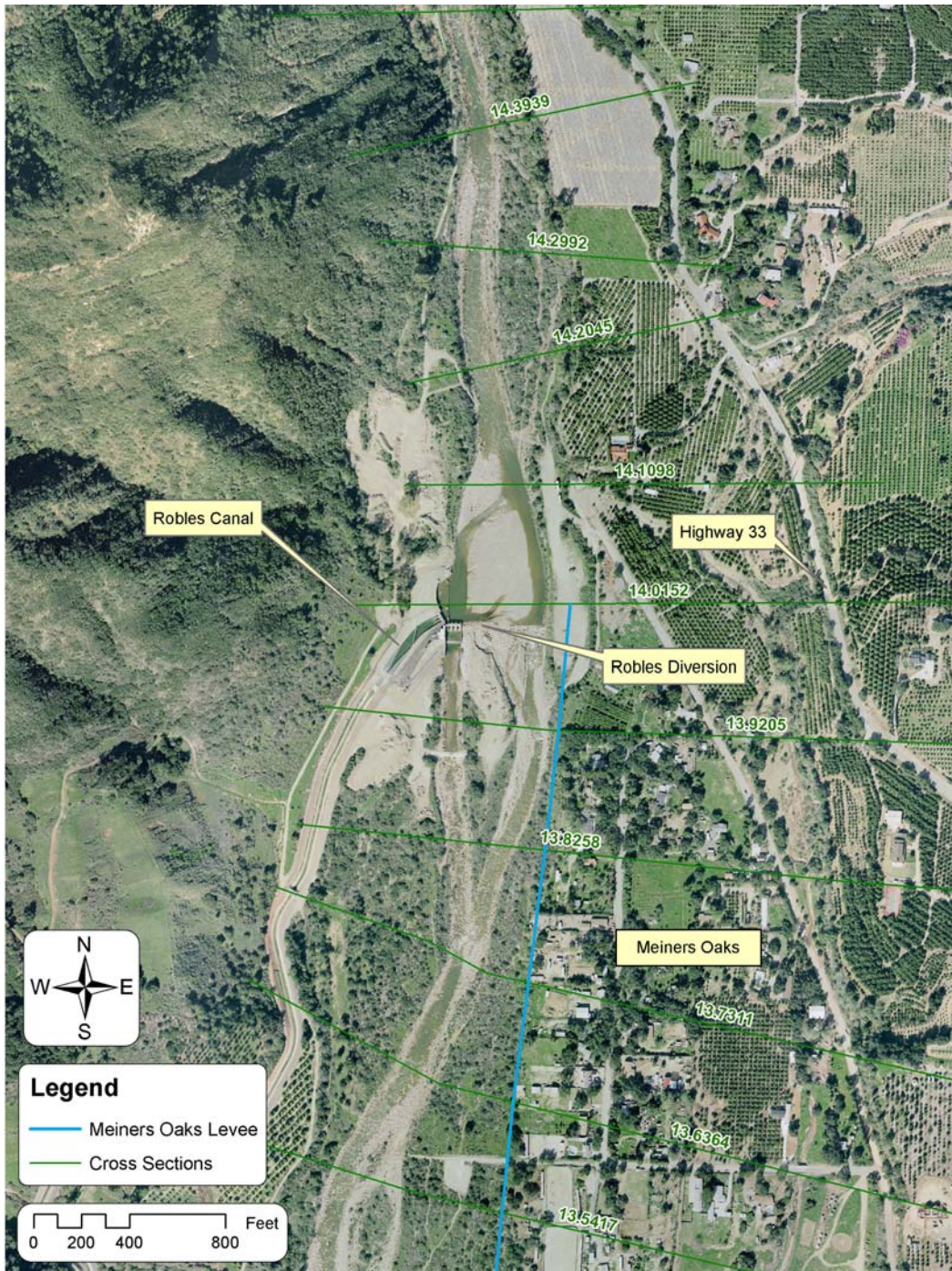


Figure 1. Aerial view of Robles Diversion taken in 2005.

2.0 Numerical Model Study Benefits

The numerical model study was carried out to assist, complement, and extend the physical model results as documented in Mefford et al. (2008). Combined results

from physical and numerical models provide relatively complete data that helps develop an informed design and selection of alternatives. Anticipated specific benefits of the numerical modeling for the current project are as follows:

- (1) The physical model includes only a small section of the river with the upstream boundary located at a meander bend. Conditions at the upstream inlet of the physical model may be obtained by the numerical model.
- (2) The discharge and sediment input are limited for the physical model. The numerical model has the capability to simulate higher flows once verified at the lower flows.
- (3) Issues of the upstream fish migration at the Robles diversion are hard to be resolved with the physical model due to limited modeling of the downstream reach. The numerical model includes a much longer river reach and the data provide information about fish migration issues.
- (4) The scale issue of sediment modeling is well known for the physical model. The numerical model provides a check on the scale effect.

3.0 Field Data

Data related to the physical model tests are presented in the physical model sections of the report, and they are not repeated. This Chapter focuses on the field data used for the current 2D numerical modeling.

3.1 Topographic and Bathymetric Data

The current study uses SRH-2D, which is a two-dimensional (2D) depth-averaged hydraulic and sediment transport model. SRH-2D simulates water surface elevation, flow velocity, and channel bed change in an unsteady manner for a specified flow hydrograph, sediment load, and other input parameters. The topographic and bathymetric data are needed for the numerical modeling. The model results can only be as detailed and accurate as the bathymetric data used.

In this study, LiDAR data collected in March, 2005 were used to represent the topography of the river section to be modeled. The survey data were imported into the SMS software for mesh generation. A perspective view of the topography near the Robles Diversion Dam is shown in Figure 2.

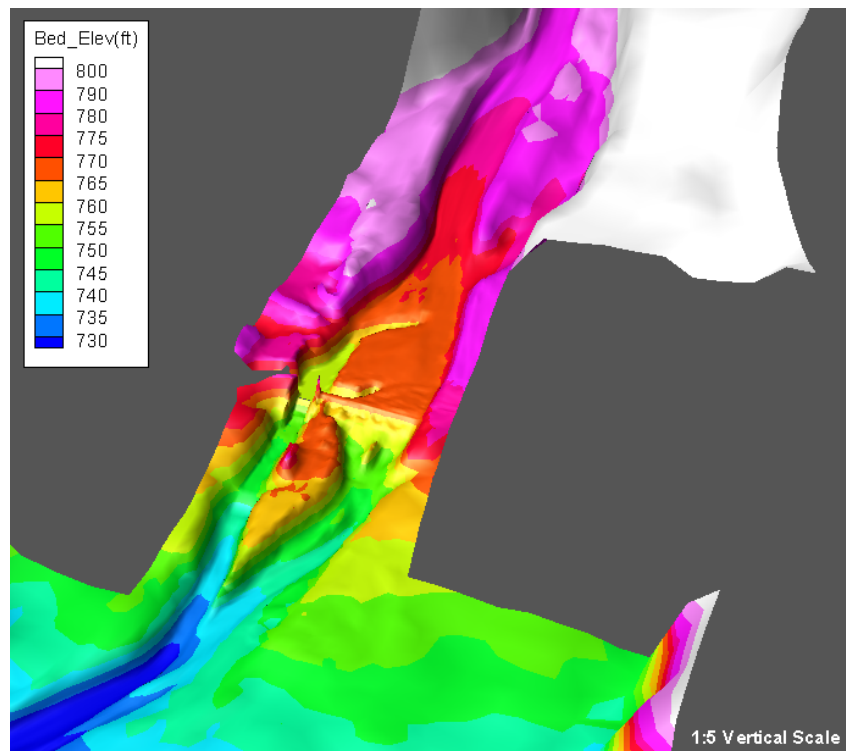


Figure 2. Topography near the Robles Diversion Dam based on the LiDAR data in March 2005

3.2 Hydrologic Data

The hydrologic data have been discussed in great detail in previous studies (Greimann, 2004 and 2006). In the current study, the flood frequency analysis reported by Greimann (2004) (Table 22) was followed. The peak flows downstream of the confluence with N. Fork Matilija Creek were used and they are listed in Table 1. The water surface elevations shown in Table 1 are the elevations at cross section RM 12.7841; as obtained by the one-dimensional (1D) model results reported by Greimann (2006).

Table 1. Peak flows downstream of the confluence with N. Fork Matilija Creek and the water elevation at RM 12.7841

Return Period (yr)	2	5	10	20	50	100	500
Flow (cfs)	3,250	7,580	15,000	18,800	24,000	27,100	35,200
Water surface elevation(ft)	660.7	662.2	663.7	664.2	664.8	665.2	665.9

Further, specific flood events were selected for the sediment routing study. Two flow events were chosen: the 1991 flood and the 1998 flood. The flow hydrographs for the two events are shown in Figure 3. About 200 hours of the hydrograph were modeled. The 1991 hydrograph had a peak of 6,065 cfs at time 78.3 hour and represented the 3 to 4 year flood. The 1998 hydrograph had a peak of 20,240 cfs at time 59.8 hour which corresponded approximately to the 15 year flood.

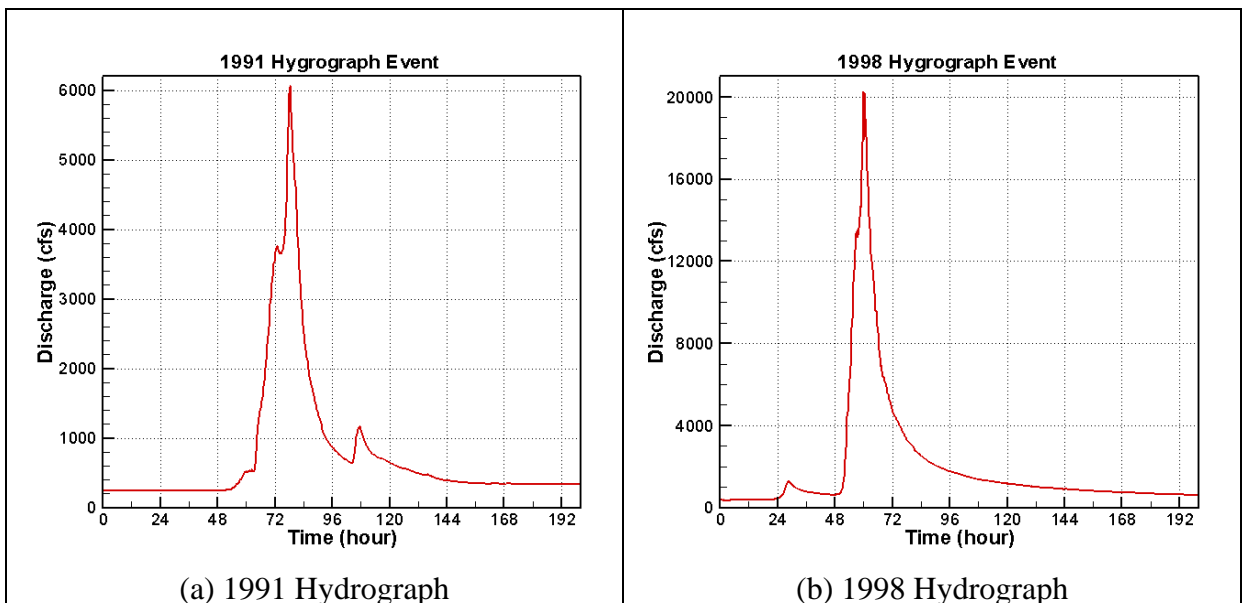


Figure 3. The 1991 and 1998 hydrographs used for the sediment modeling

3.3 Sediment Data

Input data required for the numerical modeling include the sediment load (input) at the upstream boundary and the sediment gradations of the bed material, in addition to the flow hydrograph and topography/bathymetry.

The cross section RM 14.8674 was chosen as the upstream boundary of the 2D numerical model. The sediment input at this location was obtained using results of the SRH-1D (formerly GSTAR-1D) model. The input rates of each sediment size class were computed by SRH-1D and used as input boundary conditions. Two scenarios were modeled, before and after the removal of Matilija Dam. The before-dam removal scenario represented the existing conditions with the Matilija Dam in place; and the after-dam removal scenario represented the case of removing the Matilija Dam.

The total sediment load at RM 14.8674 is shown in Figure 4 for the two dam removal scenarios and two different flood events. The total amount of sediments moving through the cross section RM 14.8674 over the 200 hour period is compared in Table 2.

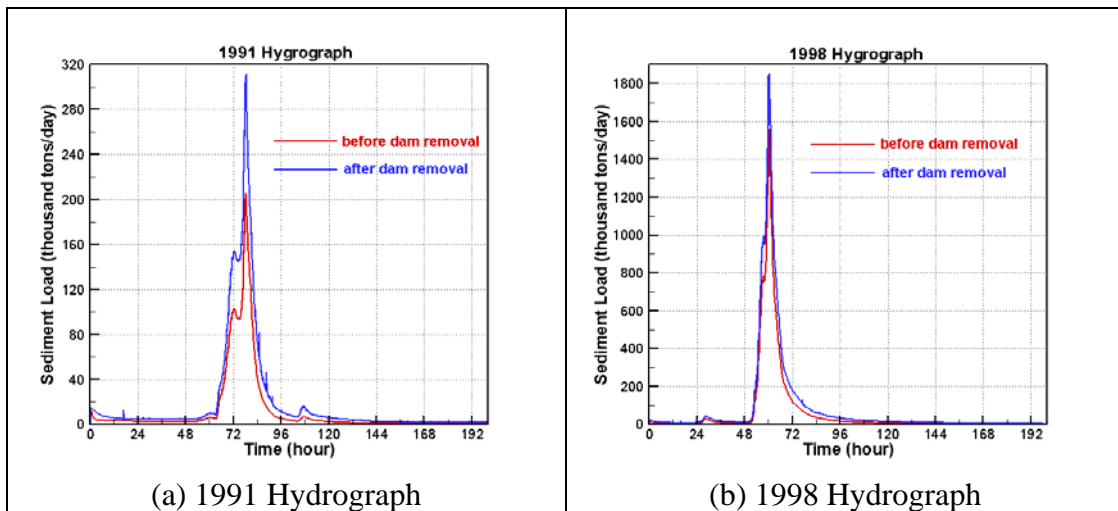


Figure 4. Total sediment load (input) at RM 14.8674 computed from the SRH-1D model

Table 2. Total sediment volume (yd³) moving through RM 14.8674 over the 200-hour period (volume is without voids)

	Before dam removal	After dam removal
1991 Hydrograph	43,930	72,130
1998 Hydrograph	233,650	318,490

Limited bed material gradation measurements were available as discussed in the reports of Greimann (2004, 2006). Bed gradation data near RM 14.4, about 0.4 miles upstream of the Robles Diversion Dam, were used for the current numerical modeling study. These surveyed gradation data were applied to the entire solution domain. The cumulative size distribution of the bed materials is shown in Figure 5. It is seen that sediments upstream of the Robles Diversion Dam are quite coarse having a medium diameter of 154 mm.

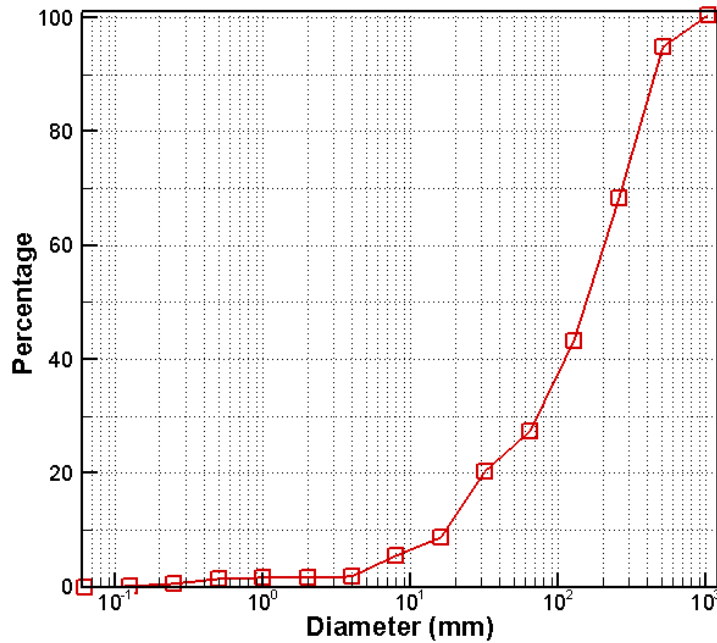


Figure 5. Size distribution of the bed materials at a location about 0.4 mile upstream of the Robles Diversion Dam (d_{50} is about 154 mm)

4.0 Methods of Analysis

4.1. SRH-2D model

Sedimentation and River Hydraulics – Two-Dimensional model (SRH-2D) is used for this study. The model is a 2D depth-averaged hydraulic and sediment transport model for river systems, and is a product of research and development at the Bureau of Reclamation. SRH-2D is based on SRH-W (Lai, 2006) for its flow modeling capability, while its sediment module is based on the Reclamation's latest sediment modeling concept (Greimann et al. 2007). SRH-2D is chosen for several reasons. First, there are not many mature 2D mobile-bed models readily available. Second, the hydraulic flow capability is based on SRH-W which is a mature and flexible tool. Its robustness and accuracy have been demonstrated by many Reclamation project applications. Detailed technical information and application cases may be obtained from the following Reclamation website: <http://www.usbr.gov/pmts/sediment/>. Third, one of the project team members, Dr. Yong G. Lai, is the lead developer of SRH-2D and SRH-W. Expert knowledge of a numerical model is critical for the success of the modeling and interpretation of the numerical results.

One of the major features of SRH-2D is the adoption of the arbitrarily shaped element method of Lai et al. (2003) for geometry representation. This allows use of the unstructured hybrid mesh for river modeling which has been shown to be flexible and has led to increased accuracy and efficiency.

Major capabilities of SRH-2D are listed below:

- 2D depth-averaged solution of the dynamic wave equations for flow hydraulics;
- An implicit solution scheme for solution robustness and efficiency;
- Unstructured or structured meshes with arbitrary mesh cell shapes may be used. In most applications, a combination of quadrilateral and triangular meshes works the best;
- Steady or unsteady flows;
- All flow regimes can be evaluated: subcritical, supercritical, or transcritical flows;
- Unsteady, non-equilibrium, and non-uniform modeling of the sediment transport;
- Multi-size sediment transports, with bed sorting and armoring;
- Effects of gravity and secondary flows; and
- Non-cohesive or cohesive sediments.

SRH-2D is a two-dimensional (2D) model, and it is particularly useful for problems where 2D effects are important. Examples include flows with in-stream structures such as weirs, diversion dams, release gates, coffer dams, etc.; bends and point bars; perched rivers; and multi-channel systems. 2D models may also be needed if some hydraulic characteristics are important such as flow recirculation and eddy patterns, lateral variations, flow overtopping banks and levees, differential flow shears on river banks, and interaction between the main channel, vegetated areas and floodplains. Some of the scenarios listed above may be modeled in 1D, but additional empirical models are used and extra calibration must be carried out with unknown accuracy.

Similar to any numerical model, uncertainty is inherent in SRH-2D due to assumptions made by the model and uncertainties in user-supplied input data. Specific assumptions and the associated uncertainties are discussed in Section 7 of the report.

4.2. Modeling Scenarios

The 2D numerical model study consisted of three categories of simulations: (1) simulation of the physical model scenarios; (2) calibration study using flows in the field; and (3) simulation of the field scenarios.

Simulation of the physical model scenarios was carried out for two purposes: to verify and validate the mobile-bed sediment model and to investigate various cases under different conditions. Cross check of results between the physical and numerical model results may provide further confidence in using the model data to develop the recommended measures.

Calibration study of the field flows was conducted for developing and testing the numerical model for the field cases so that the appropriateness of the developed model may be assessed and the flow resistance of the model may be calibrated. The study lends credence to the validity of the numerical model. Additionally, the numerical model provided the necessary flow data for designing and conducting the physical model study.

The numerical model simulated the field scenarios and represented the mobile-bed conditions present at the site. The numerical model covered a much larger reach of the river than the physical model, which eliminated sensitivity of the results to the inlet conditions. In addition, the results of the numerical model eliminated the complication of the scale effects in the physical model. Comparison of the physical model scale and the field prototype scale may shed further light on the recommended measures for the project.

A number of simulation cases were developed and performed within each category. Table 3 is a list of all simulation cases which may be used as a summary and a reference.

Table 3. List of model simulation cases and associated conditions

Model Category	Scenario Description	Case Name	Flow Hydrograph	Case Description
Physical Model Simulation	Flow Calibration	PM-FLOW-1	6,000 cfs	
		PM-FLOW-2	6,000 cfs	
	Sediment: Existing	PM-SED-EX-91	1991	
		PM-SED-EX-98	1998	
	Sediment: RHFB	PM-SED-RHFB-91	1991	
		PM-SED-RHFB-98	1998	
	Sediment: LHFB	PM-SED-LHFB-91	1991	
		PM-SED-LHFB-98	1998	
Field Scale Simulation	Flow Calibration & Application	FD-CA-2005	12,400 cfs	2005 Flood
		FD-CA-100Year	27,100 cfs	100-Yr Flood
		FD-AP-24K	24,000 cfs	
		FD-AP-15K	15,000 cfs	
		FD-AP-6K	6,000 cfs	
	Sediment; Existing	FD-EX-1991-1	1991	before-dam
		FD-EX-1991-2	1991	after-dam
		FD-EX-1998-1	1998	before-dam
		FD-EX-1998-2	1998	after-dam
	Sediment: RHFB	FD-RHFB-1991	1991	after-dam
		FD-RHFB-1998	1998	after-dam
	Sediment: LHFB	FD-LHFB-1991	1991	after-dam
		FD-LHFB-1998	1998	after-dam

4.3. Numerical Model Details

2D modeling, in general, includes the following steps:

- (1) Selection of the solution domain;
- (2) Mesh generation for the solution domain;
- (3) Zonal representation of bed properties such as flow roughness and sediment gradation;
- (4) Model development and calibration; and
- (5) Model applications.

The first three steps are discussed in this section.

4.3.1. Solution Domain and Mesh Generation

A 2D analysis begins by defining a solution domain and then generating a mesh that covers the domain. The solution domain of the field cases for the present analysis was based on the objectives of the project, the available data, and the limit of the computing power. This process largely relied on the past experience of applying the model to other similar rivers. The final solution domain for the present study is shown in Figure 6, and it has the following characteristics:

- Downstream boundary: It is located about 1.2 miles downstream of the Robles Diversion Dam, at the cross-section RM 12.7841, with a relatively straight section.
- Upstream boundary: It is located about 0.9 miles upstream of the Robles Diversion Dam, at the cross-section RM 14.8674, with a relatively straight channel.
- Lateral extent: It is wide enough laterally that the domain would fully contain the 500-year flood; based on the results of the 1D numerical modeling (Greimann, 2004).
- The total length of the river reach modeled is about 2.1 miles.

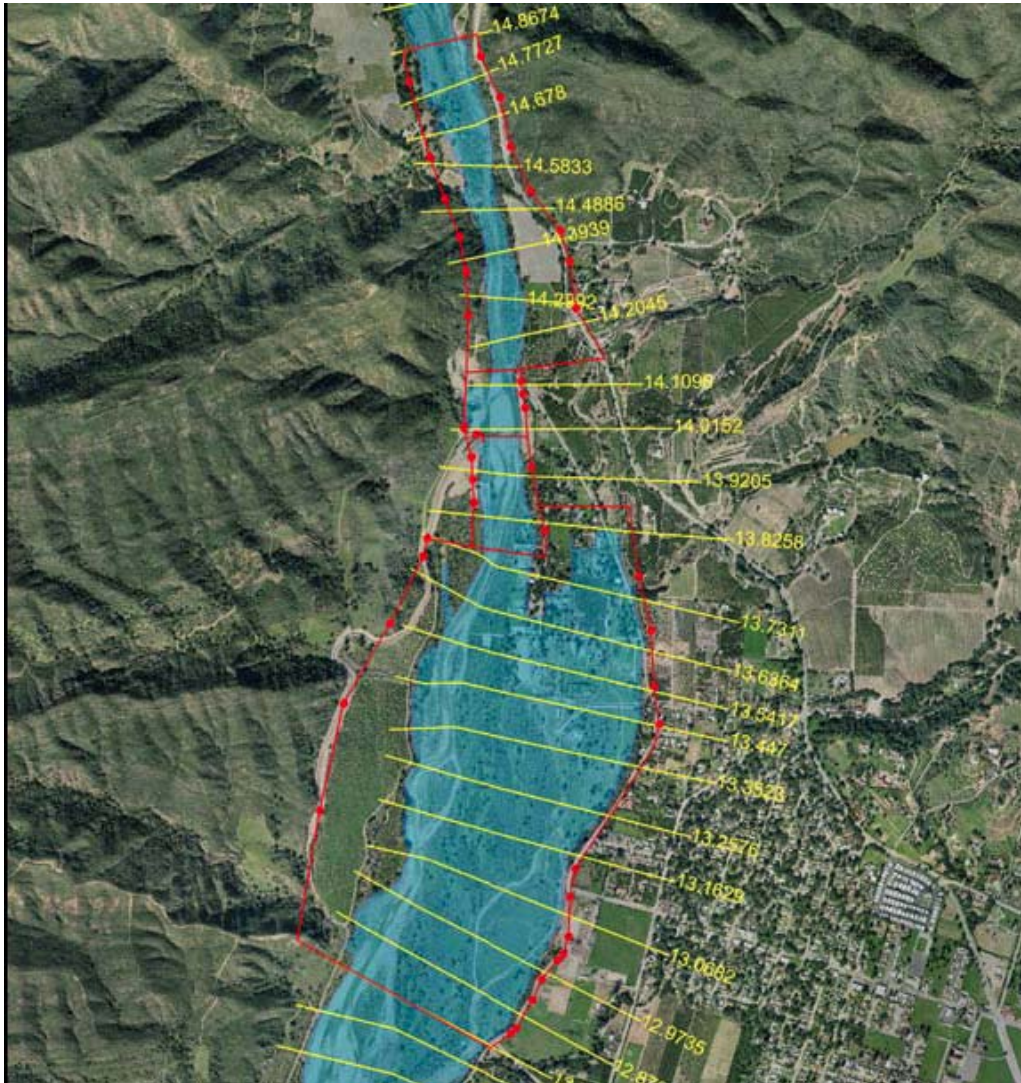


Figure 6. Solution domain (red) of the 2D numerical model for the field simulation

A 2D mesh was generated using the Surface water Modeling System software (SMS). The following website link provides more information for the software: www.ems-i.com. Additionally, the SRH-W manual (Lai, 2006) may be consulted for discussion on how the SRH-2D model interacts with SMS. Different meshes were generated for each scenario and they are discussed. In reference to the following discussion, the mesh used for the calibration study of field flows is shown in Figure 7. A total of about 10,000 hybrid quadrilateral and triangular mesh cells were used to represent the solution domain. The topography/bathymetry of the solution domain represented by the mesh is shown in Figure 8. Note that the bathymetry was based on the March 2005 LiDAR survey as discussed in Chapter 3.0.

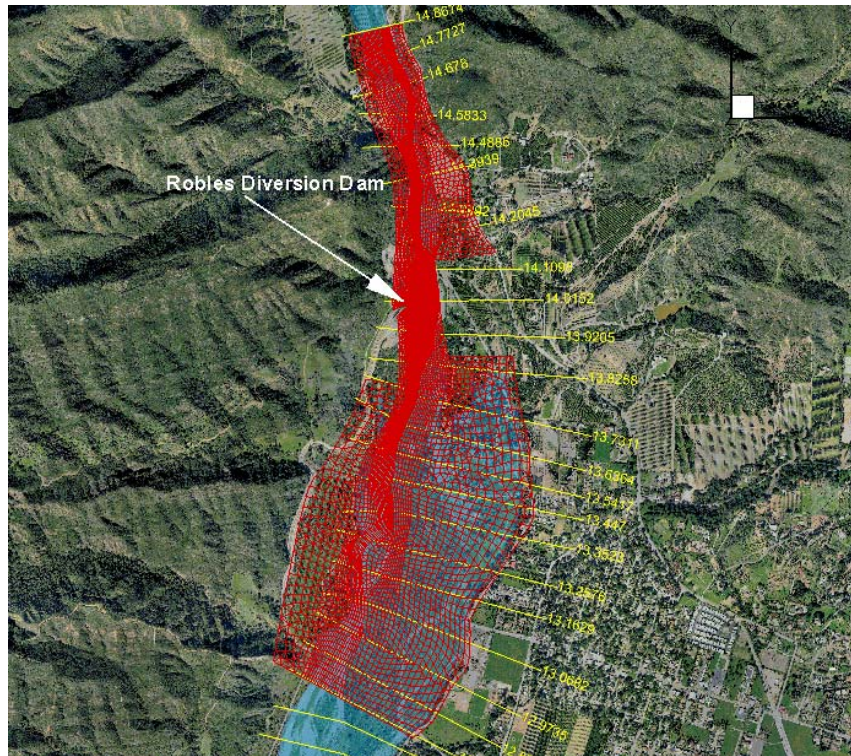


Figure 7. Mesh generated for the calibration study of field flows discussed in Chapter 5.0

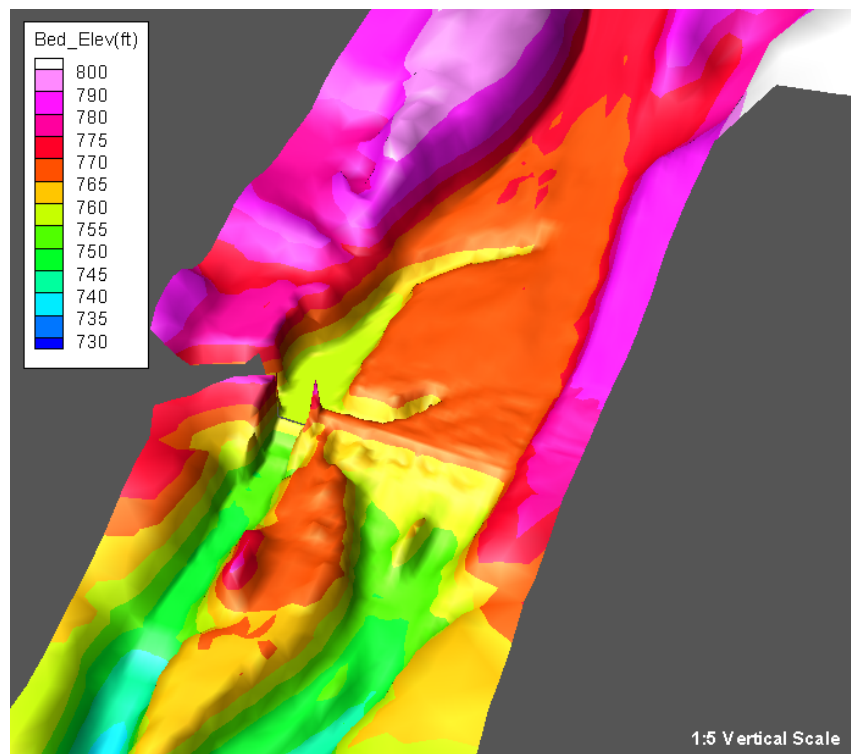


Figure 8. 3D perspective view of the topography for the existing condition scenario based on March 2005 LiDAR survey data

4.3.2. Representation of Flow Roughness and Bed Gradation

Flow resistance was calculated with the Manning's roughness equation in which the Manning's coefficient (n) was used as one of the model inputs. Major bed properties include the Manning's coefficient and the bed gradation. The bed properties may be spatially distributed over the solution domain. The zonal representation approach was used: the solution domain was partitioned into a number of bed-property zones and each zone was assigned different properties of the roughness and bed gradation.

In this study, the solution domain was divided into three bed-property zones based on the aerial photo: main channel, light vegetation, and heavy vegetation. The zonal partition is shown in Figure 9. Each zone is assigned a different Manning's coefficient n . Based on the report of Greimann (2006) (p.67), the previous 1D model study used the Manning's roughness coefficient of 0.04 for the main channel, and 0.08 for the floodplain. In general, 2D models use smaller roughness coefficients than the 1D model, as some energy losses are taken into account by the 2D model. In this study, the main channel has $n = 0.035$, light vegetation has $n = 0.045$, and heavy vegetation $n = 0.075$. These initial values were confirmed to give good results during the calibration study reported in Chapter 5.0, and they were used unchanged for all field simulations reported.

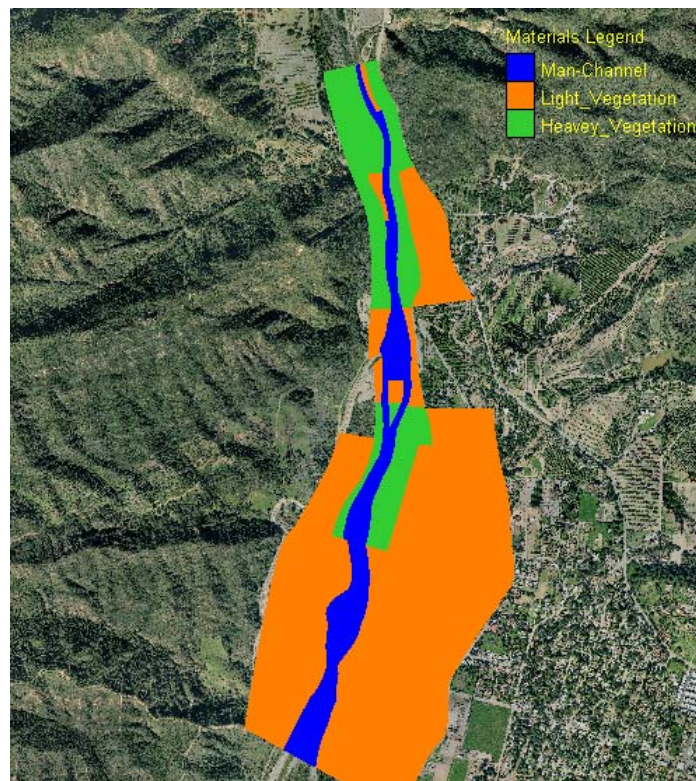


Figure 9. Three zones were used to represent the bed properties on the solution domain: the main channel, light vegetation and heavy vegetation

4.4. Sedimentation Analysis Method

The mobile-bed sediment analysis was carried out with SRH-2D. The flow modeling capability is well documented by Lai (2006); but the sediment module is not. Readers may consult a few recent papers for details (e.g., Greimann et al. 2007; Lai and Greimann 2007; Lai and Greimann 2008a.). In the following, a brief description of the sediment analysis methodology and the related modeling parameters is provided.

4.4.1. Sediment Transport Equations

Sediment transport in a mobile-bed river depends on many input variables such as topographic and bathymetric features, flow hydraulics, bed gradation, and upstream sediment supply. The bed gradation changes from its initial state as sediment particles are eroded from or deposited on the bed, which in turn changes flow hydraulics and fractional sediment transport rates.

In general, a water column and a river bed may be divided into four separate vertical layers, from a computational point of view:

- **Suspended Load Layer:** a top layer in the water column where sediment particles are in suspension and are transported as suspended load (including wash load);
- **Bed Load Layer:** a layer near the bed where sediment particles roll, slide, or saltate. Particles are transported as bed load;
- **Active Layer:** a layer on the top surface of the bed where sediment exchange occurs between the sediment load above and the bed underneath;
- **Subsurface Layers:** one or several bed layers, which have not been mobilized by flow and are underneath the active layer.

In this project, transport of the bed material load is considered. That is, the combined suspended load and bed load, but without the wash load, is simulated. The wash load refers to those fine sediments that are transported from the upstream boundary to the downstream exit without interaction with the bed sediments. Wash load is ignored as it does not contribute to the bed morphological changes.

Furthermore, the general modeling approach of the non-uniform and non-equilibrium sediment transport is adopted. Non-uniform transport refers to the representation of sediments with multiple sediment size classes and transport of each size class is tracked separately. The non-uniform approach may be compared with the alternative of the uniform transport method in which all sediments are represented by one size class (d_{50} is usually used). The non-uniform approach is closer to field conditions and is the choice if sediment sorting and other related features are of interest. Non-equilibrium transport refers to the use of the full sediment transport equation in which the sediment concentration does not equal

the sediment transport capacity. This is in contrast to the commonly used Exner equation, an equilibrium model, which assumes instant exchange between the transported loads and the bed materials. With the non-equilibrium method, the sediment concentration is allowed to vary in response to local flow features such as convection and dispersion, local transport capacity, and local bed gradation.

With the non-uniform non-equilibrium approach, sediments are divided into a number of size classes and each sediment size class (k) obeys the following transport equation derived from mass conservation:

$$\frac{\partial hC}{\partial t} + \frac{\partial \cos(\alpha)V_t hC}{\partial x} + \frac{\partial \sin(\alpha)V_t hC}{\partial y} = S_E \quad (1)$$

where C is the depth-averaged sediment concentration, h is water depth, t is time, x and y are two horizontal Cartesian coordinates, respectively, V_t is the depth-averaged total sediment velocity, α is the angle of sediment transport direction relative to the x -axis, and S_E is the sediment exchange term between the total sediment load and the active layer. Specific models for a number of variables in the above equation will not be discussed and may be found in Greimann et al. (2007). It is sufficient to point out that the angle of sediment transport direction is not the same as the water flow. Instead, the angle depends on whether or not the size class is suspended load, bed load, or mixed load, and the impacts of secondary flows and gravity are also included.

The sediment exchange term is discussed next. For the non-cohesive sediments, the exchange term may be expressed as:

$$S_E = \frac{1}{L_{tot}}(q_{tot}^* - V_t hC) \quad (2)$$

where q_{tot}^* is the equilibrium transport capacity for the total load, and L_{tot} is the adaptation length of the total load and is calculated as:

$$L_{tot} = (1 - f)L_b + f \zeta V_t h / \omega_s \quad (3)$$

where f is the fraction of the suspended sediments in the total load, ζ is the parameter for the rate of suspended load exchange, L_b is the bed load adaptation length, and ω_s is the particle fall velocity. The bed load adaptation length characterizes the distance for sediments to adjust from the non-equilibrium state to the equilibrium state, and is related to scales of sediment transport, bedform, and geometry. In this study, a constant L_b was specified. The suspended sediment coefficient, ζ , equals 1.0 for net erosion and 0.25 for net deposition.

The Parker (1990) sediment transport equation was used in this project and is suitable for rivers composed of gravel and mixed sand and gravel beds. The transport equation for sediment size class k may be expressed as:

$$\frac{q_{t,k}^* g(s-1)}{(\tau_b / \rho)^{1.5}} = p_{ak} G(\phi_k); \quad \phi_k = \frac{\theta_k}{\theta_r} \left(\frac{d_k}{d_{50}} \right)^\alpha \quad (4)$$

In the above, $q_{t,k}^*$ is the volumetric sediment transport rate per unit width, p_{ak} is the volumetric fraction of sediment size class k on the bed surface, $s = \rho_s / \rho - 1$, ρ and ρ_s are the water and sediment density, respectively, g is the gravitational acceleration, τ_b is bed shear stress, $\theta_k = \tau_b / [\rho g(s-1)d_k]$ is Shield's parameter of sediment size class k ; θ_r is the reference Shield's parameter, d_k is diameter of sediment size class k , and d_{50} is the median diameter of the sediment mixture in bed. The function in the transport equation was fit to the field data by Parker (1990) and is expressed as:

$$G = \begin{cases} 11.933(1 - 0.853 / \phi)^{4.5}, & \phi > 1.59 \\ .00218 \exp[14.2(\phi - 1) - 9.28(\phi - 1)^2], & 1.0 \leq \phi \leq 1.59 \\ .00218 \phi^{14.2}, & \phi < 1.0 \end{cases}$$

Two parameters must be defined by a user to apply the Parker equation: θ_r and α . The parameter θ_r is a reference value above which sediment is mobilized and α is the exposure (or hiding) factor to account for reduction in critical shear stress for larger particles and increase in critical shear stress for smaller particles. In this project, $\theta_r = 0.055$ and $\alpha = 0.65$ were used.

Dynamics of the bed sediments and the bed interaction with the sediment load were also simulated, and details may be found in Greimann et al. (2008).

4.4.2. Boundary Conditions and Other Input Data

At the upstream boundary, conditions include the flow discharge and the sediment supply rate (load) for each size class. In this study, a constant flow discharge or a time series flow hydrograph was imposed as discussed in Chapter 3.0. The upstream sediment supply was obtained from the SRH-1D simulation results as discussed in Chapter 3.0 for the filed scenarios and was estimated from the total sediment added for the physical model cases.

At the downstream boundary, the water surface elevation (stage) was specified. A rating curve was generated at the downstream boundary based on the SRH-1D model results and was tabulated in Table 1.

Ten sediment size classes, as shown in Table 4, were used to represent the sediments on the river bed and at the inlet. The bed gradation has been presented in Figure 5 and it was used throughout the solution domain. Note that size class 10 was used to represent the non-erodible bed such as the radial gates and at spillways. Each size class will be transported and modeled individually.

Table 4. Size ranges of each sediment size class

Sediment Size Class	Size Range (mm)
1	0.0064 to 0.0625
2	0.0625 to 0.25
3	0.25 to 1
4	1 to 4
5	4 to 16
6	16 to 64
7	64 to 256
8	256 to 1028
9	1028 to 4096
10	Non-erodible

5.0 Physical Model Scenarios

5.1. Discussion of Physical Model Scenarios

Different physical model scenarios have been discussed and results are presented in the physical model results portion of the report. Only information relevant to the numerical simulation is summarized and discussed next.

Three test scenarios were performed in the physical model: Existing Condition, Right High Flow Bypass (RHFB), and Left High Flow Bypass (LHFB). The existing condition has the existing radial gates and the diversion canal gates in operation. With the RHFB and LHFB, the new high flow bypass radial gates are added to the existing condition. Layouts of the three scenarios are illustrated in Figure 10.

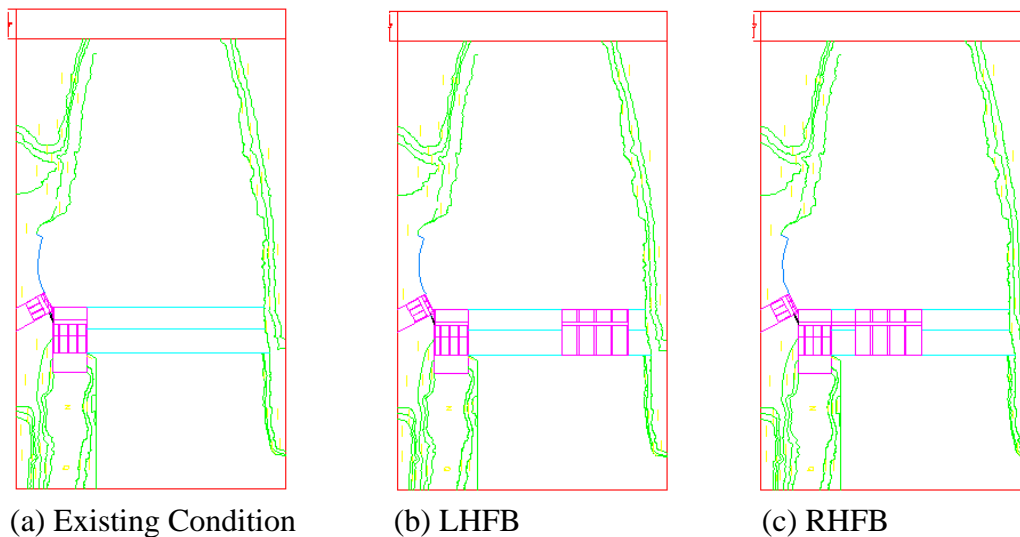


Figure 10. Layouts of three physical model scenarios (looking upstream)

The flow capacities of the existing gates, the diversion canal gates, and the new high flow bypass gates are about 3.3538 cfs, 0.2795 cfs, and 6.149 cfs, respectively. These correspond to 6,000 cfs, 500 cfs, and 11,000 cfs, respectively, in the prototype field scale.

For each scenario, two flow hydrographs were tested: 1991 hydrograph and 1998 hydrograph. The 1991 hydrograph has a peak flow of about 6,000 cfs in the prototype scale and 1998 hydrograph has a peak of 14,000 cfs in the prototype scale. The actual peak of the 1998 flood was more than 20,000 cfs and the smaller value of 14,000 cfs was used for the physical model due to the limit of sediment feed at the laboratory. The two hydrographs in the physical model scale, along

with the sediment input rate at the model inlet, are shown in Figure 11 and Figure 12. Only the total sediment input was recorded during the physical model test: an average of about 3.5 yd³ and 6.85 yd³ for the 1991 and 1998 hydrographs, respectively. In the numerical modeling, the curves of the total sediment rates in Figure 11 and Figure 12 were determined as follows. The numerical model was first run assuming that the sediment transport rate at the inlet equaled the sediment capacity. Integration of the resultant curve gave the total amount of sediments into the test box. In general, however, the calculated input volume would not equal the actual one used. The sediment rating curve was then scaled up or down so that the total sediment input volume would be the same as the recorded volume used during the test. It is interesting to point out that the total input volume based on the transport capacity was approximately the value of 3.5 yd³ for the 1991 hydrograph case while it was about 11.5 yd³ for the 1998 hydrograph case.

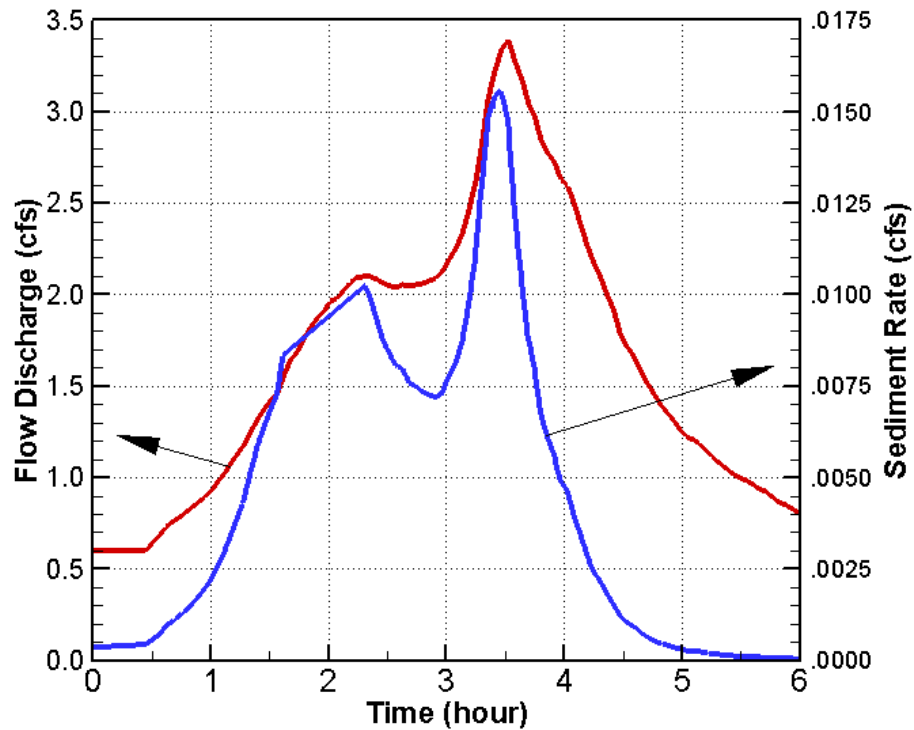


Figure 11. Flow hydrograph and total sediment load at the inlet with the 1991 hydrograph

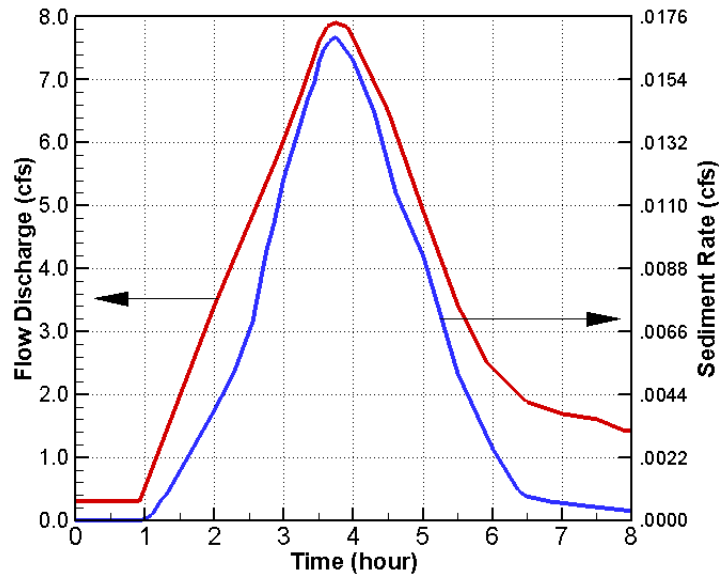


Figure 12. Flow hydrograph and total sediment load at the inlet with the 1998 hydrograph

A sediment mixture with medium diameter $d_{50}=1.75$ mm was used for the physical model test. It was used as the initial bed and it was also used as the sediment feed at the inlet. The gradation sample analysis provided the cumulative size distribution as plotted in Figure 13. For the numerical modeling, the sediment mixture was divided into seven size classes listed in Table 5. The bed upstream of the weir was initially filled with the sediments while the test section downstream of the weir was non-erodible.

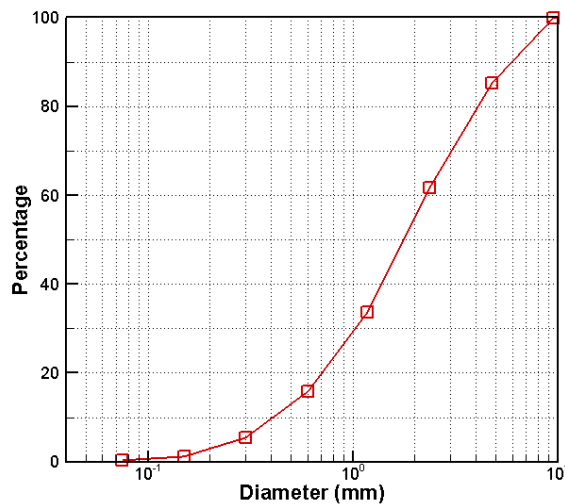


Figure 13. Size distribution of the base sediment mixture used for the physical model test ($d_{50}=1.75$ mm)

Table 5. The lower (d_{low}) and upper (d_{upp}) diameter of each sediment size class used for the numerical modeling of the physical model scenarios

Size ID	1	2	3	4	5	6	7
$d_{low}(mm)$	0.0625	0.15	0.30	0.60	1.18	2.36	4.75
$d_{upp}(mm)$	0.15	0.30	0.60	1.18	2.36	4.75	9.5

5.2. Calibration Using the Measured Flow Data

With SRH-2D, the major flow calibration parameter is the Manning’s roughness coefficient. In the physical model, flow velocity measurements were made under a constant flow discharge of 3.3538 cfs (6,000 cfs at the prototype field scale) under several gate scenarios. The data were used to calibrate the Manning’s coefficient and then used to verify the numerical model. The final calibrated Manning’s coefficient for the physical model scenarios was 0.026 which was a constant uniformly distributed over the solution domain.

The RHFB scenario was set up for the flow measurement in the laboratory. The layout of the flow case is shown in Figure 14. In this setting, the existing gate, the diversion canal gates, and the RHFB gates were all in place. The solution domain was the same as the test box. The mesh generated for the numerical modeling, along with the bathymetry represented by the mesh, is displayed in Figure 15. A perspective view of the bathymetry is shown in Figure 16.

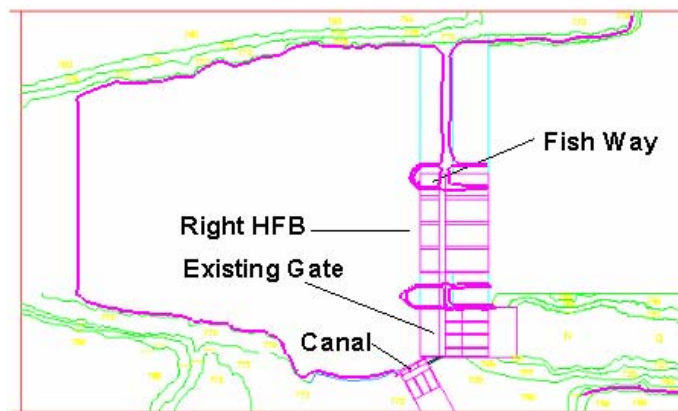


Figure 14. Layout of the right HFB case

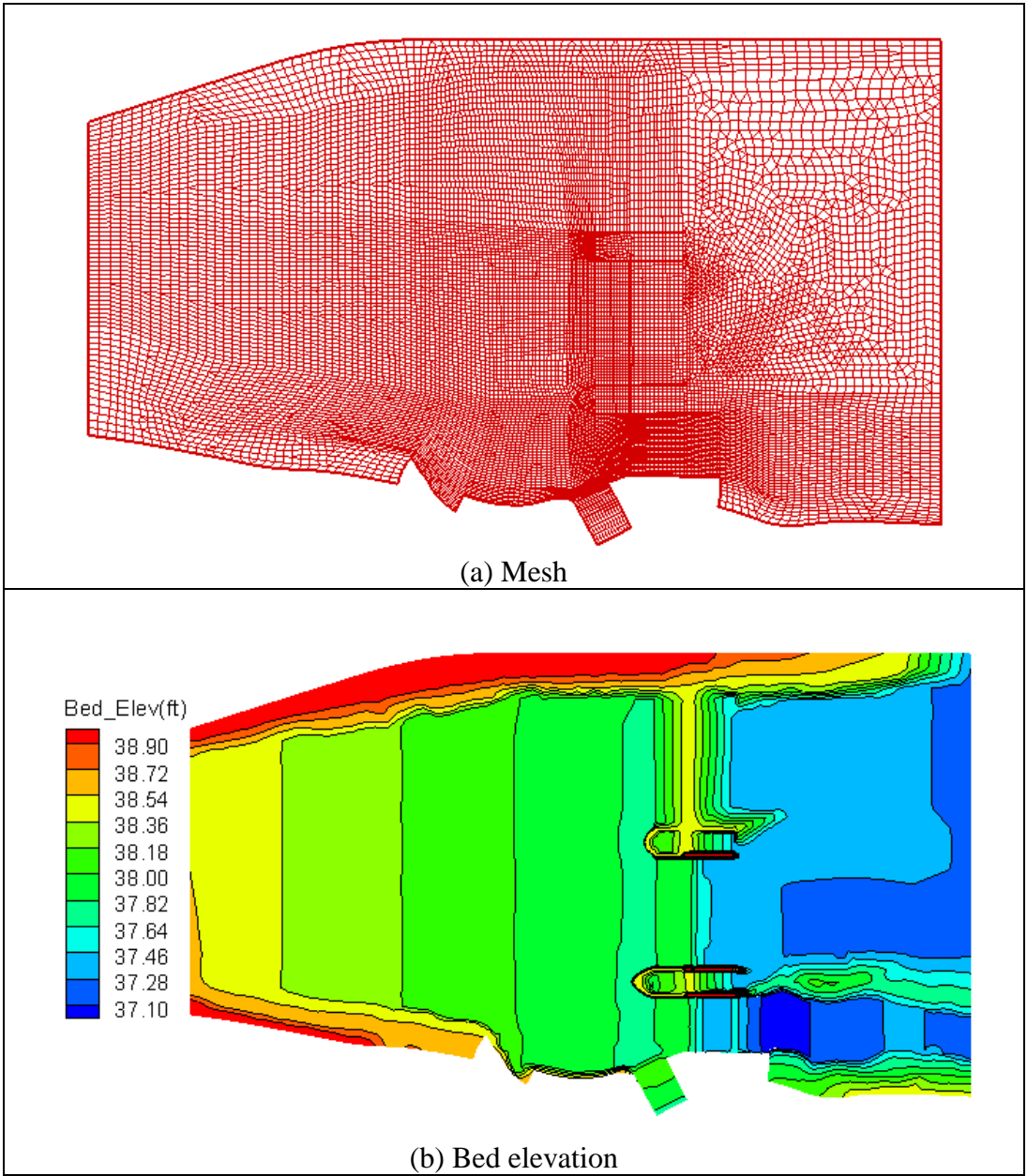


Figure 15. Mesh and bathymetry of the RHFb numerical model used for the calibration study

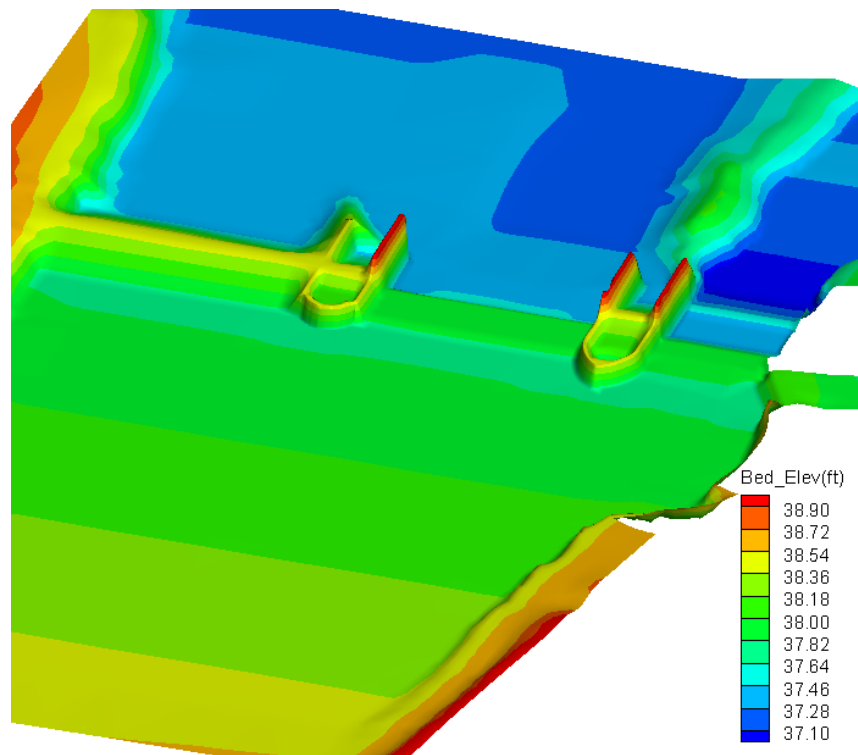


Figure 16. Perspective view of the bathymetry of the RHFB case in the physical model used for the calibration study

Two flow cases were simulated and results were compared with the measurements. The first case was named PM-FLOW-1 for which the existing gates were fully open while the RHFB gates were closed completely. The second case, PM-FLOW-2, reversed the gate operation: the RHFB gates were fully open while the existing gates were closed. The diversion canal gates were fully open for both cases.

A comparison of the measured and computed depth-averaged velocity along several transects is shown in Figure 17 and Figure 18. It is seen that agreement between the measurement and computation is reasonably good. The measured depth-averaged velocity was obtained at the 60% flow depth. Some of the measurement points, particularly at the upstream transects, were not accurate as they were strongly influenced by the delta movement.

The predicted flow streamlines and flow patterns are also shown in the figures. The computed recirculation location, size and shape at the top right corner were in agreement with the observation made during the physical model test.

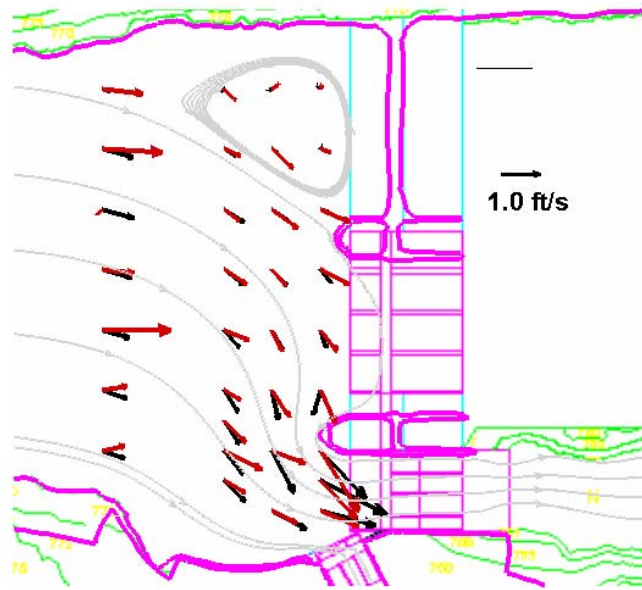


Figure 17. Comparison of measured (red) and computed (black) depth-averaged velocity for case PM-FLOW-1

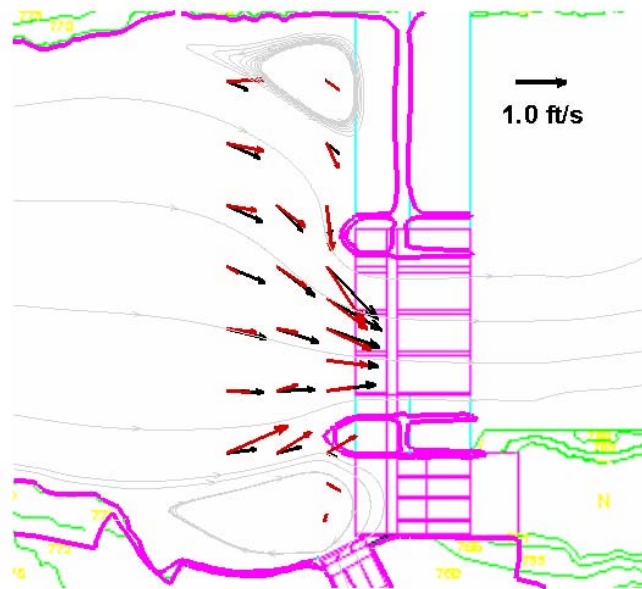


Figure 18. Comparison of measured (red) and computed (black) depth-averaged velocity for case PM-FLOW-2

5.3. Mobile-Bed Simulation with the Existing Condition

The mobile-bed simulation was carried out for the existing condition scenario. The mesh is shown in Figure 19, and the bathymetry of the initial bed is displayed in Figure 20. The mesh has a total of 10,285 combined quadrilateral and triangular cells.

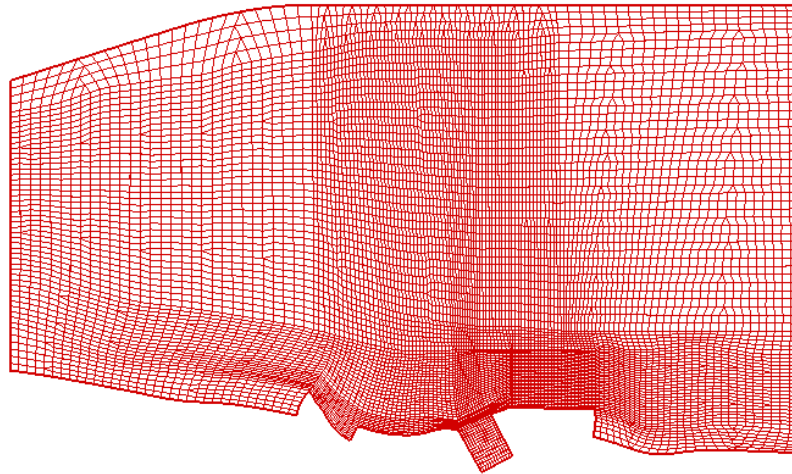


Figure 19. Mesh for the existing condition scenario mobile-bed simulation (physical model)

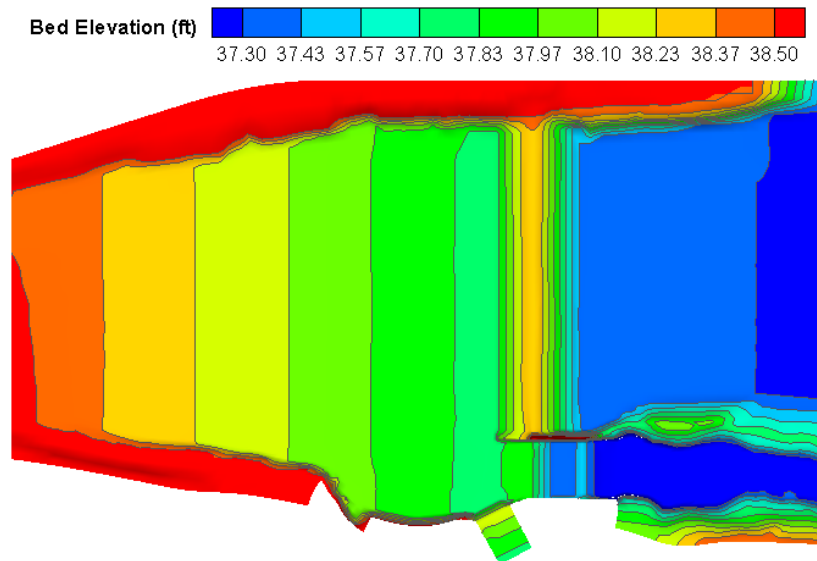


Figure 20. Bed elevation of the existing condition scenario for the mobile-bed simulation (Physical model)

Two unsteady mobile-bed simulations were carried out in the physical model corresponding to the 1991 hydrograph and the 1998 hydrograph (see Figure 11

and Figure 12). They are labeled as PM-SED-EX-91 and PM-SED-EX-98, respectively. The diversion canal gates were open all the time with a flow capacity of 0.2795 cfs (500 cfs in the prototype). Operation of the existing gates followed the operation of the physical model test as closely as possible and the discharge capacity of the gates is shown in Figure 21 which was used for both simulation cases. The existing gates were open to a capacity of 0.2 cfs for the first 1.16 hours; the capacity was jumped to 1.0 cfs for the period of 1.16 to 1.685 hours; and the gates were fully open to 3.35 cfs after 1.685 hours. The gate capacity was reduced down to 1.4 cfs after 5.94 hours.

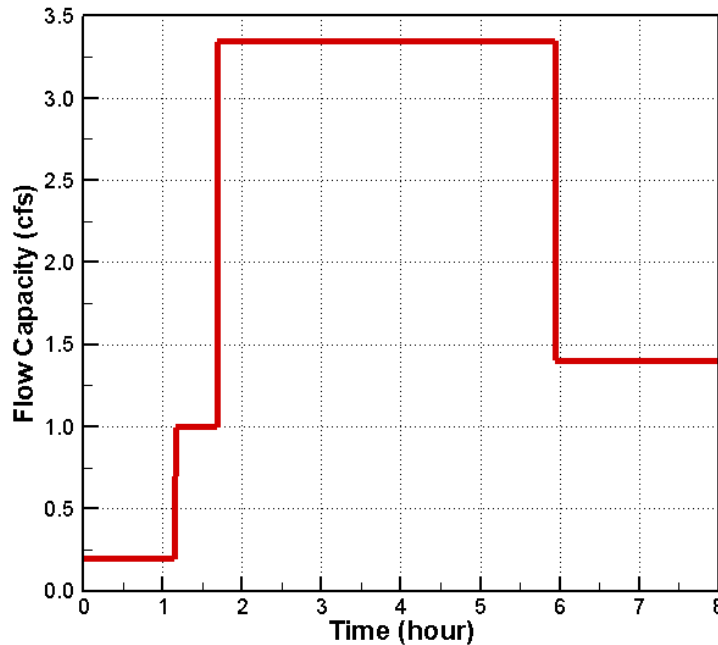


Figure 21. Gate operation curve (flow capacity versus time) of the existing radial gates for the existing condition modeling

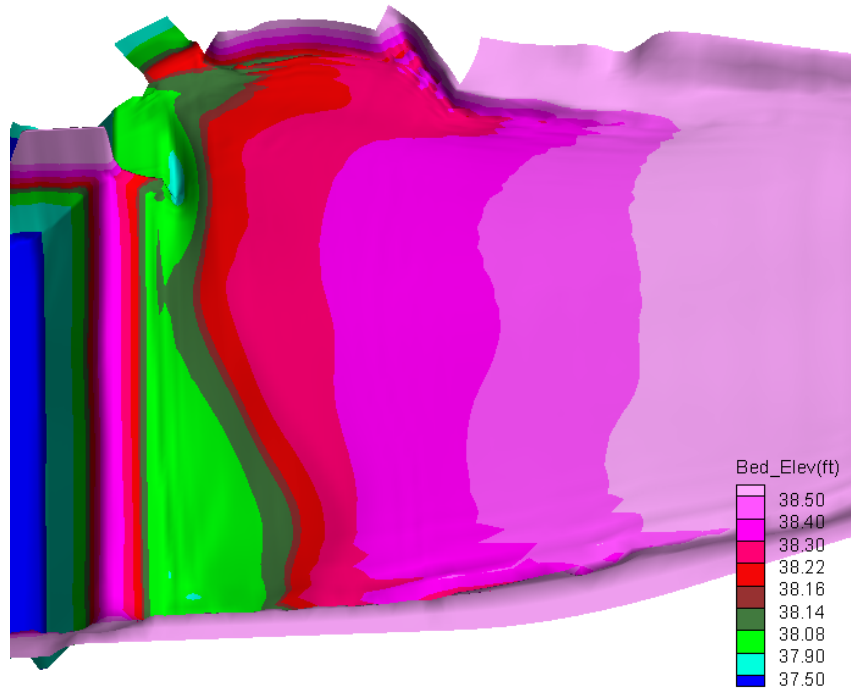
For case PM-SED-EX-91 (1991 hydrograph), the final bed topography is compared in Figure 22 at time 6 hours between the simulated results and the physical model results. The simulated bed form evolution in time is plotted in Figure 23.

The simulated final bed form is in qualitative agreement with that of the physical model test. Some discrepancy is observed and is mainly near the existing gate. It may be attributed to the possible difference in the radial gate operation during the falling limb of the hydrograph. In the numerical model, all gates (a total of four) could only be opened or closed at the same time and they were not allowed to operate separately. In the physical model test, each individual gate may be operated to different capacity. In addition, the gate operation during the falling limb was not well documented during the physical model test. Another source of uncertainty is related to the spatial distribution of the input sediments. During the

physical model tests, sediments addition at the inlet was not uniform laterally, but the numerical model assumed a uniform distribution of the sediment concentration across the inlet.



(a) Photo taken at the end of the physical model test



(b) Simulated bed elevation

Figure 22. Comparison of bed topography at the end of the hydrograph (6 hours) between the physical model and the simulation for PM-SED-EX-91

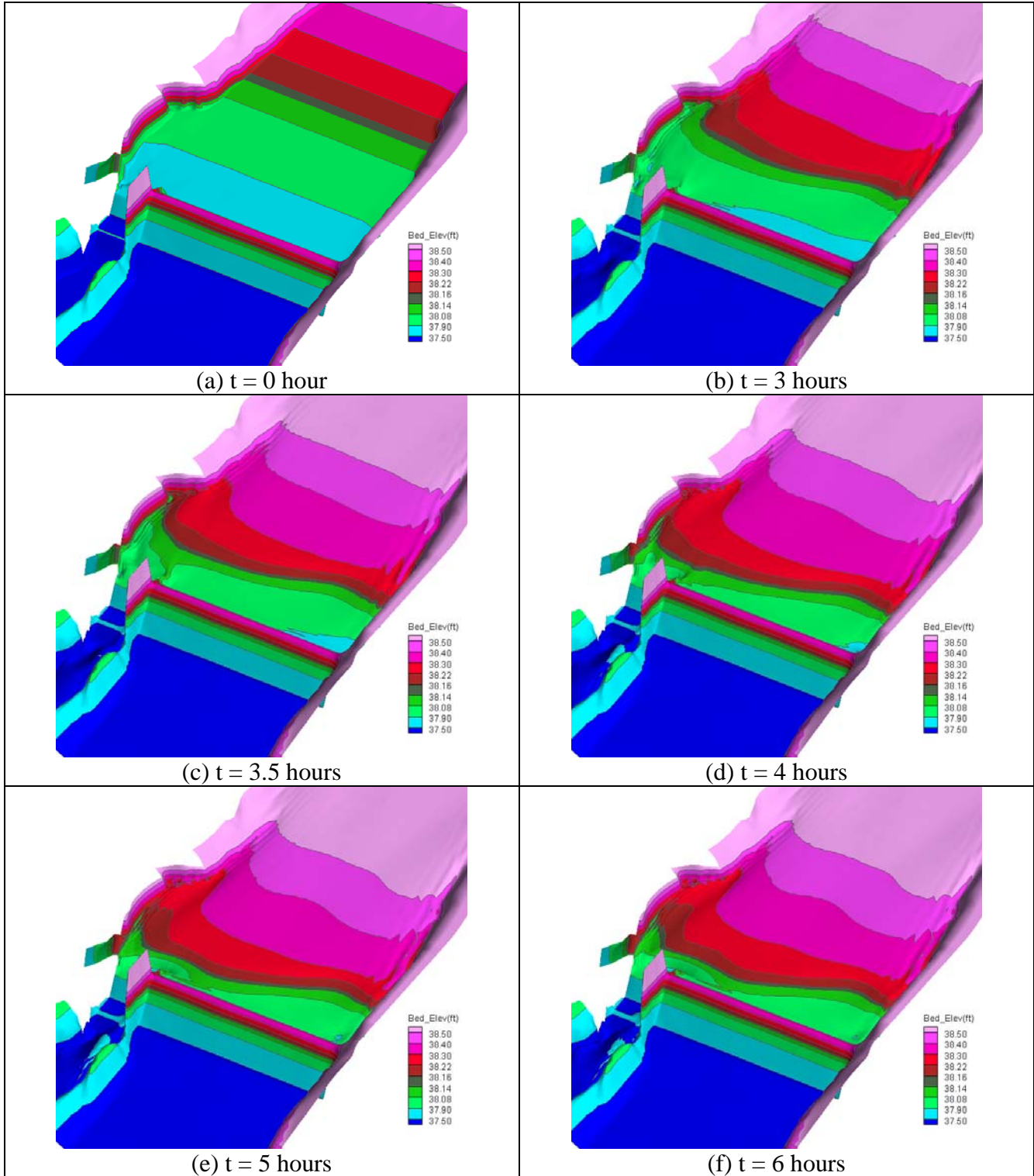


Figure 23. Simulated bed form evolution at different times for case PM-SED-EX-91 (1:4 vertical distortion)

For case PM-SED-EX-98 (1998 hydrograph), the bed topography is compared in Figure 24 and Figure 25 at the end of the hydrograph (8 hours) between the simulated and physical model test results. The simulated bed form evolution in time is plotted in Figure 26.

Figure 24 and Figure 25 show that the model results were in qualitative agreement with the physical model results. In the area upstream of the existing gates and the diversion canal gates, greater deposition occurred in the middle while “channel”-type topography appeared on the two sides. The “channel” on the left was more significant in the numerical model as shown in Figure 24 and it was due to sluicing by the existing gates. The sluicing effect can be seen by comparing results of 5.5 hours and 8.0 hours in Figure 26. The right “channel” was less significant near the canal diversion gate (Figure 24) but more significant upstream (Figure 25). The right “channel” was only marginally captured by the numerical model as shown in Figure 25 and this may be attributed to the difference in sediment feeding at the inlet upstream. Much less sediments were added on the right side of the inlet during the physical model tests but uniform constant sediment concentration was assumed in the numerical model. The final bed form may be sensitive to the existing gate operation particularly during the falling limb of the hydrograph, and to a lesser degree, also sensitive to the spatial distribution of the sediment input at the inlet.

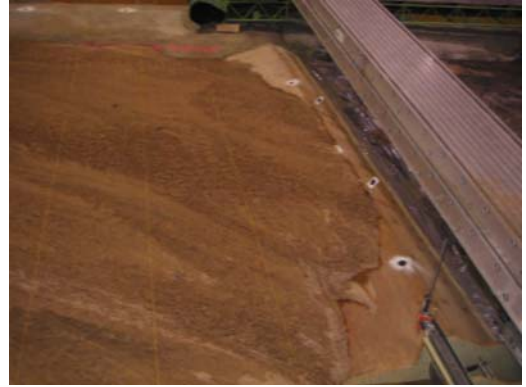
High sediment deposition was observed in the middle section of the weir and it was captured by the numerical model as shown in Figure 24.

Model results of the case PM-SED-EX-98 point to the possibility of using the existing radial gates to remove the sediments deposited in front of the existing gates and the diversion canal gates by opening the existing gates as much as possible during the falling limb of the hydrograph. Since the sluicing does not take place for case PM-SED-EX-91, an estimate may be made based on the model results. It is found that a discharge above 1.5 cfs (2,236 cfs in the prototype) is needed for effective sluicing using the existing gates. However, the numerical model assumed that all four gates are open; it is expected that much less flow is needed if only one of the four gates is open for sediment sluicing.

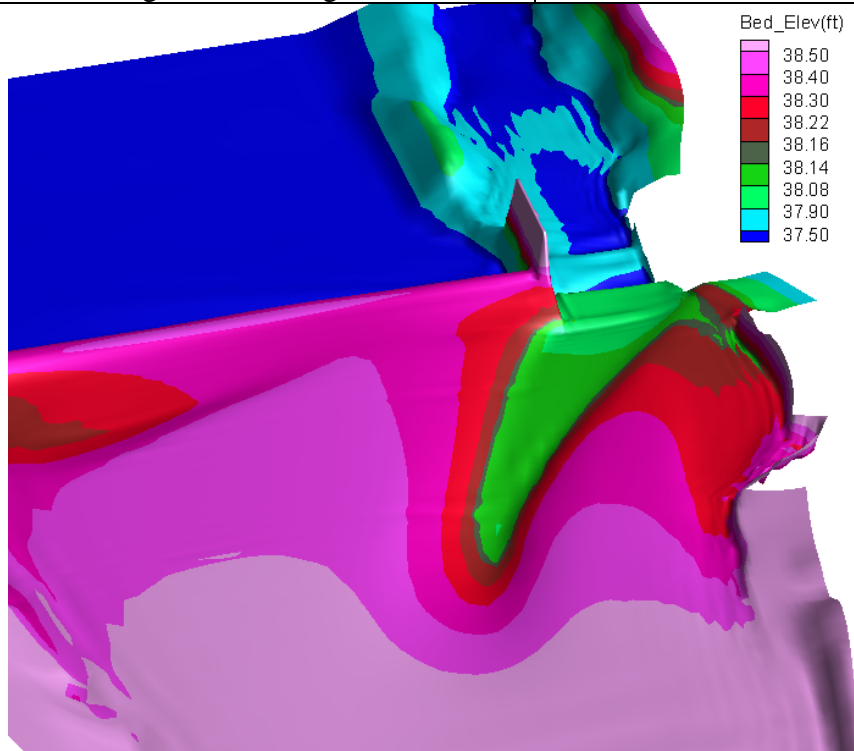
The bed evolution pattern in Figure 23 showed that the delta has reach the canal diversion gates but the delta elevation in front of the gate is still less than the gate sill elevation. Figure 26 clearly showed the risk of bed load sediments transported into the diversion canal during the flood as the delta elevation in front of the canal gates is about the same as the gate sill.



(a) Photo looking towards the gates



(b) Photo looking at the weir



(c) Simulated bed elevation

Figure 24. Comparison of bed topography at time 8 hours between the physical model and the simulation for PM-SED-EX-98

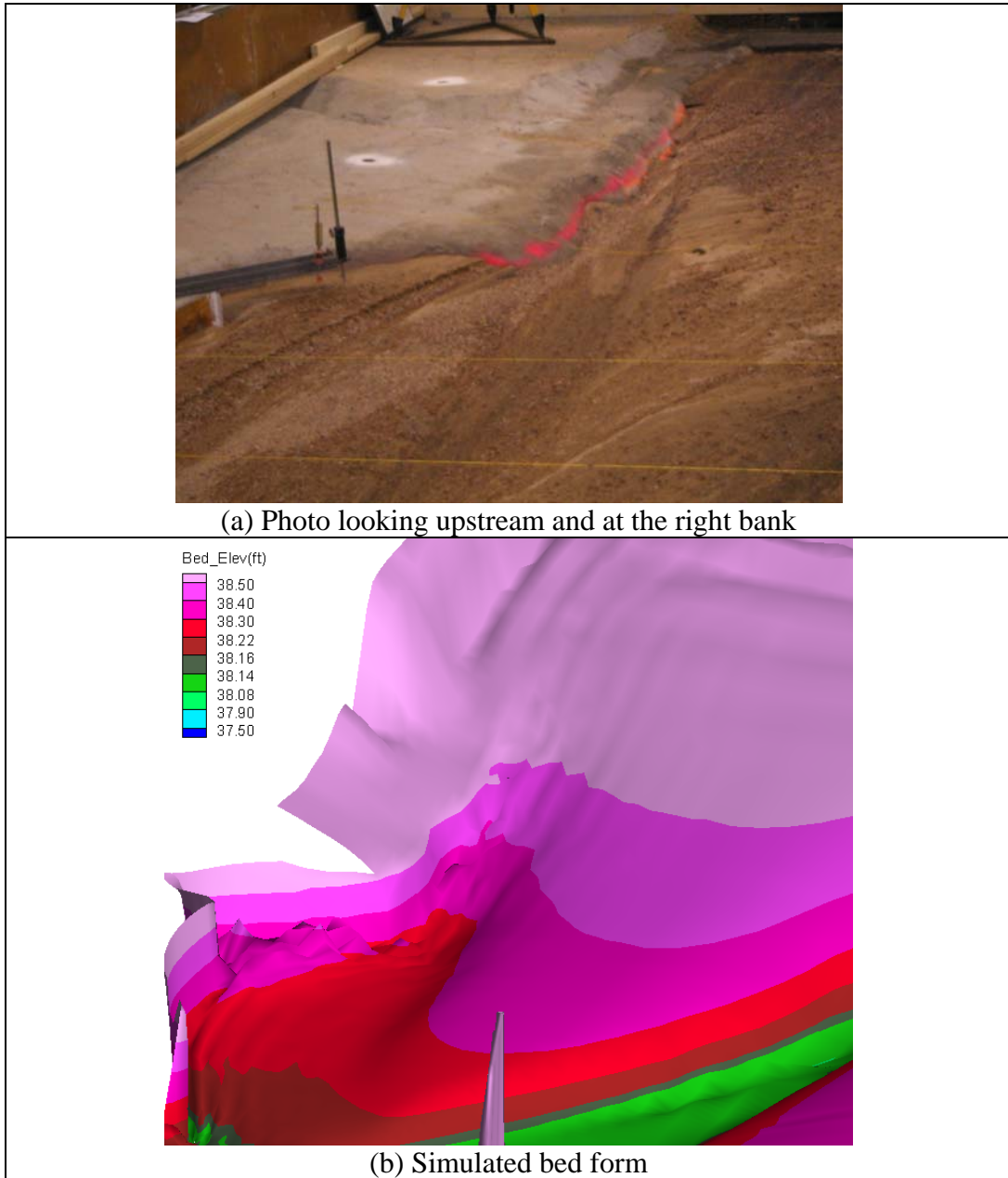


Figure 25. Comparison of bed topography near the right bank between the physical and numerical models for PM-SED-EX-98 at the end of the hydrograph (8 hours)

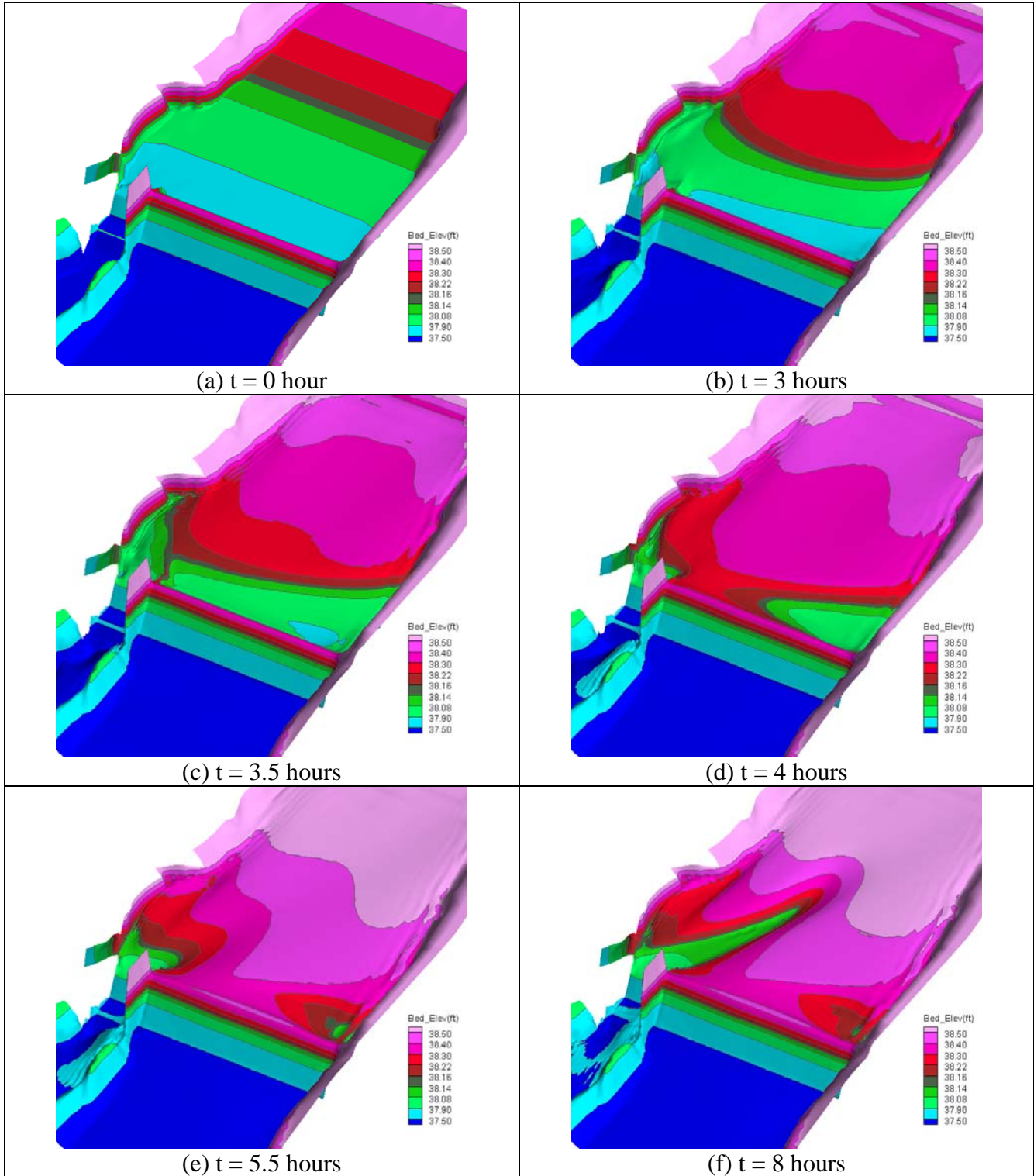


Figure 26. Simulated bed form evolution with time for case PM-SED-EX-98 (1:4 vertical distortion)

5.4. Mobile-Bed Simulation with the Right HFB

The right high flow bypass (RHFB) scenario was simulated with both the 1991 and 1998 hydrographs, and the two cases are labeled as PM-SED-RHFB-91 and PM-SED-RHFB-98. The mesh generated for the scenario is shown in Figure 27. The bathymetry of the initial bed is displayed in Figure 28. The RHFB mesh has a total of 13,513 combined quadrilateral and triangular cells.

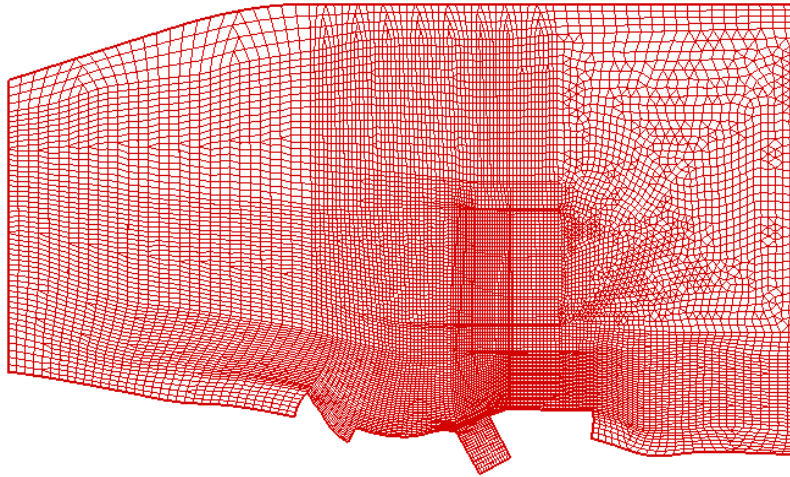


Figure 27. Mesh used for the RHFB scenario for the mobile-bed simulation of the physical model cases

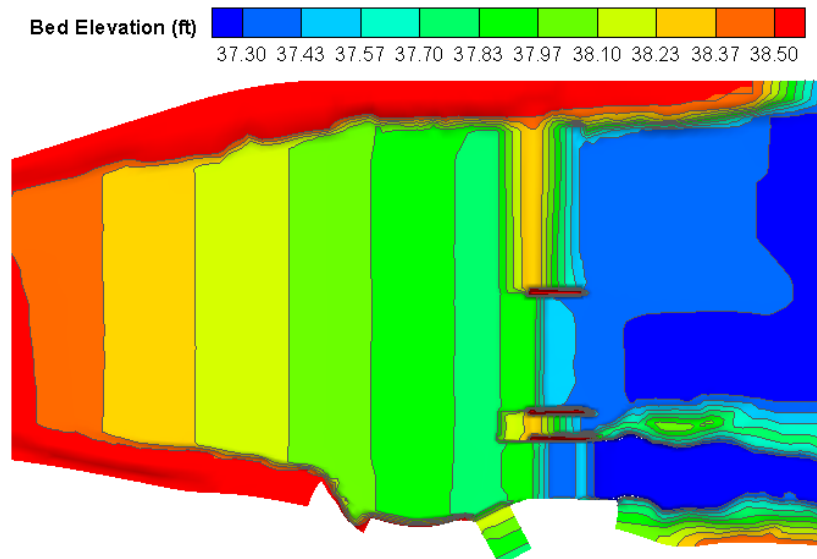


Figure 28. Bed elevation of the RHFB scenario for the mobile-bed simulation of the physical model cases

The gate operation was prescribed as follows. The diversion canal gates were open all the time with a flow capacity of 0.2795 cfs (500 cfs in the prototype). The high flow bypass has four gates and were numbered as 5 to 8 from right to left (looking downstream). The four HFB gates were divided into two groups: 5 and 8 gates as one group and 6 and 7 as another. The two gates within each group were operated the same way but each group may be operated independently. For case PM-SED-RHFB-91 (1991 hydrograph), the existing gates were closed all the time and the flow capacity for gates 5/8 and gates 6/7 were as shown in Figure 29. For case PM-SED-RHFB-98 (1998 hydrograph), gate operation of the existing gates and the HFB gates were specified as in Figure 30. The gate operation used by the numerical models followed the physical model tests as closely as possible. However, the operation during the falling limb of the hydrograph was not documented and there might be unknown differences between the physical model and numerical model.

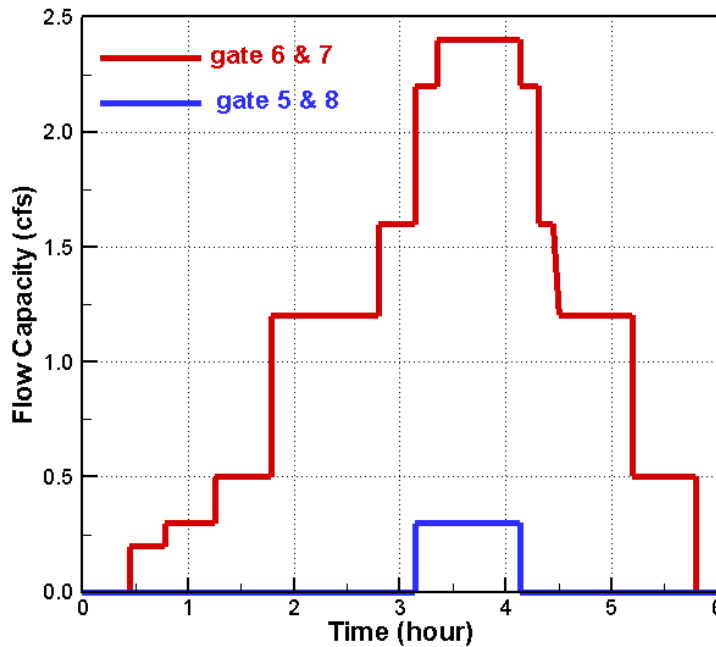


Figure 29. Gate operation capacity of the high flow bypass gates for the right HFB scenario for case PM-SED-RHFB-91 (1991 hydrograph)

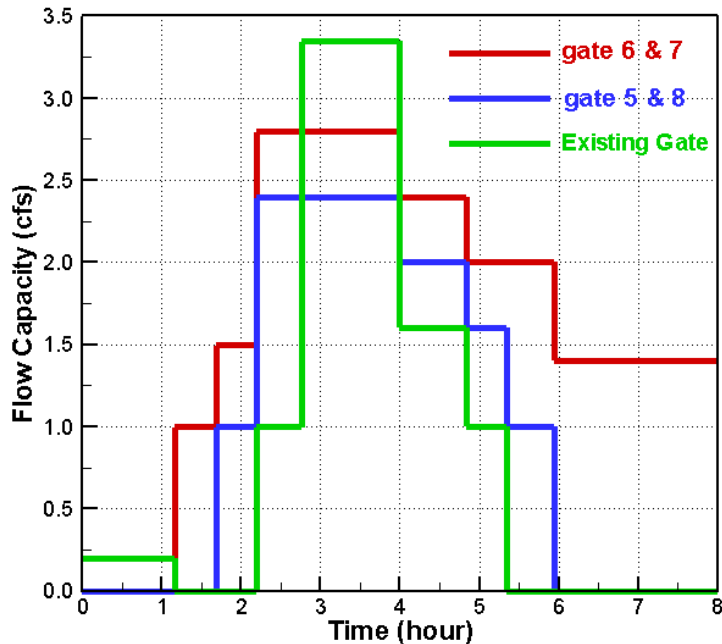


Figure 30. Gate operation capacity of the existing gates and the HFB gates for the right HFB scenario for case PM-SED-RHFB-98 (1998 hydrograph)

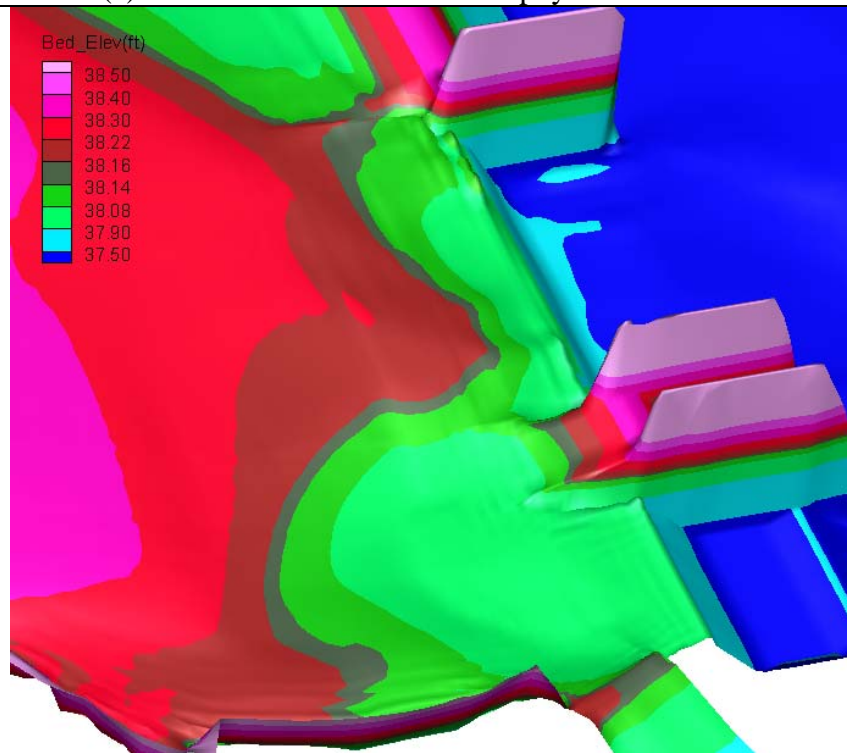
For case PM-SED-RHFB-91 (1991 hydrograph), the bed topography between the simulated and physical model results is compared in Figure 31 and Figure 32 at the end of the hydrograph (6 hours). The simulated bed form evolution in time is plotted in Figure 33.

The simulated final bed form is qualitatively in agreement with the physical model test. Particularly, the delta front reached the high flow bypass first for both the numerical and physical models. The main discrepancy was in the area upstream of the exiting gates. As discussed before it may be due to the difference in the gate operation during the falling limb of the hydrograph. The numerical model assumed that the existing gates were completely closed but non-negligible flow leaking was present at the existing gates during the physical model test.

Both models showed that the sediment delta has not reached the diversion canal gates. The result points to a decreased likelihood of bed load sediments being transported into the diversion canal.



(a) Photo taken at the end of the physical model test

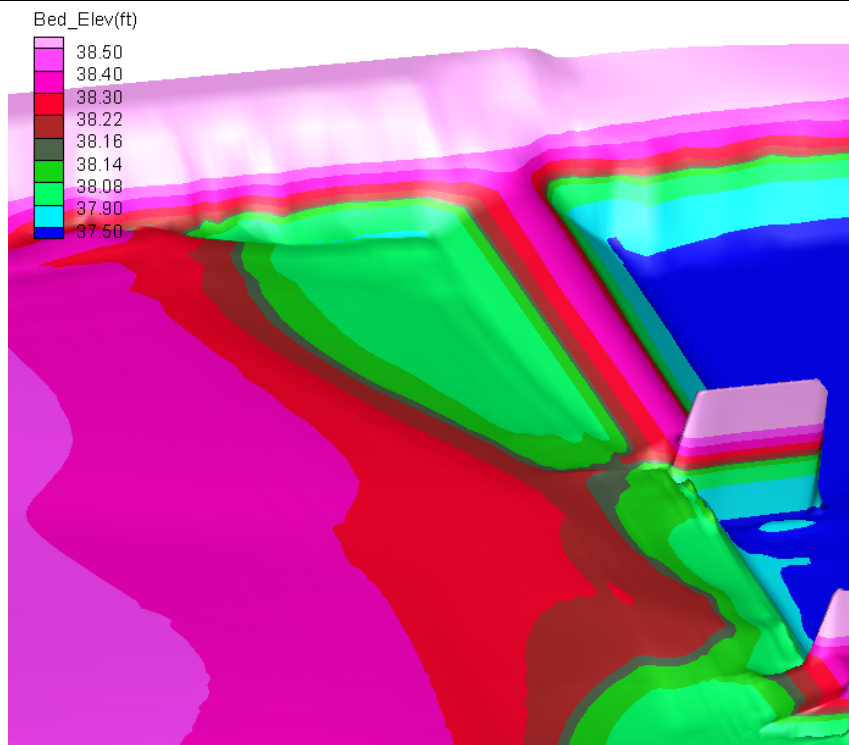


(b) Simulated bed elevation

Figure 31. Comparison of bed topography at the end of the hydrograph (6 hours) between the physical and numerical models for PM-SED-RHFB-91



(a) Photo taken at the end of the physical model test



(b) Simulated bed elevation

Figure 32. Comparison of bed topography at the end of the hydrograph (6 hours) between the physical and numerical models PM-SED-RHFB-91

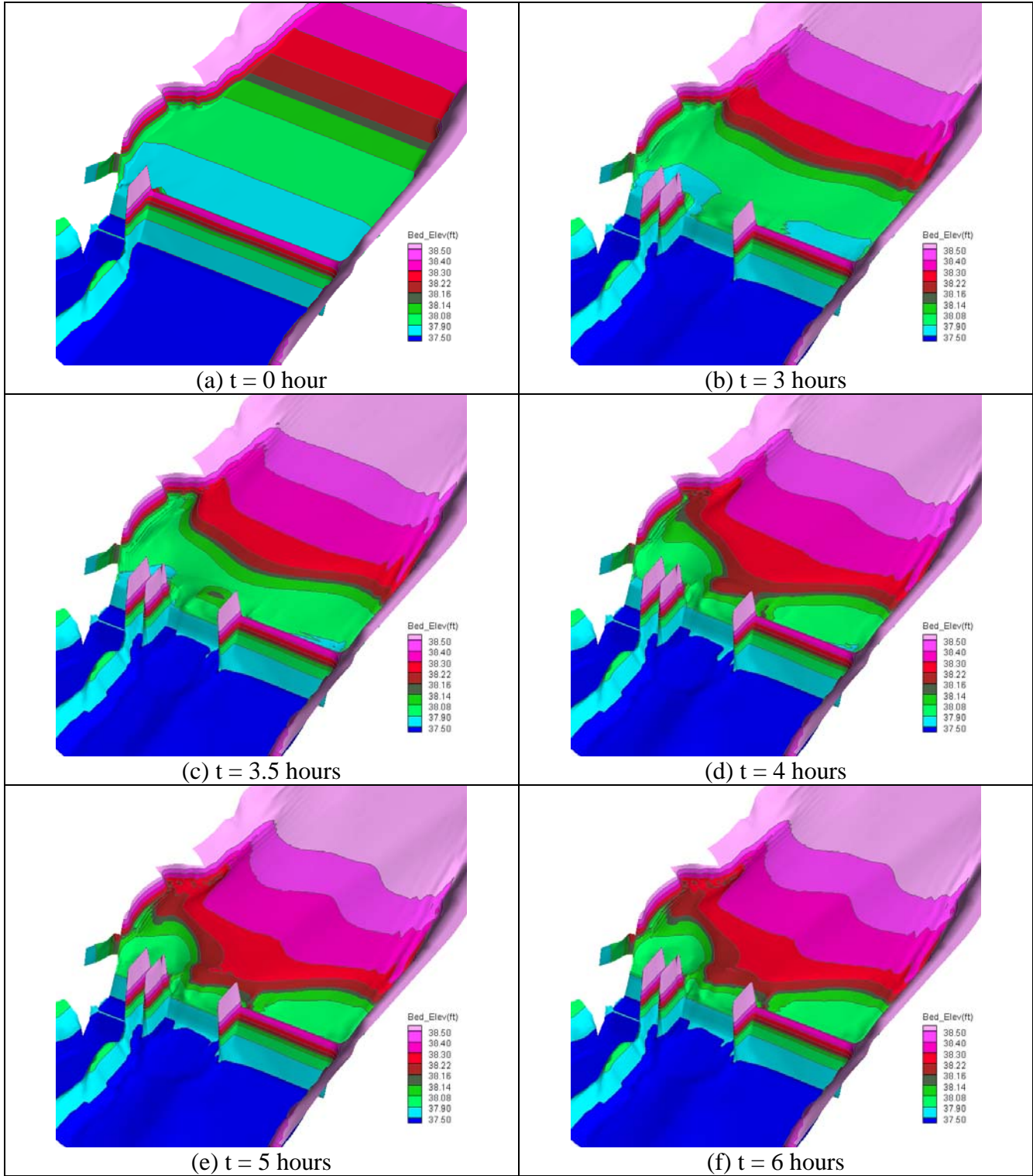


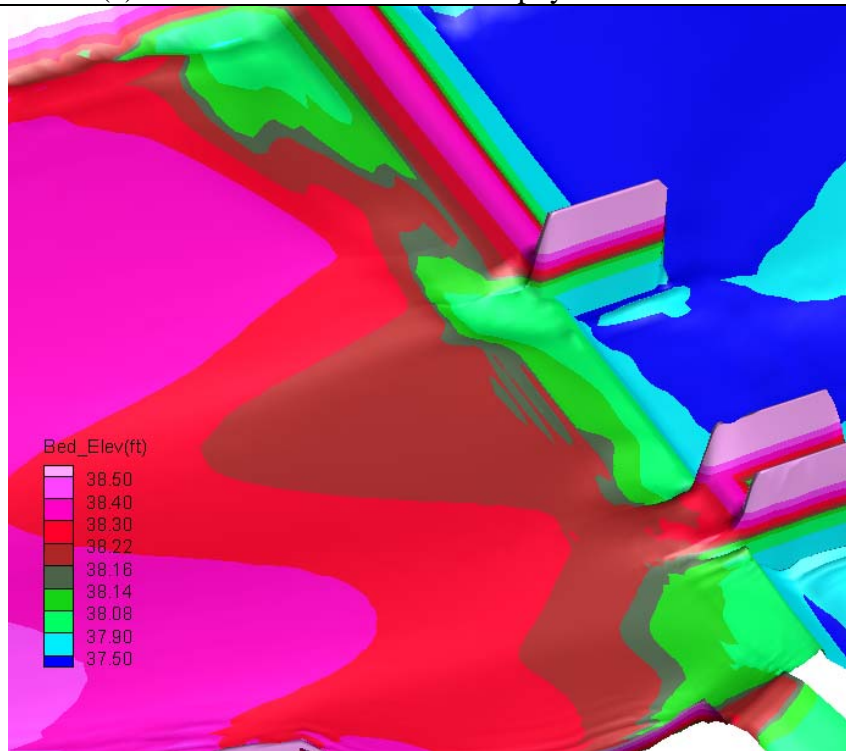
Figure 33. Simulated bed form evolution in time for case PM-SED-RHFB-91 (1:4 vertical distortion)

For case PM-SED-RHFB-98 (1998 hydrograph), the bed topography between the physical and numerical model results is compared in Figure 34 at the end of the hydrograph (8 hours). The simulated bed form evolution in time is plotted in Figure 35.

It is seen that the model results were in qualitative agreement with the physical model results. The sediment delta has reached both the high flow bypass gates and the existing gates. However, the elevation of the delta was relatively low in comparison with the sill elevation of the diversion canal. Therefore, it can be concluded that there is much less likely that the bed load sediments will be transported to the diversion canal under the RHFB scenario. Both the PM-SED-RHFB-91 and PM-SED-RHFB-98 cases have much less deposition in front of the canal gates than the existing condition scenario.



(a) Photo taken at the end of the physical model test



(b) Simulated bed elevation

Figure 34. Comparison of bed topography at the end of the hydrograph (8 hours) between the physical and numerical models for PM-SED-RHFB-98

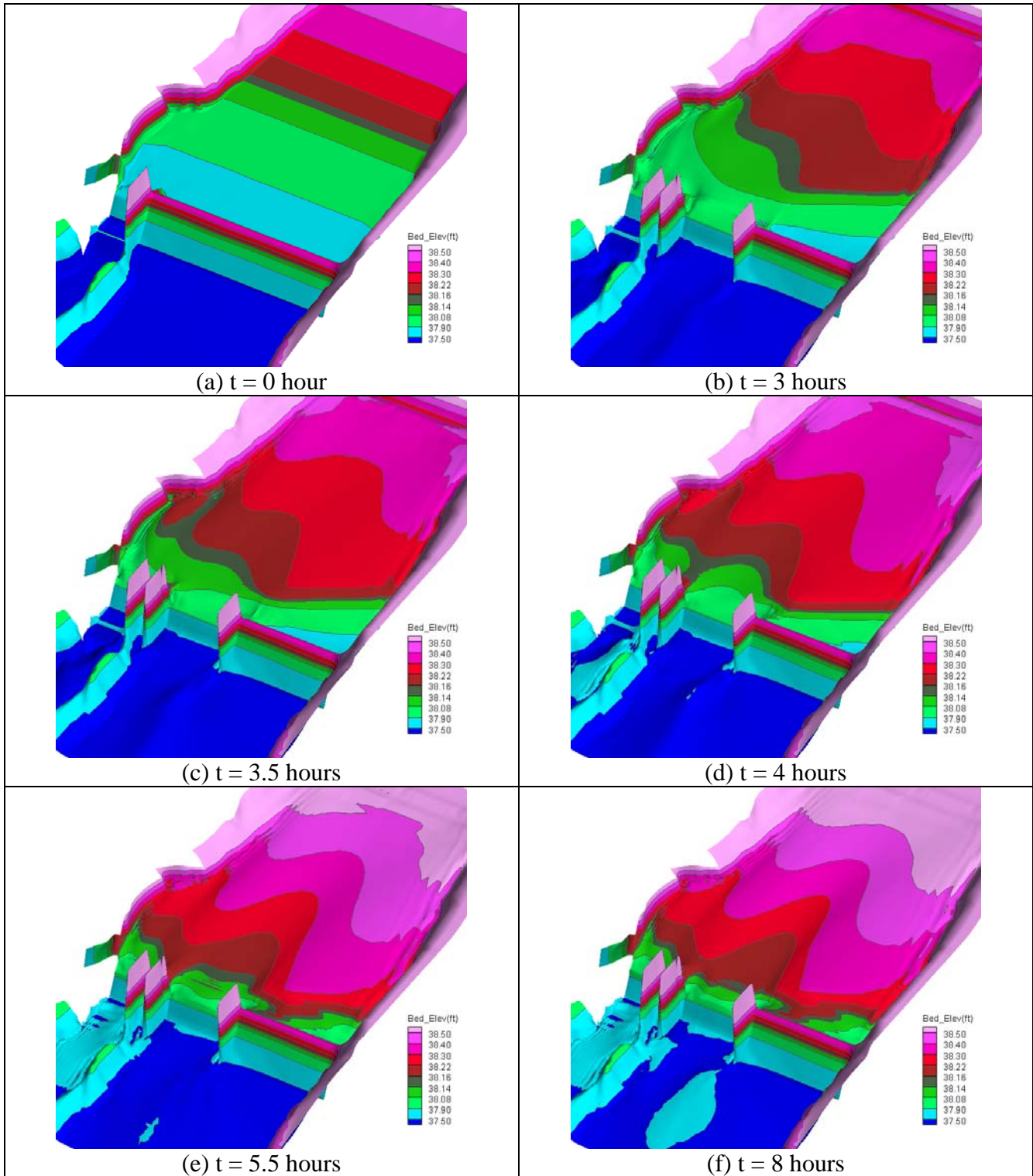


Figure 35. Simulated bed form evolution in time for case PM-SED-RHFB-98 (1:4 vertical distortion)

5.5. Sediment Results with the Left HFB Gate

The left high flow bypass (LHFB) scenario was simulated with both the 1991 and 1998 hydrographs and results are reported in this section. The mesh generated for the scenario is shown in Figure 36. The bathymetry of the initial bed is displayed in Figure 37. The LHFB mesh has a total of 14,417 combined quadrilateral and triangular cells.

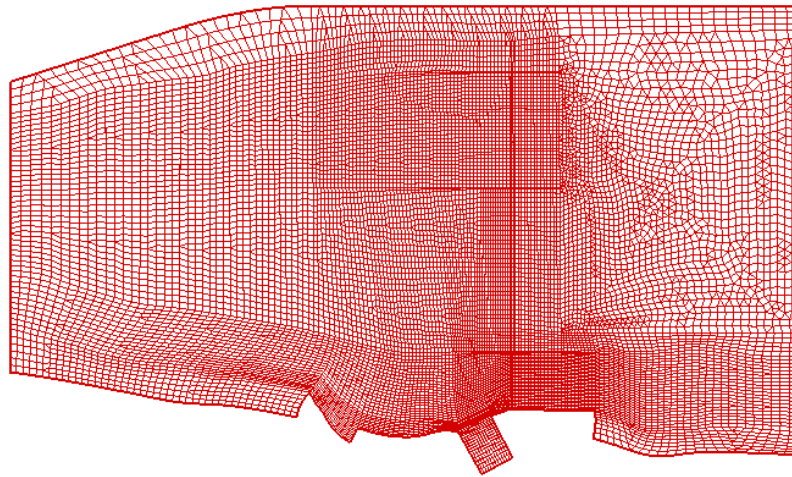


Figure 36. Mesh used for the LHFB scenario mobile-bed simulation of the physical model cases

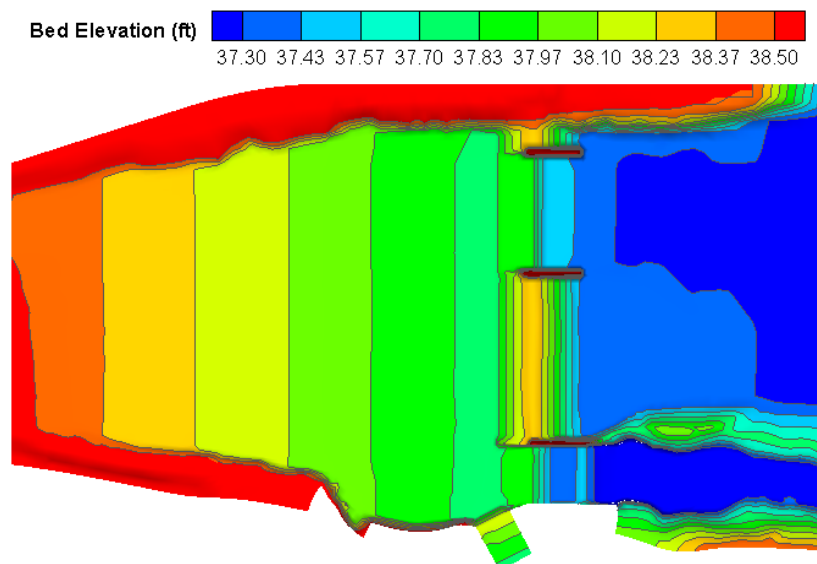


Figure 37. Bed elevation of the LHFB scenario for the mobile-bed simulation of the physical model cases

Two cases were simulated using the 1991 hydrograph and the 1998 hydrograph, and they are labeled as PM-SED-LHFB-91 and PM-SED-LHFB-98, respectively. The diversion canal gates were open all the time with a flow capacity of 0.2795 cfs (500 cfs in the prototype). For case PM-SED-LHFB-91 (1991 hydrograph), the existing gates were always open with a capacity of 0.25 cfs; the flow capacity for gates 5 and 8 and gates 6 and 7 are shown in Figure 38. For case PM-SED-LHFB-98 (1998 hydrograph), gate operation of the existing gates and the HFB gates are specified as in Figure 39. The gate operation used by the numerical model followed the physical model tests as closely as possible; but again, the operation during the falling limb of the hydrograph was not documented and was estimated.

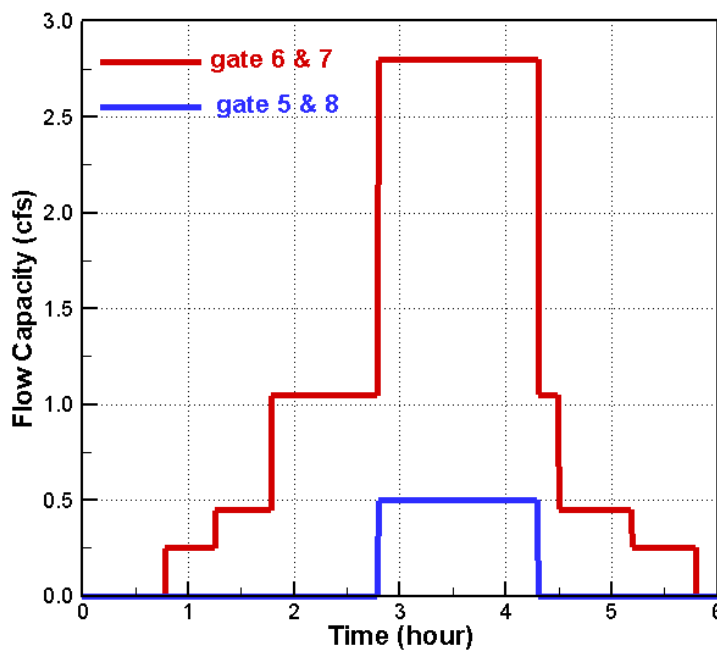


Figure 38. Gate operation capacity of the high flow bypass gates for case PM-SED-LHFB-91 (1991 hydrograph)

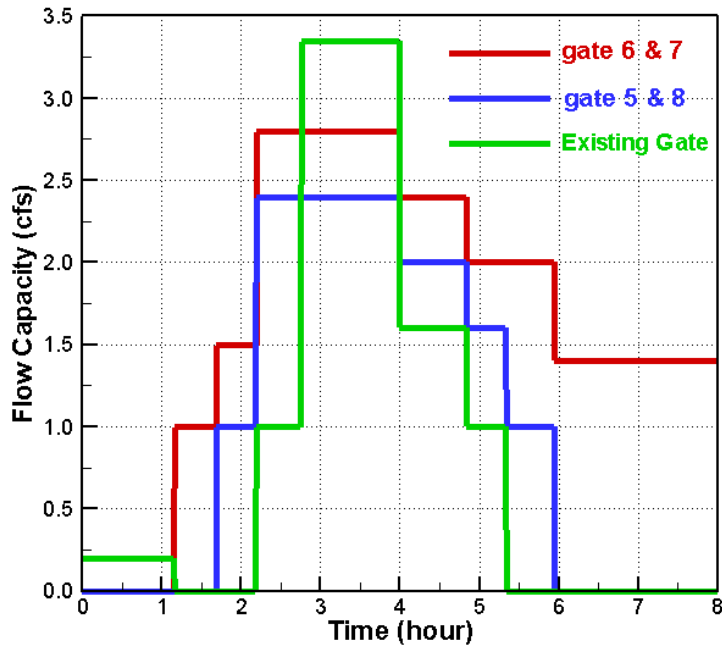


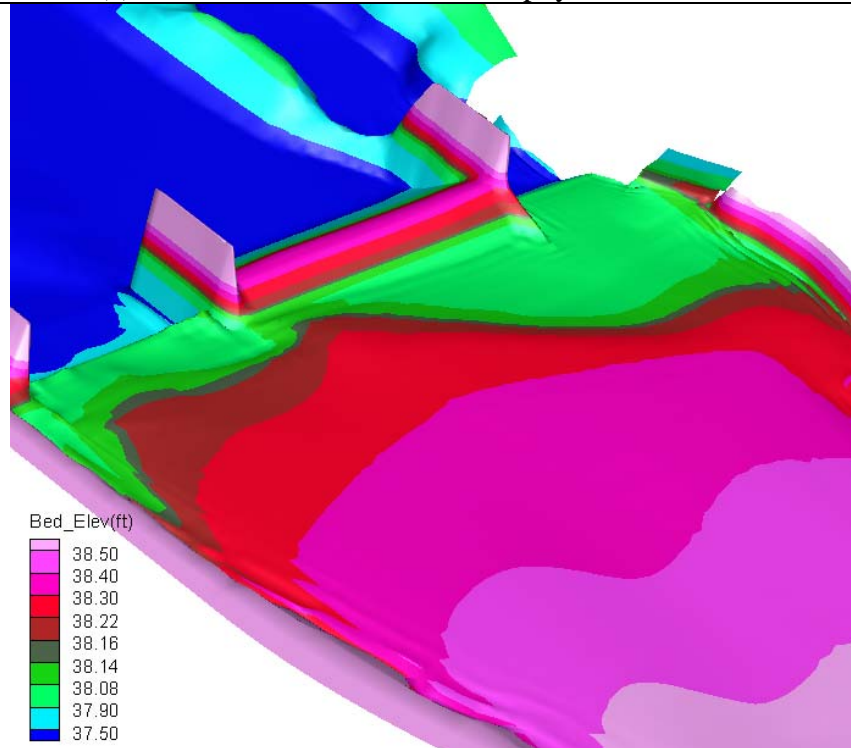
Figure 39. Gate operation capacity of the existing gates and the HFB gates for case PM-SED-LHFB-98 (1998 hydrograph)

For case PM-SED-LHFB-91 (1991 hydrograph), the bed topography between the physical and numerical model results is compared in Figure 40 at the end of the flow hydrograph (6 hours). The simulated bed form evolution in time is plotted in Figure 41.

The simulated final bed form is qualitatively in agreement with the physical model test. Both the numerical and physical models predicted that the delta front reached the high flow bypass on the left bank first, and front shape of the delta was in agreement with each other. It is seen that the delta did not reach the area in front of the diversion canal. The result points to a decreased likelihood of bed load sediments being transported into the canal.



(a) Photo taken at the end of the physical model test



(b) Simulated bed elevation

Figure 40. Comparison of bed topography at the end of the hydrograph (6 hours) between the physical and numerical models for PM-SED-LHFB-91

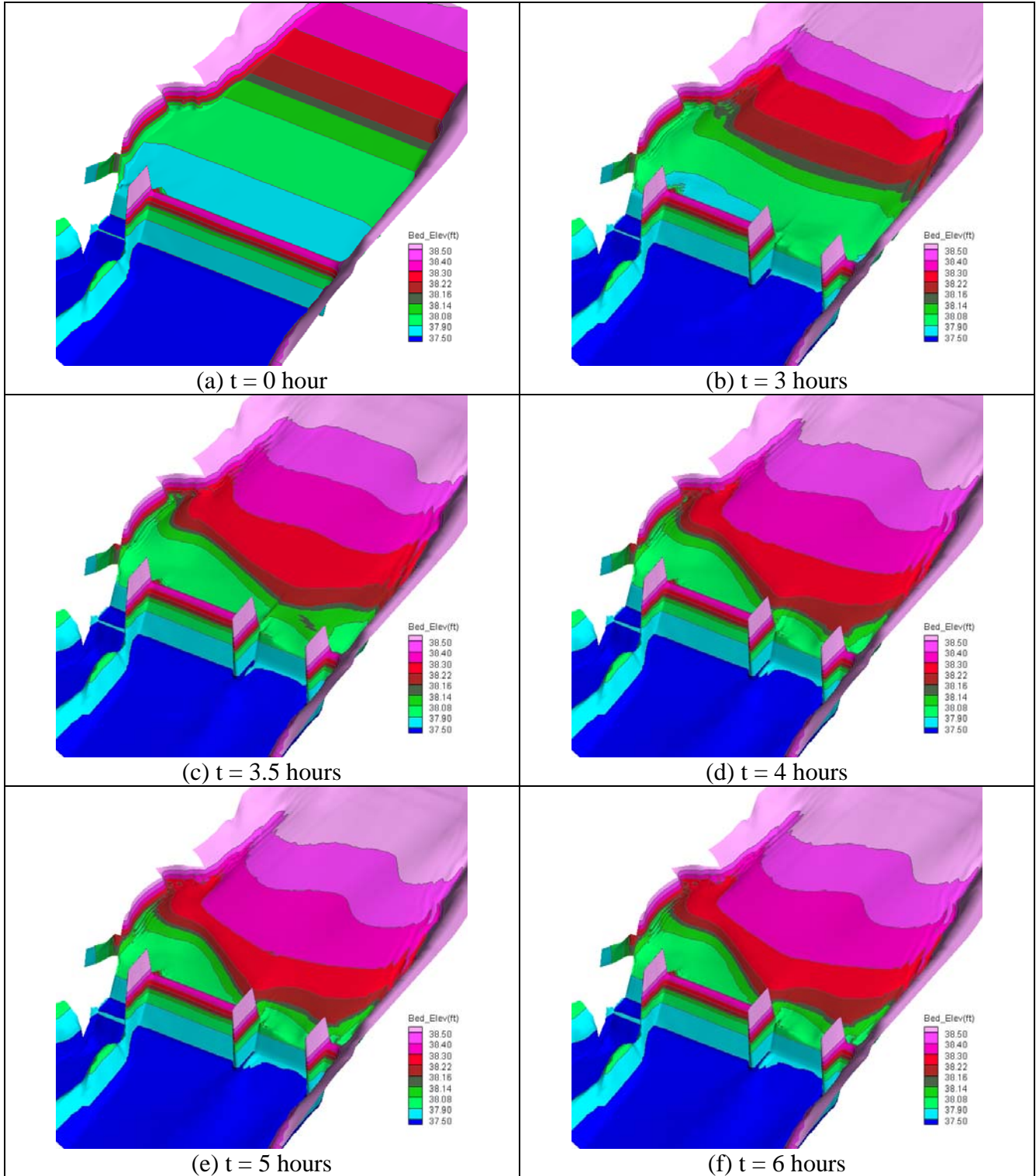


Figure 41. Simulated bed evolution in time for case PM-SED-LHFB-91 (1:4 vertical distortion)

For case PM-SED-LHFB-98 (1998 hydrograph), the bed topography between the physical and numerical models is compared in Figure 42 at the end of the flow hydrograph (8 hours). The simulated bed form evolution in time is plotted in Figure 43.

It is seen that the model results were in qualitative agreement with the physical model results. The delta has reached both the high flow bypass gates and the existing gates.

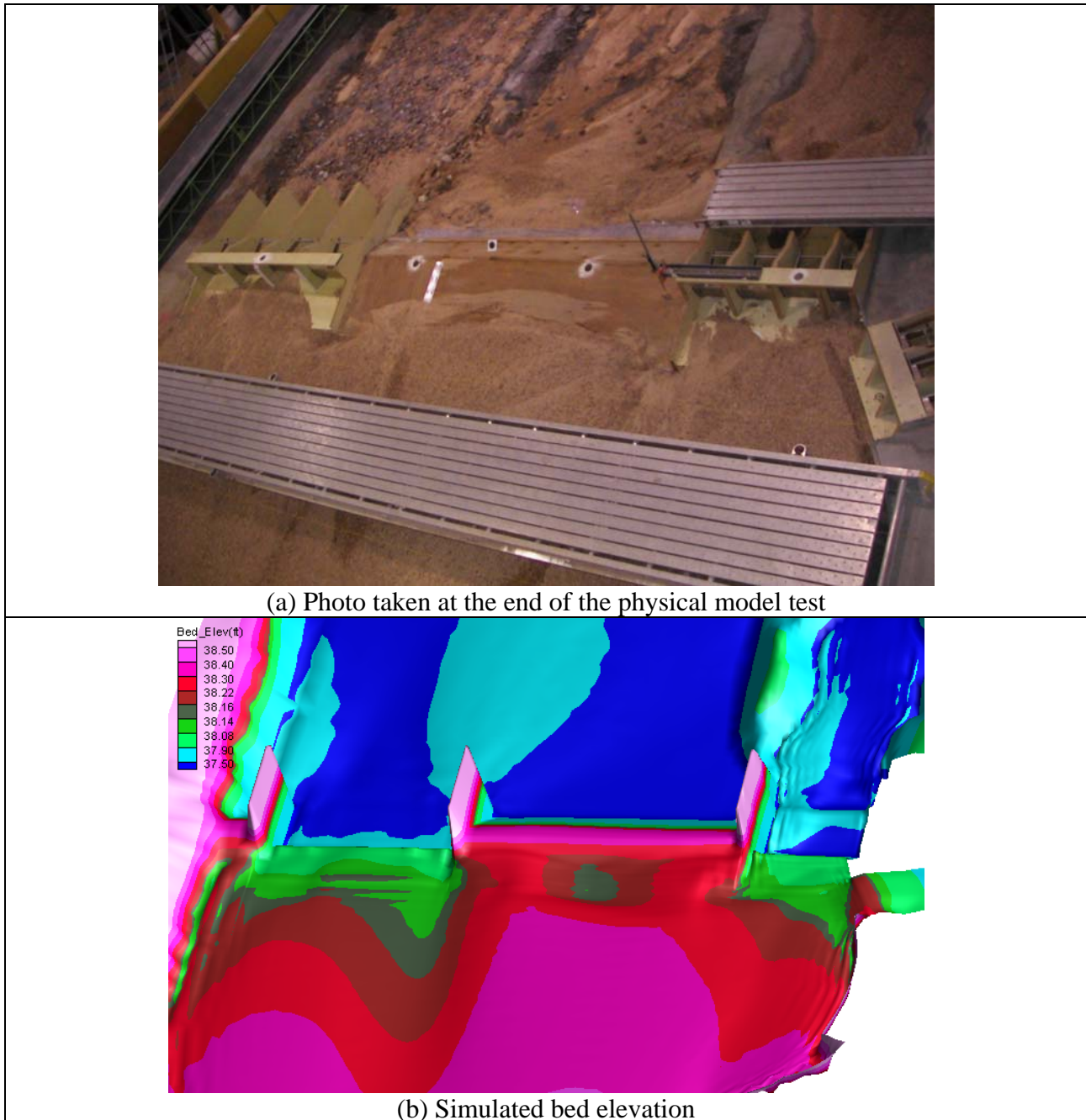


Figure 42. Comparison of bed topography at the end of hydrograph (8 hours) between the physical and numerical models for PM-SED-LHFB-98

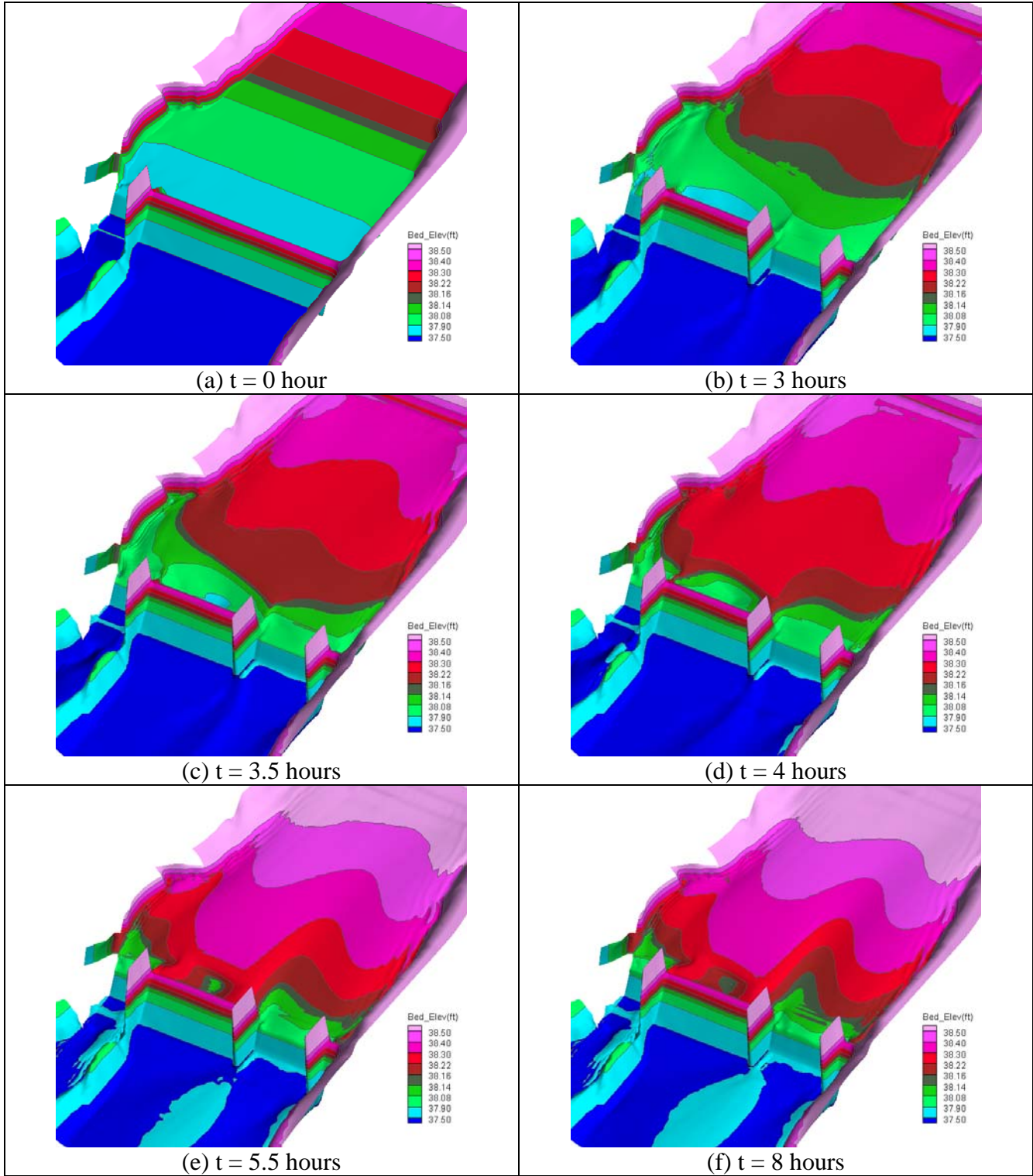


Figure 43. Simulated bed evolution in time for case PM-SED-LHFB-98 (1:4 vertical distortion)

6.0 Field Model Scenarios

Modeling of field scenarios consisted of two categories: the calibration study with the field flows and the mobile bed simulations. In this Chapter, the calibration results were presented first and the field model results are then discussed.

6.1. Calibration with Field Flow Cases

Two field flow simulations were performed and compared with the available flow data. They served as the calibration study to ensure the adequacy of the numerical model and the selection of the Manning's roughness coefficient. One simulation was carried out for the 12,400 cfs flood which occurred in 2005 (7,400 cfs was from Matilija Creek and 5,000 cfs was from North Fork). High water marks were surveyed in 2005 after the flood and two high water mark survey points were located within the solution domain. The second calibration simulation was carried out for the 100 year flood (27,100 cfs) so that a comparison may be made with the previous 1D models. The results of the two cases are reported below.

6.1.1. 2005 Flood Flow

In 2005 a flood with a peak flow of about 12,400 cfs occurred, and this flow was simulated with the SRH-2D model. A constant flow discharge of 12,400 cfs was imposed at the upstream boundary while the water surface elevation at the downstream boundary, cross-section RM 12.7841, was 663.2 ft based on the 1D model result. Also, the flow through the existing gate at the Robles diversion dam was calculated to be 8,540 cfs if the flow through the gate was assumed to be fully open channel flow (versus pressurized flow). It is known that the design capacity of the existing gates is about 7,000 cfs, and the above open channel gate flow assumption cannot be right. Therefore, special boundary treatment was applied at the gate so that only 7,000 cfs was allowed to pass through the gates. In addition, it was assumed that 500 cfs was diverted into the canal upstream of the gate which leaves 11,900 cfs to be passed downstream.

A comparison of the simulated water surface elevation and surveyed high water marks at two survey points is shown in Table 6. The difference between the simulation and survey is 0.22 ft and 0.36 ft, respectively, for the two survey points. It is seen that the numerical model compares well with the surveyed data.

Table 6. Comparison of simulated and surveyed water elevation at two points

High Water Mark Point	Northing Coordinate (ft)	Easting Coordinate (ft)	Surveyed Elevation (feet)	Simulated Elevation (feet)
#1	1991570.69	6172432.59	724.04	724.26
#2	1991939.71	6172523.82	728.82	729.18

6.1.2. 100 Year Flood

The model was next applied to compute the 100 year flood. A discharge of 27,100 cfs was imposed at the upstream boundary, and a water surface elevation of 665.2 ft, from the 1D model, was applied at the downstream exit boundary. Similarly, 7,000 cfs was passing through the existing gate at the Robles diversion dam and 500 cfs was diverted to the canal. The simulated water surface elevation along the main channel thalweg is compared with the HEC-RAS model in Figure 44. Note that the water surface elevation from the HEC-RAS model is the cross section averaged value.

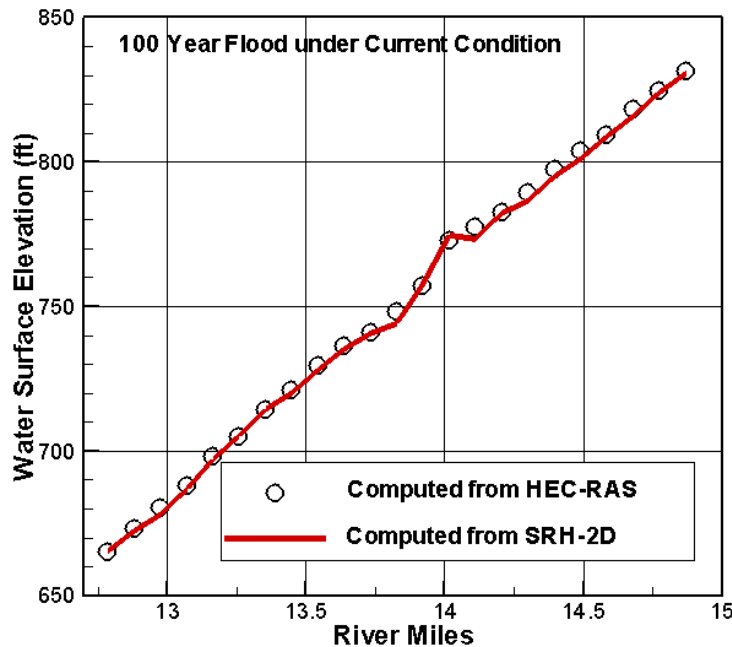


Figure 44. Comparison of the water surface elevation (WSE) from SRH-2D and HEC-RAS; SRH-2D represents the WSE along the channel thalweg, and HEC-RAS is cross section averaged WSE.

6.2. Flow Simulation Results at Other Discharges

Three more flow discharges, 24,000 cfs, 15,000 cfs, and 6,000 cfs, were simulated to provide the flow data for the physical model portion of the project. Major parameters are summarized in Table 7. Note that 500 cfs was diverted to the canal for all three cases.

Table 7. Flow parameters for the three simulations

Discharge (cfs)	24,000	15,000	6,000
WSE at exit (ft)	664.80	663.70	661.65
Flow at the existing gate (cfs)	7,000	7,000	5,381

Simulated results are shown from Figure 45 to Figure 50.

Figure 45 and Figure 47 display the simulated water depth near the Robles diversion dam, Figure 48 and Figure 49 show the predicted water surface elevation at two cross sections: 14.2045 RM and 13.9205 RM, and the velocity distribution is plotted in Figure 50 for three flows. All these results were used to decide the boundary conditions for the physical model study.

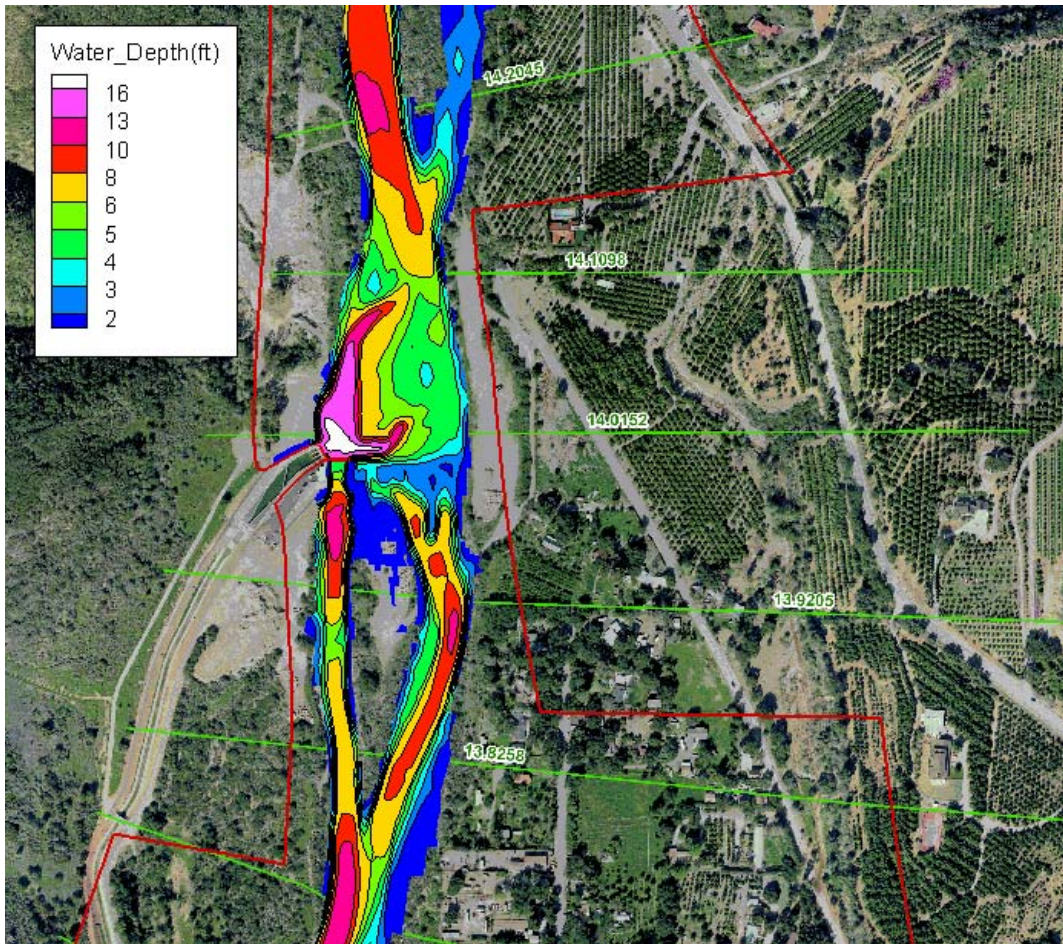


Figure 45. Simulated water depth for the 24,000 cfs flow discharge in the Robles dam area.

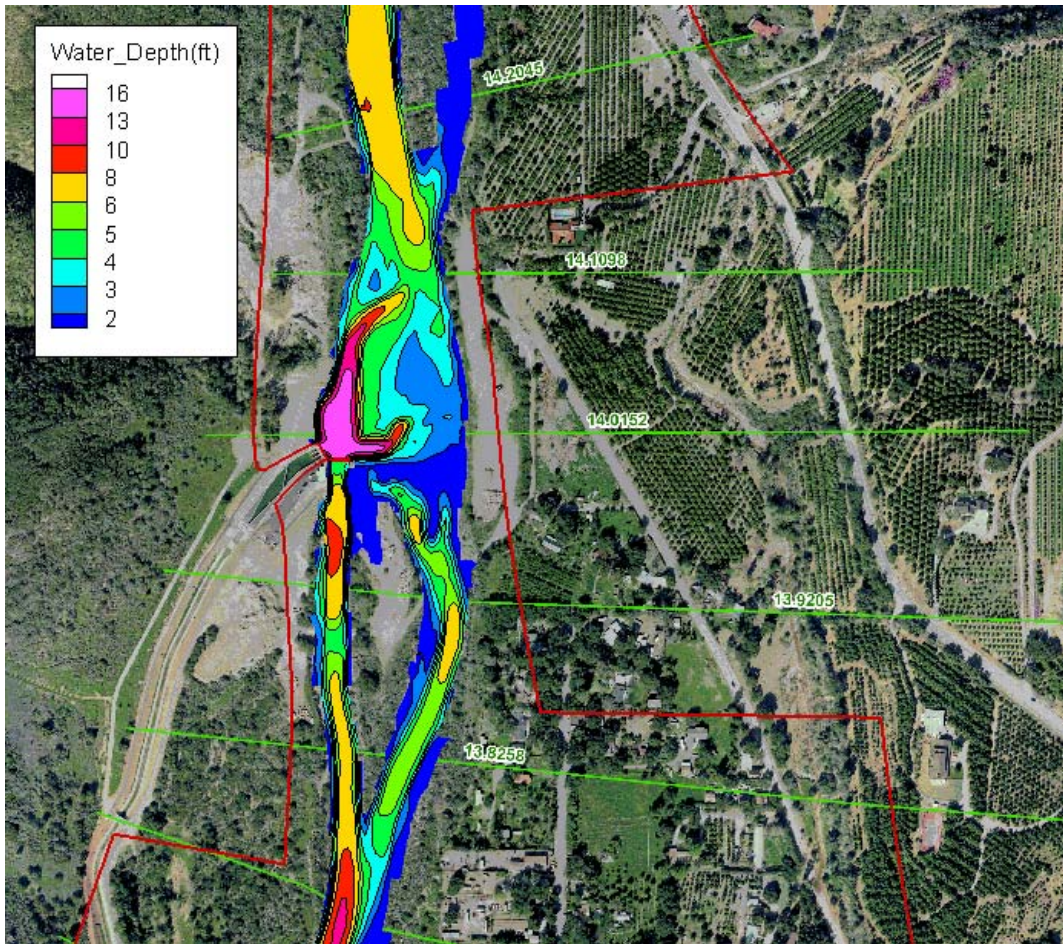


Figure 46. Simulated water depth for the 15,000 cfs flow discharge in the Robles dam area.

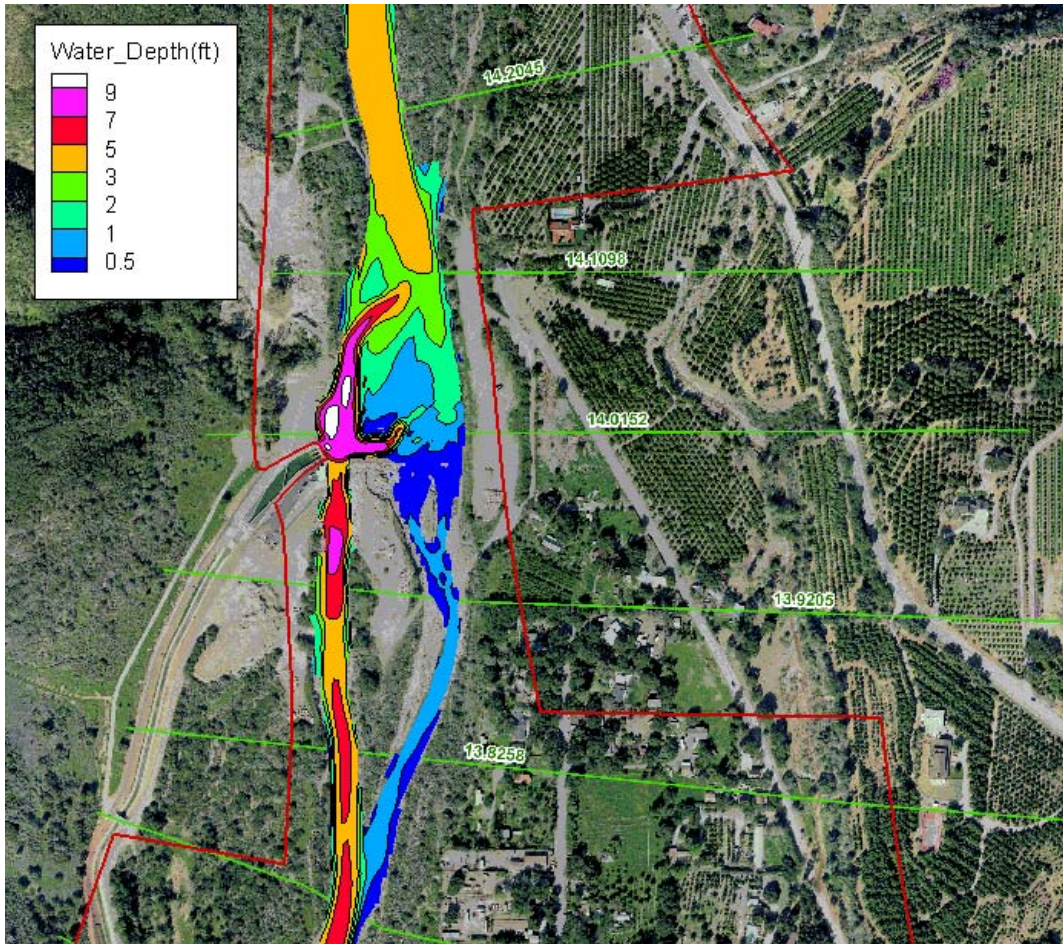


Figure 47. Simulated water depth for the 6,000 cfs flow discharge in the Robles dam area.

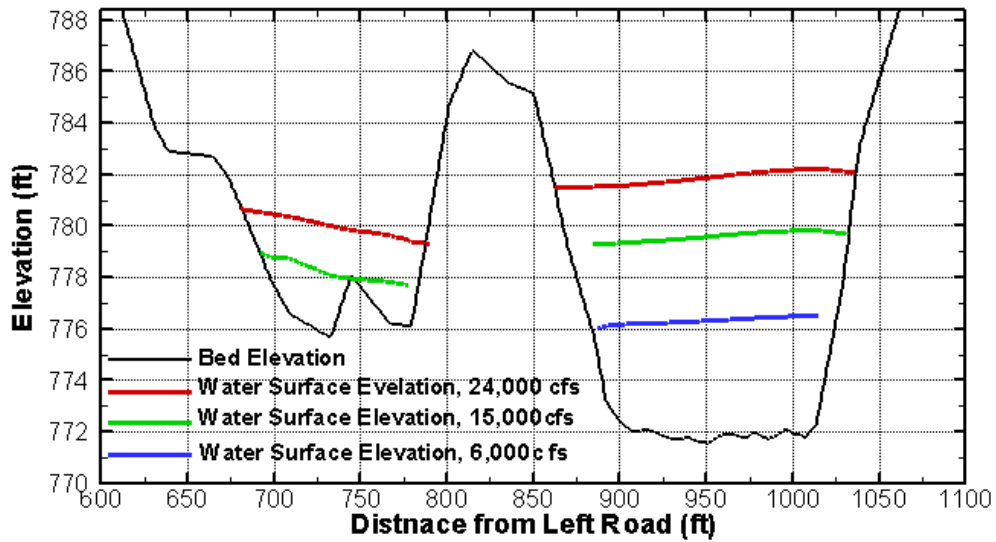


Figure 48. Simulated water surface elevation at cross section 14.2045 for three discharges; Distance is measured from the middle of road on the left side of the river (looking downstream).

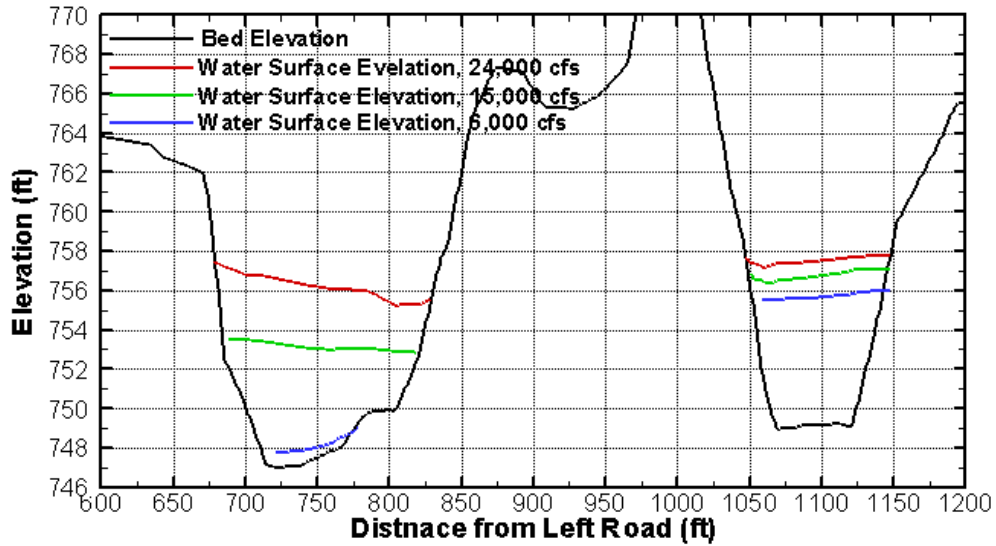


Figure 49. Simulated water surface elevation at cross section 13.9205 for three discharges; Distance is measured from the middle of road on the left side of the river (looking downstream).

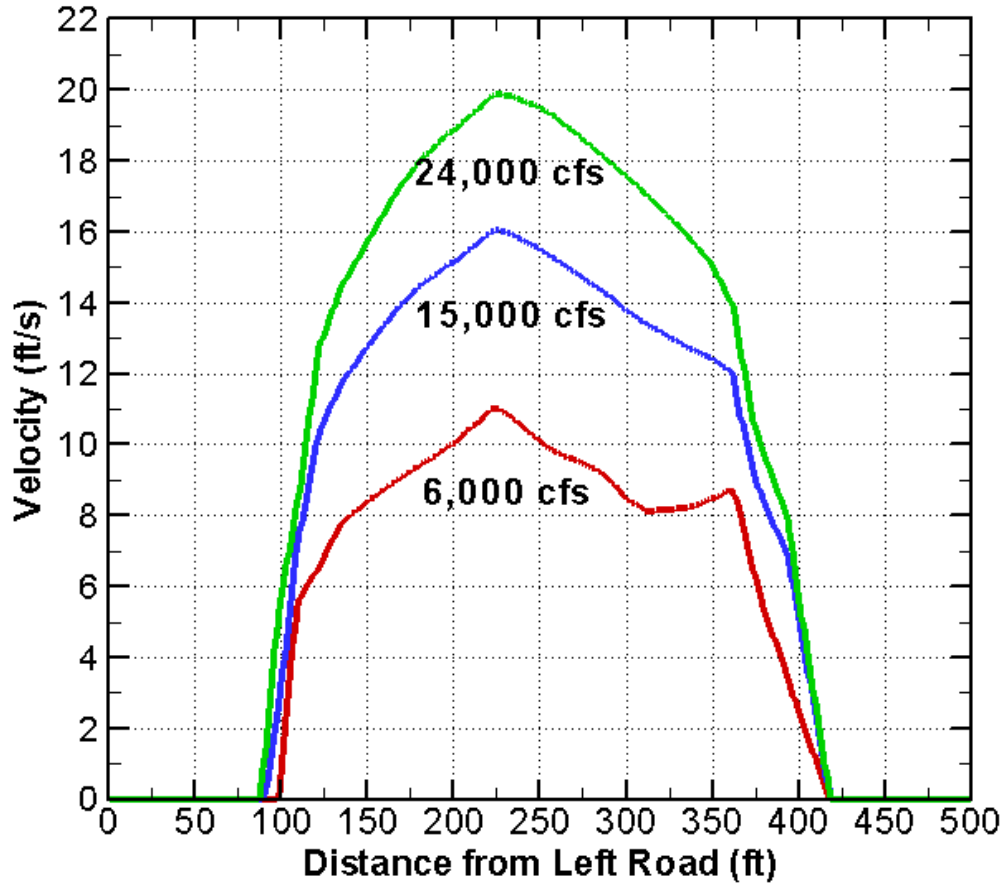


Figure 50. Computed velocity distribution at cross section 14.1089 RM.

6.3. Mobile-Bed Model Inputs

Three topographic scenarios, the existing, the right high flow bypass (RHFB), and the left high flow bypass (LHFB) were modeled. For each scenario, two flow hydrographs, 1991 and 1998 hydrographs as discussed in Chapter 3, were used. There were also two inlet sediment load conditions: before-dam and after-dam removal (see discussion in Chapter 3). Most simulations were carried out for the after-dam removal sediment input and a few used the before-dam removal sediment input.

The topography was based on the March 2005 LiDAR data as discussed in Chapter 3. For the mobile-bed simulations, the bathymetry upstream of the Robles diversion weir was modified through “excavation” since the 2005 survey showed that the dam was almost filled upstream of the weir. This way the simulation

would reveal how the area upstream of the dam would be filled again after excavation.

The excavation was performed as follows. An area between the weir and the cross section RM 14.1098, shown in Figure 51 as a red box, was excavated to create a constant slope. At the face of the weir, approximately 10 feet of material was removed in order to make the elevation equal to 757.8 ft, the sill elevation of the existing radial gate. If the bed elevation at the cross section RM 14.1098 remains the same, a constant slope of about 1.6% was created. The total excavated sediment volume was estimated to be about 20,000 cubic yards excluding the voids and 33,000 cubic yards including the voids. Periodic excavation at the Robles Diversion was performed after a major flood and a record of the sediment removal was tabulated in the report of Greimann (2004) and was reproduced in Table 8.

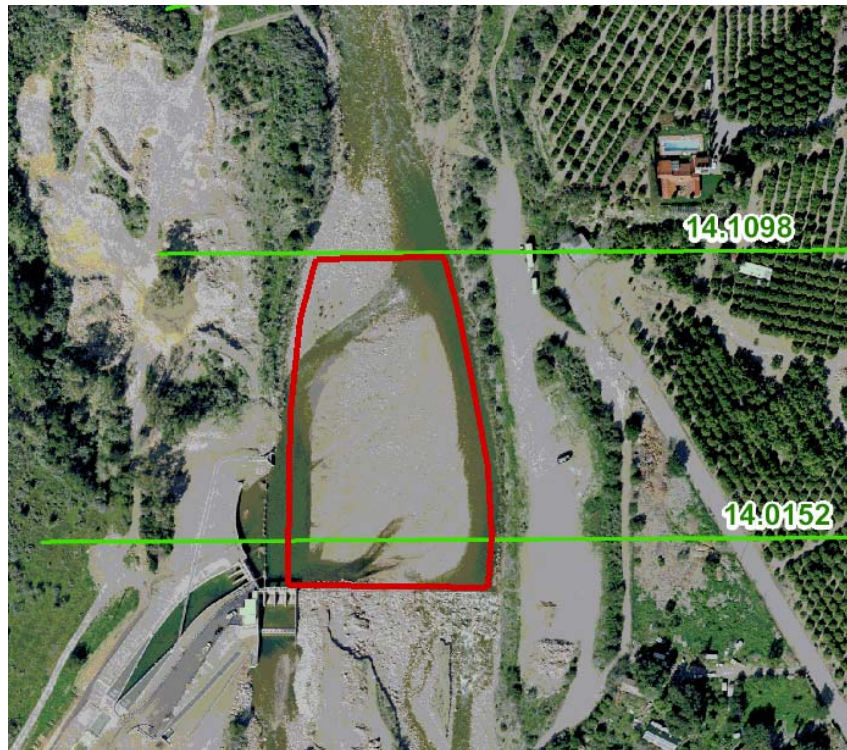


Figure 51. Excavation area, shown in red box, for the mobile-bed simulation

Three topographic scenarios were developed using the excavated bathymetry and they are compared in Figure 52. Some characteristic bed elevations are as follows: the sill elevation at the existing gate is 757.8 ft; the sill elevation of the canal diversion gate is 762.7 ft; the top elevation of the weir is about 767.5 ft; the width of the high flow bypass is 131.25 ft. Note that the geometry did not include the small features added later such as the fish way, etc.

Three corresponding meshes are displayed in Figure 53 and only the portion of the mesh near the Robles dam is shown. The total number of hybrid quadrilateral and triangular mesh cells is 12,184, 13,373, and 14,050 cells, respectively for the existing, RHFB, and LHFB scenarios.

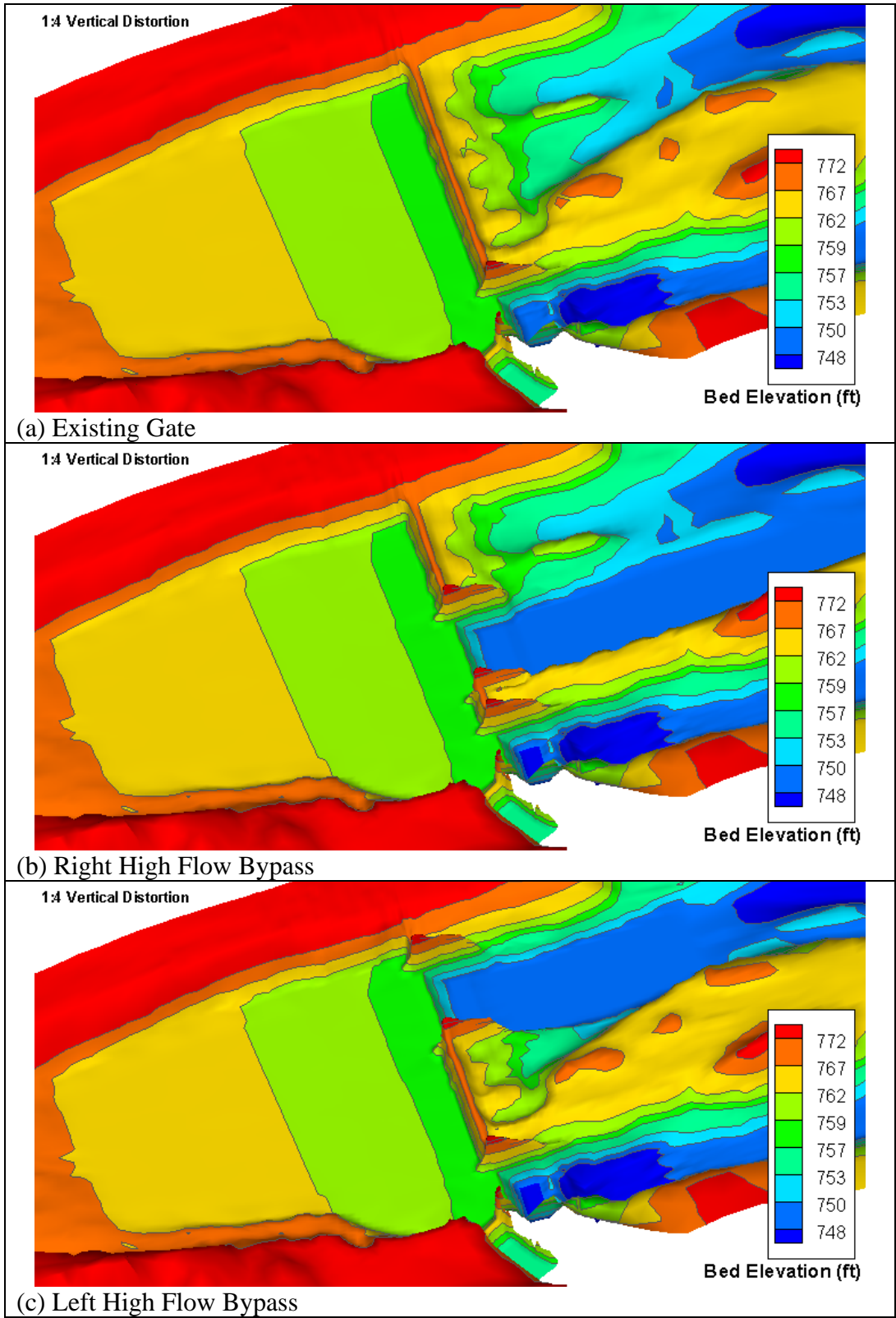


Figure 52. Perspective view of the three topographic scenarios

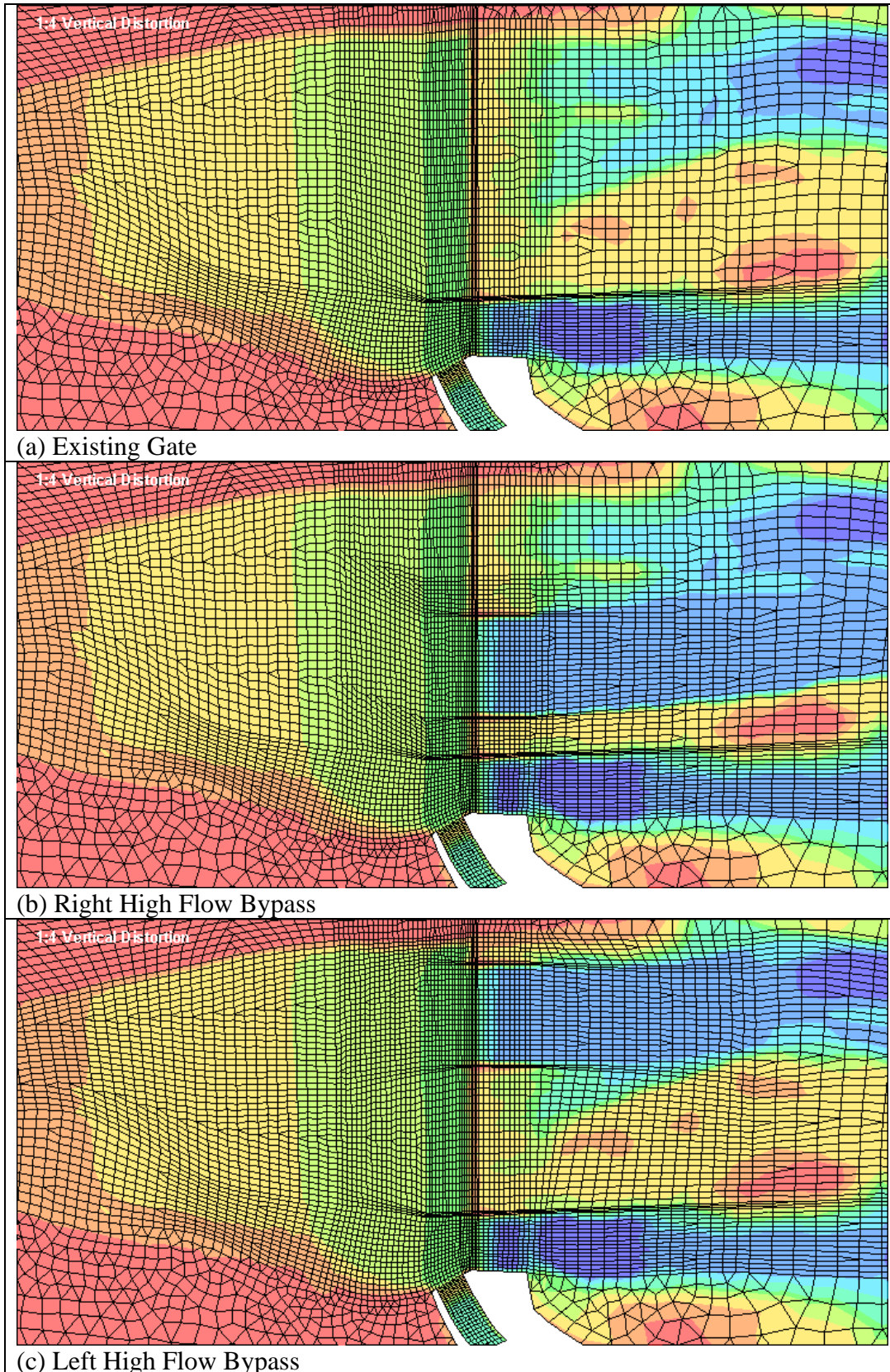


Figure 53. Zoom-in view of the meshes for the three topographical scenarios

Gate operation needs to be specified for both the existing radial gates and the new high flow bypass gates (HFB). For the field modeling reported below, gate operation was incorporated by specifying the flow capacity (the maximum discharge allowed) for each gate structure. If the actual flow through the gate structure is below the capacity, regular open channel flow is assumed; but if the flow is above the capacity, it is limited to the capacity and the pressurized flow is assumed. Figure 54 shows the capacity used for the existing gates under the existing condition and the high flow bypass (HFB) scenarios and the capacity for the HFB gates.

Under the existing condition scenario, the operation of the existing gates is different for the two hydrographs. With the 1991 hydrograph, the gates were open to a capacity of 100 cfs for the first 64.5 hours and were fully open (6,000 cfs capacity) afterwards. With the 1998 hydrograph, the existing gates were open to a capacity of 200 cfs for the first 27.5 hours. They were fully open (6,000 cfs capacity) from 27.5 to 80.0 hours. After 80 hours, the gate capacity was gradually reduced. The capacity remained at 300 cfs from 160 to 200 hours. The existing gate capacity for the existing condition scenario is shown in Figure 54.

Under the high flow bypass (HFB) scenarios, the same gate operations were used for the 1991 and 1998 hydrographs. The existing gates were closed except for the period of 55.7 to 65 hours during which the capacity was set at 6,000 cfs. The high flow bypass (HFB) gates started to open at 27 hours with a capacity of 600 cfs. HFB gates were fully open from 52.3 to 91 hours with a capacity of 10,000 cfs and back to 600 cfs capacity from 91 to 200 hours.

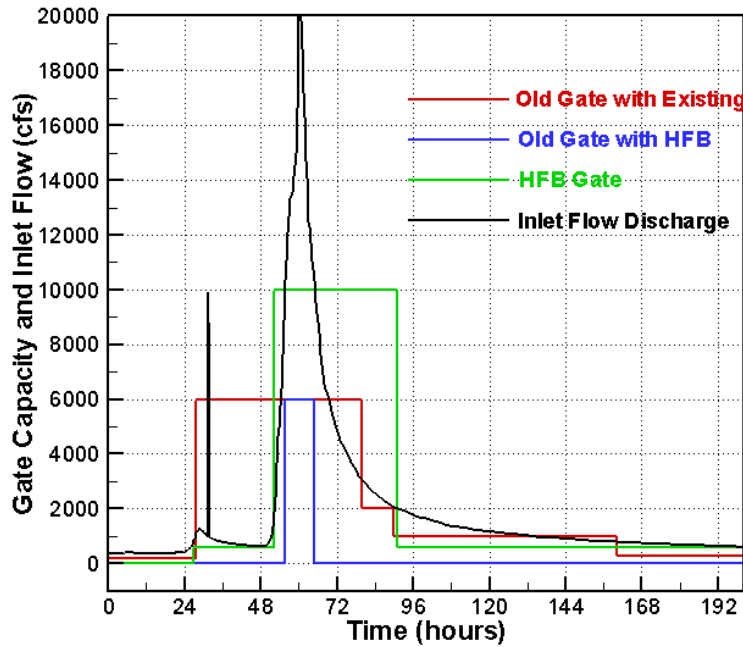


Figure 54. Gate capacity versus time for the existing and HFB gates for the field modeling; the 1998 hydrograph is also shown as a reference

6.4. Qualitative Comparison of Results under the Existing Condition

Numerical model results were examined for the existing condition scenario with the before-dam removal sediment inputs. A comparison of the net deposited depth after 200 hours for the 1991 and 1998 hydrographs is shown in Figure 55. Note that the deposition depth reported in this study refers to the sediment depth including the voids (porosity) while the sediment volume reported is without the voids unless it is explicitly stated otherwise.

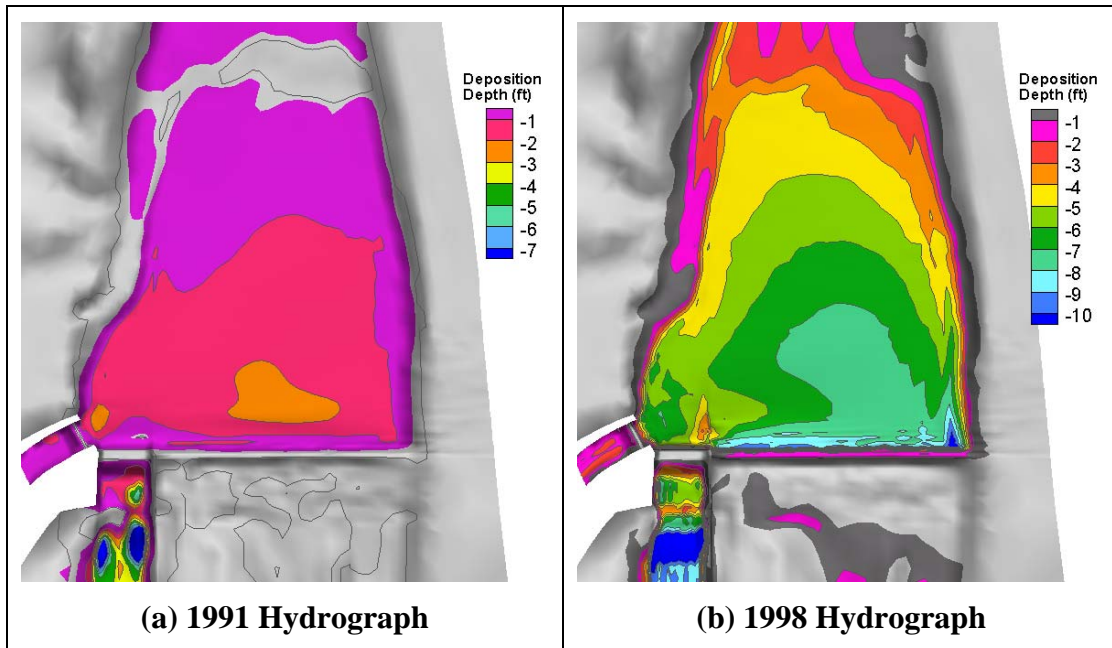


Figure 55. A comparison of the deposition depth after 200 hours between the 1991 hydrograph and 1998 hydrograph for the existing condition with the before-dam removal sediment input

The model predicted that the average deposition depth in front of the diversion weir, after 200 hours, was about 2.0 ft and 7.0 ft, respectively, for the 1991 and 1998 hydrographs. It showed that a flood with the magnitude of 1991 hydrograph would not cause serious sedimentation problem at the diversion canal. However, with the 1998 flood, the deposition in front of the canal gates would be high enough that there would be a risk of bedload sediments being transported into the diversion canal.

With the 1991 hydrograph, it was estimated that a total of 34,190 yd³ of sediments (excluding voids) was moving through the cross section RM 14.1098, and about 4,130 yd³ of sediments were deposited behind the Robles diversion weir. In contrast, with the 1998 hydrograph, about 205,500 yd³ of sediments (excluding voids) were moving through RM 14.1098 and about 21,900 yd³ of sediments were deposited behind the weir.

The model results indicated that a flood similar to the 1998 event (near 15-year flood) would move a majority of the sediments towards the diversion dam and fill the area upstream of the weir almost completely even if excavation had been done before the flood. The result is in agreement with the field observation that significant sediment deposition occurred after each major flood and sediment removal was often necessary. A record of sediment removal from 1966 to 1998 was shown in Table 8 and a total of 419,000 yd³ of sediments (including the voids) was removed in the period from 1966 to 1998. Each removal was about 46,000 yd³ (including the voids) on average. The simulation estimated that sediment deposition between the weir and RM 14.1098 (Figure 51) is 21,900 yd³

without the voids, which is equivalent of 36,500 yd³ with the voids. This amount is in agreement with the recorded sediment removal of 35,000 yd³ in 1998. For 1991, the simulated deposition is about 8,300 yd³ (including the voids) which was much less than the reported removal of 20,000 yd³ in 1991. Several possibilities might contribute to this discrepancy. For one, the modeling assumed that the gate was fully open during the flood which would maximize the sediment sluicing through the gates. Another possibility may be that the reported removal was the result of accumulated sediment depositions for the period of 1987 to 1991.

Table 8. Record of sediment removal at Robles Diversion Dam

Year	Amount of Sediment Removal (yd ³)
1966	30,000
1969	N/A
1973	50,000
1978	91,000
1980	71,000
1983	57,000
1986	30,000
1991	20,000
1993	N/A
1995	35,000
1998	35,000

The simulated flow velocity and topographic pattern for the 1998 hydrograph and before-dam removal scenario are shown in Figure 56 at the end of the flood (200 hours). The results may be compared with the aerial photo which represents typical flow pattern upstream of the Robles Diversion Dam. It is seen that the predicted flow pattern at low flow after major floods is qualitatively in agreement with the field observation.

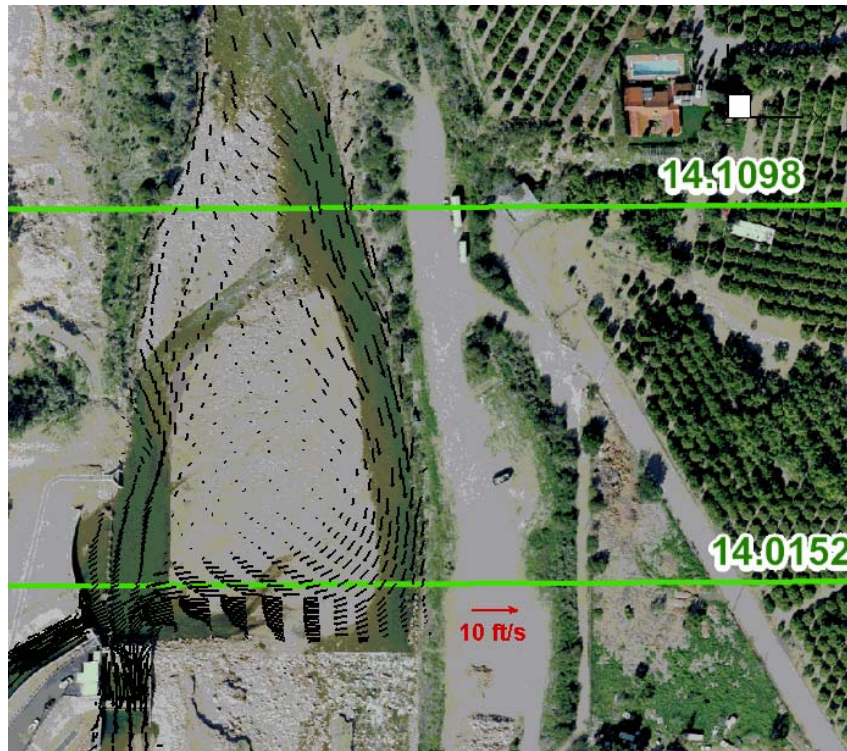


Figure 56. Simulated flow velocity and pattern for the 1998 hydrograph before-dam removal scenario at 200 hours

6.5. Results with the 1991 Hydrograph

The 1991 hydrograph is shown in Figure 3a. It is seen that the flow was relatively low (less than 500 cfs) before hour 60, rose to a maximum of 6,065 cfs at about 78.5 hours, receded below 1,000cfs after 109 hours. Under the after-dam removal scenario (see Figure 4a), the simulated bed elevation evolution in time, along with the net deposited depth, is displayed in Figure 57 and Figure 59 for all three scenarios.

The following observations may be made based on the simulation results:

- (1) No appreciable sediment deposition was observed if the flow was less than 1,000 cfs (e.g., the first 65 hours). The sediments may be mobilized only by flows larger than 1,000 cfs.
- (2) For all scenarios, sediments were accumulated behind the weir quickly. The overall deposition pattern was largely determined during the rising limb of the hydrograph.
- (3) A comparison of the deposition depth after 200 hours between the before- and after-dam removal scenarios is shown in Figure 60 and the simulated bed elevation is in Figure 61. The average deposition depth behind the weir was estimated to be 2.0 ft and 3.5 ft, respectively, for before-dam and after-dam

removal scenarios. The total predicted sediment deposition volume is tabulated in Table 9 for all cases. It is noted that the deposition volume was more than doubled for the existing condition scenario and 1991 hydrograph when the sediment input was changed from before-dam to after-dam. In numerical numbers, about 19,400 yd³ additional sediments (relative to the before-dam) were added to go through the Robles diversion after the dam removal, and 4,640 yd³ additional sediments were accumulated between RM 14.1098 and the weir. It indicates that the existing radial gates are not capable of efficiently moving the additional sediments added after dam removal.

(4) If the high flow bypass (HFB) radial gates are in place, the total sediment deposits between RM 14.1098 and the weir would be reduced by approximately 50% (see Table 9) for the 1991 hydrograph and after-dam removal condition. The average deposition depth near the weir is reduced from 3.5 ft to less than 2.5 ft under the right HFB and 3.0 ft for the left HFB, respectively. It may be concluded that the HFB gates are capable of moving sediments efficiently under the after-dam removal condition.

(5) A comparison between the right and left high flow bypass (HFB) is shown in Figure 62. It is seen that the right HFB appeared to have an advantage over the left HFB. Firstly, the total deposited depth near the weir was lower for the right HFB case (2.5 ft for the right HFB versus 3.0 ft for the left HFB). Secondly, the total sediment volume deposited upstream of the weir is also lower for the right HFB (see Table 9). In addition, more deposition occurred in front of the canal diversion gates for the left HFB scenario.

In summary, model results suggested that there would be no sediment issues for the 1991 hydrograph for all cases simulated except for the existing condition scenario with the after-dam removal sediment input. Under the existing condition, a less severe flood such as the 1991 flood may lead to much deposition upstream of the weir after dam removal.

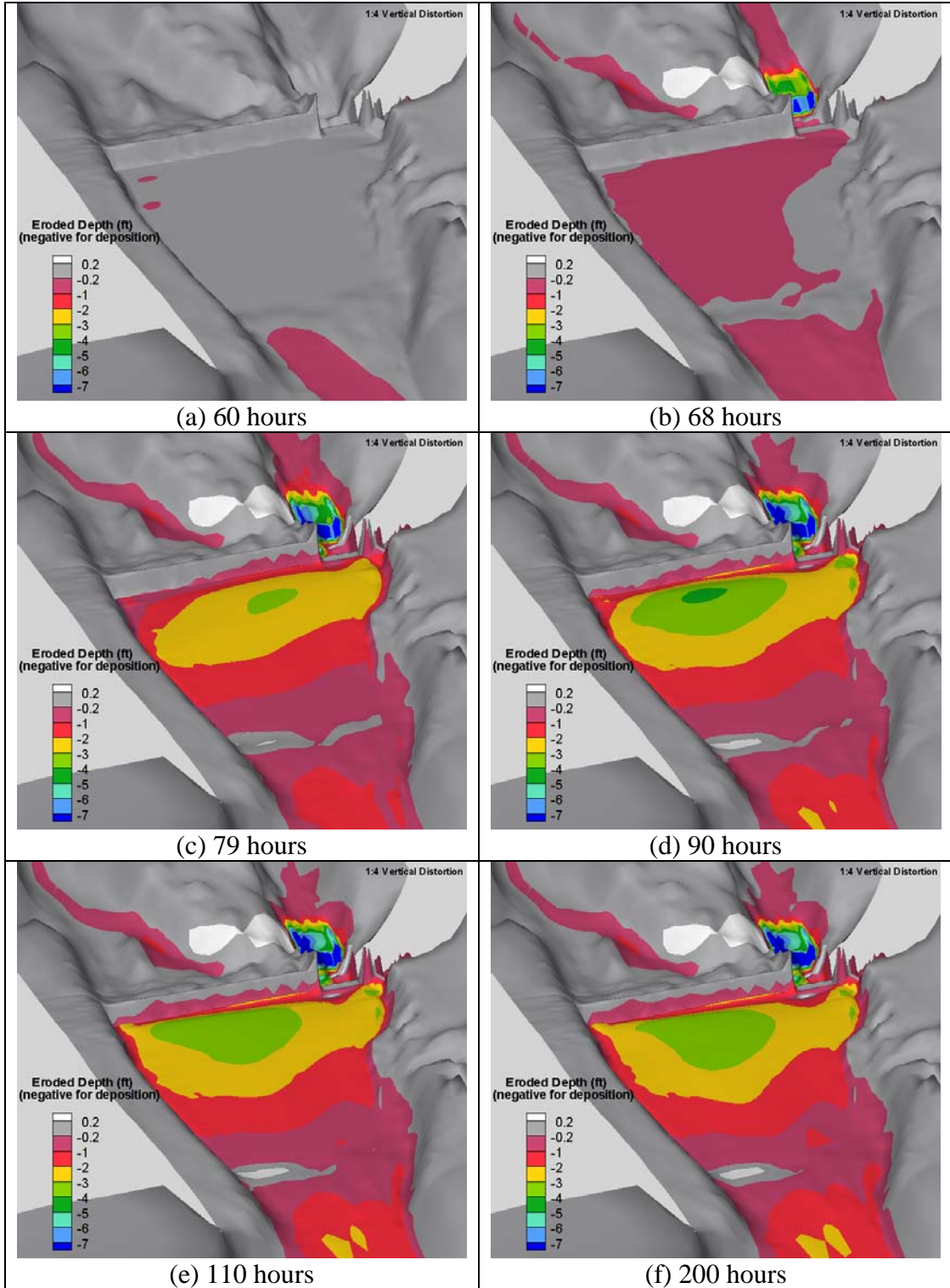


Figure 57. Simulated bed elevation and deposited depth for the existing condition with the 1991 hydrograph and after-dam removal sediment input

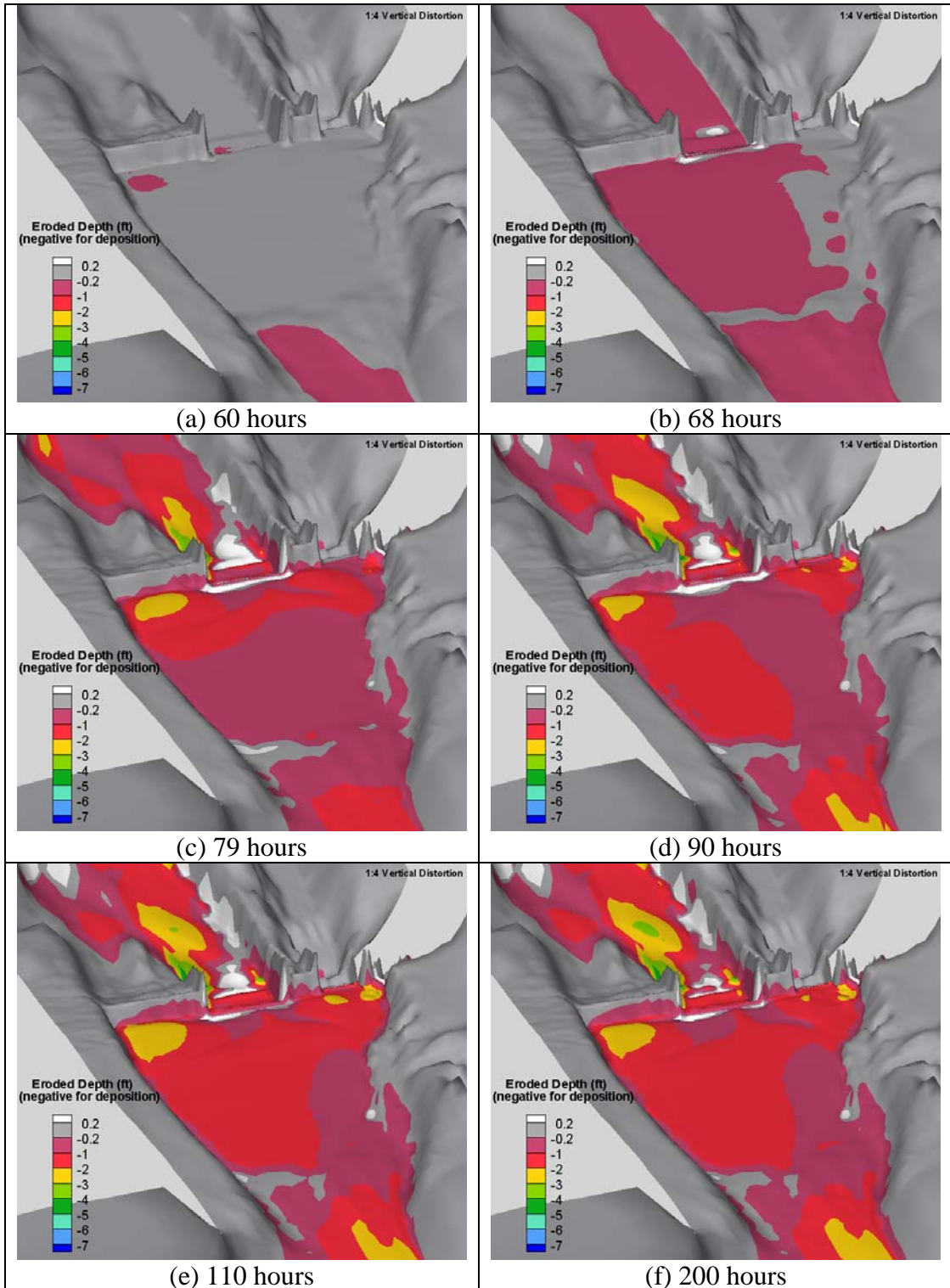


Figure 58. Simulated bed elevation and deposited depth for the RHFB scenario with the 1991 hydrograph and after-dam removal sediment input

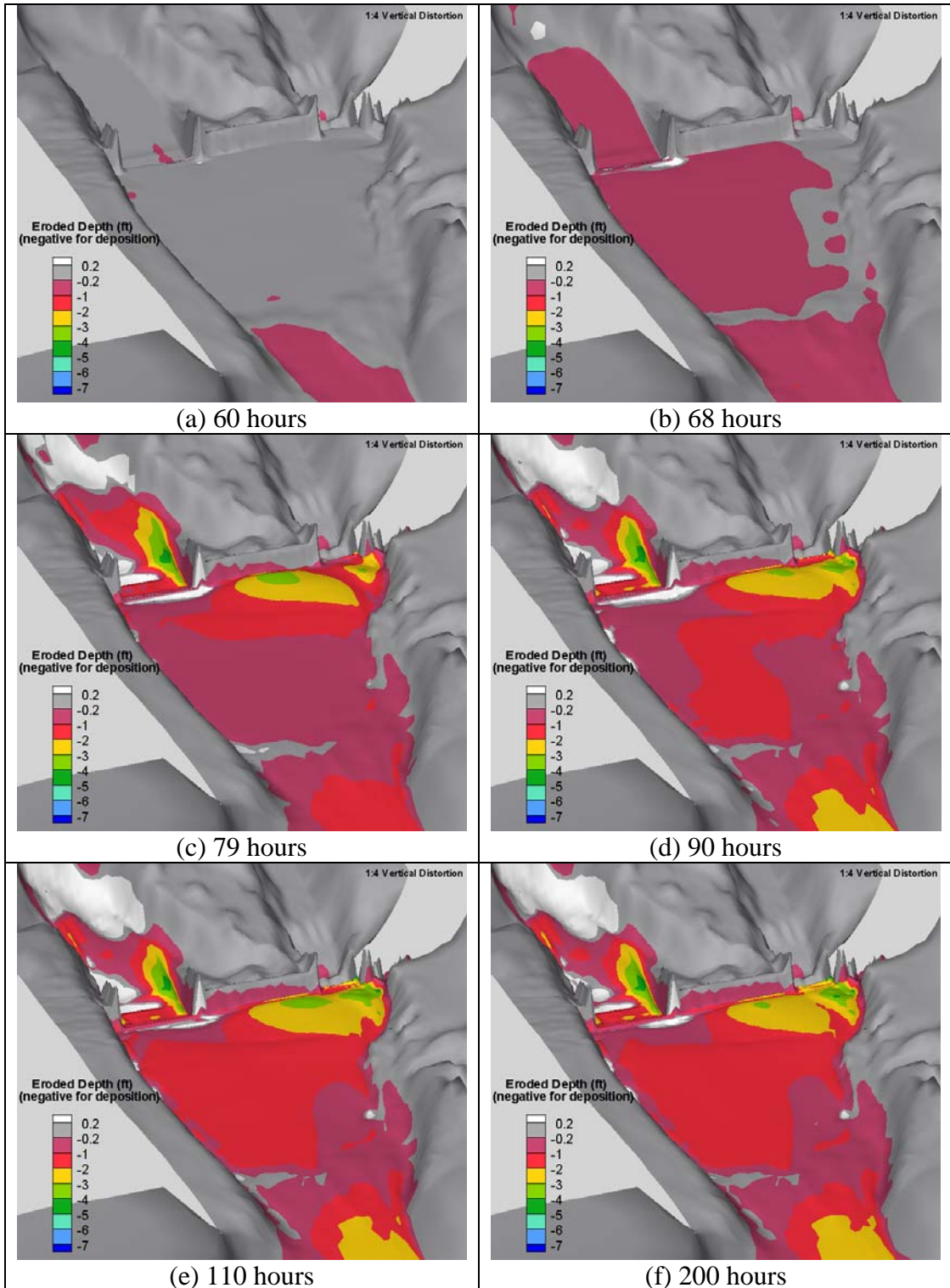


Figure 59. Simulated bed elevation and deposited depth for the LHFB scenario with the 1991 hydrograph and after-dam removal sediment input

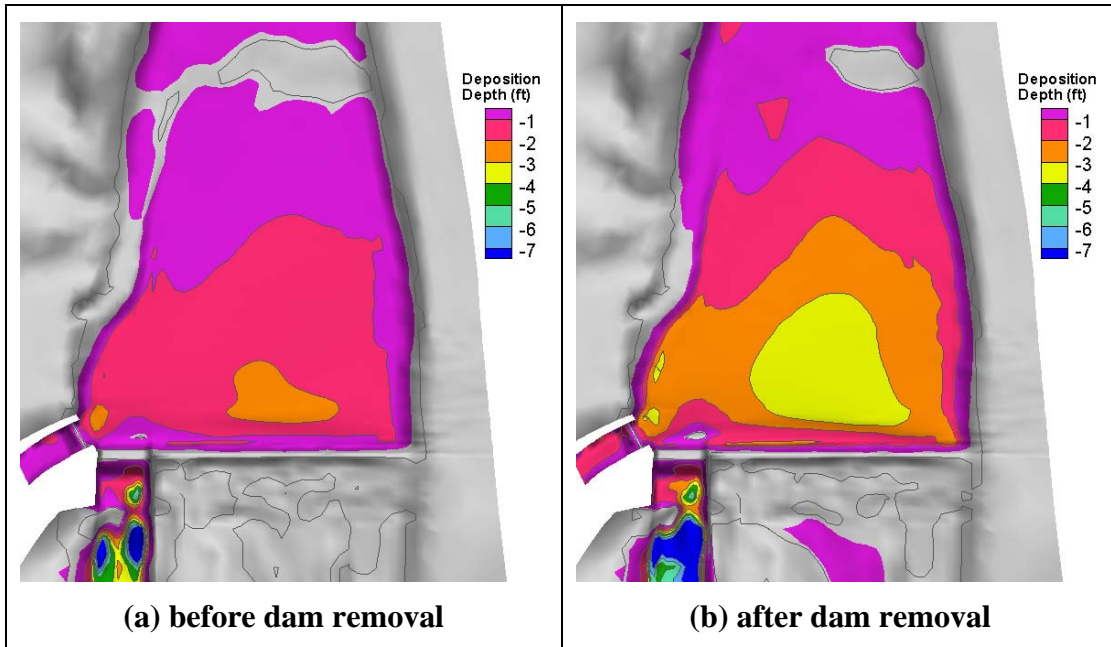


Figure 60. Comparison of deposition depth between before-dam and after-dam removal for the 1991 hydrograph and existing condition scenario

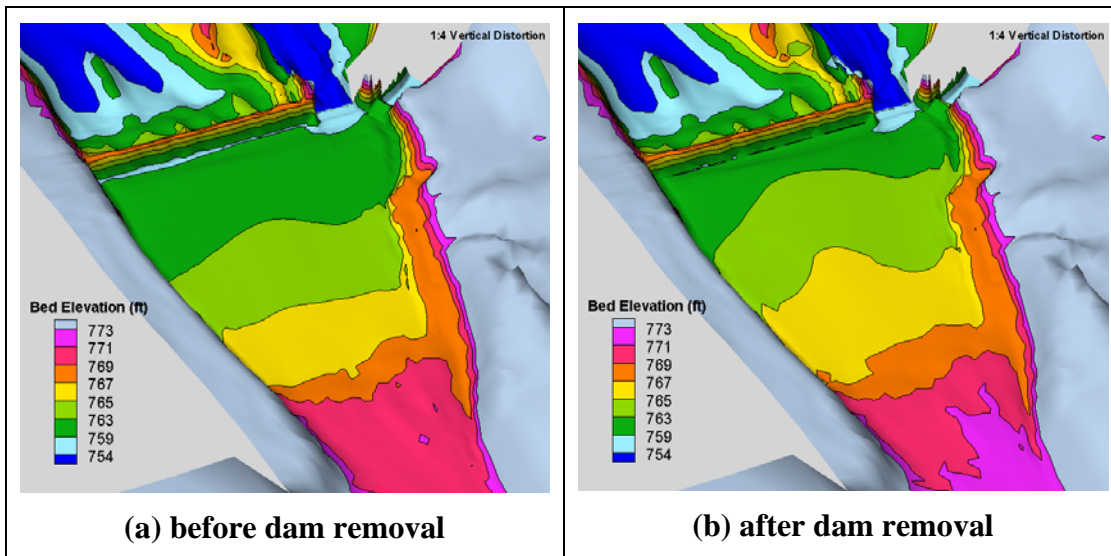


Figure 61. Comparison of bed elevation between before-dam and after-dam removal for the 1991 hydrograph and existing condition scenario

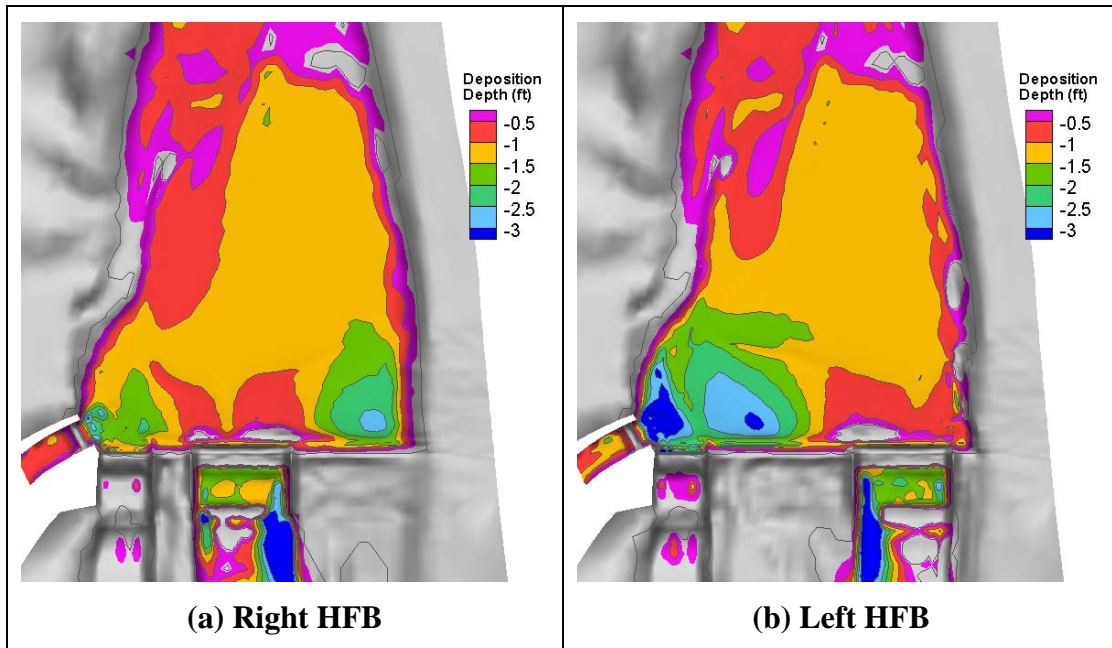


Figure 62. Comparison of deposition depth between the right and left HFB cases for the 1991 hydrograph and after dam removal

6.6. Results with the 1998 Hydrograph

The 1998 hydrograph had a relatively low flow for the first 50 hours (less than 1,000 cfs). The flow started to increase at 50 hours, reached the peak of 20,240cfs at 59.8 hours, receded below 4,000cfs after 75 hours and below 1,000cfs after 120 hours (see Figure 3b). Comparisons are mostly for the after-dam removal scenarios (see Figure 4b). The simulated bed elevation evolution in time, along with the net deposition depth, is displayed in Figure 63 to Figure 65.

Following observations may be made based on the simulation results:

(1) Similar to the 1991 hydrograph scenario, no appreciable sediment deposition was observed for the first 50 hours due to relatively low flow (less than 1,000 cfs). More deposition occurred for the existing condition scenario at 50 hours. This may be attributed to the fact that the existing gates were opened earlier (see Figure 54) which would promote faster sediment movement towards the diversion weir.

(2) For the existing condition scenario, sediments were accumulated behind the weir quickly, similar to the 1991 hydrograph scenarios. A comparison of the deposition depth between the before- and after-dam scenarios is shown in Figure 66 at 200 hours; the simulated bed elevation is compared in Figure 67. An average deposition depth behind the weir was estimated to be 7.5 ft and 10.5 ft, respectively, for before- and after-dam scenarios. The results indicate that a flood similar to the 1998 event (near 15-year flood) would move a majority of the

sediments towards the diversion dam and fill the area upstream of the weir quickly even if excavation has been done before the flood. Under the existing condition scenario, sediment deposition in front of the canal gates was predicted to be high enough that bedload would be transported into the canal for both before- and after-dam removal scenarios with the 1998 flood.

(3) If the high flow bypass (HFB) radial gates would be in place, the total amount of sediment deposits between RM 14.1098 and the weir would be reduced by about 40% (see Table 9) under the 1998 hydrograph and after-dam removal conditions, in comparison with those of the existing gates. The average deposition depth near the weir is reduced from 10.5 ft to 5.0 ft under the right HFB and 6.5 ft for the left HFB, respectively. The results show that the HFB gates would be able to move sufficient sediments through the gates that there is less likelihood for the bedload to move through the diversion canal.

(4) A comparison between the right and left high flow bypass (HFB) showed that the right HFB case would be preferred to the left HFB. Firstly, the total deposited depth near the weir was lower for the right HFB case (5.0 ft versus 6.5 ft for the left HFB) despite that the total amount of deposited sediment volume between the weir and RM 14.1098 was not much different (Figure 68). This suggests a reduced potential for the bed load sediments transported into the diversion canal directly. The difference may be explained as follows. The flow entering the cross section RM 14.1098 is not uniform laterally; the flow tends towards the left bank due to the channel meander bend upstream. With the HFB placed on the left, the sediments on the left would move through the left HFB directly while those on the right would remain on the right and be stored in front of the weir. If the HFB is placed on the right, the sediments on the left continue to be swept towards the HFB due to the stronger flow on the left; but the sediments on the right are also transported towards the HFB. The combined effect leads to increased sediment transport and reduced deposition. The above explanation is supported by the results shown in Figure 64 and Figure 65.

Table 9. Total amount of sediments moving into and stored in the area between RM 14.1098 and the weir based on model (volume excluding voids)

Case Name	Sediment Supply at Inlet	Sediment Volume (yd ³) through RM 14.1098	Sediment Volume (yd ³) stored upstream
FD-EX-1991-1	before-dam	34,190	4,130
FD-EX-1991-2	after-dam	53,600	8,770
FD-RHFB-1991	after-dam	57,530	4,330
FD-LHFB-1991	after-dam	62,340	4,923
FD-EX-1998-1	before-dam	205,500	21,900
FD-EX-1998-2	after-dam	258,400	26,500
FD-RHFB-1998	after-dam	282,500	15,700
FD-LHFB-1998	after-dam	282,500	16,100

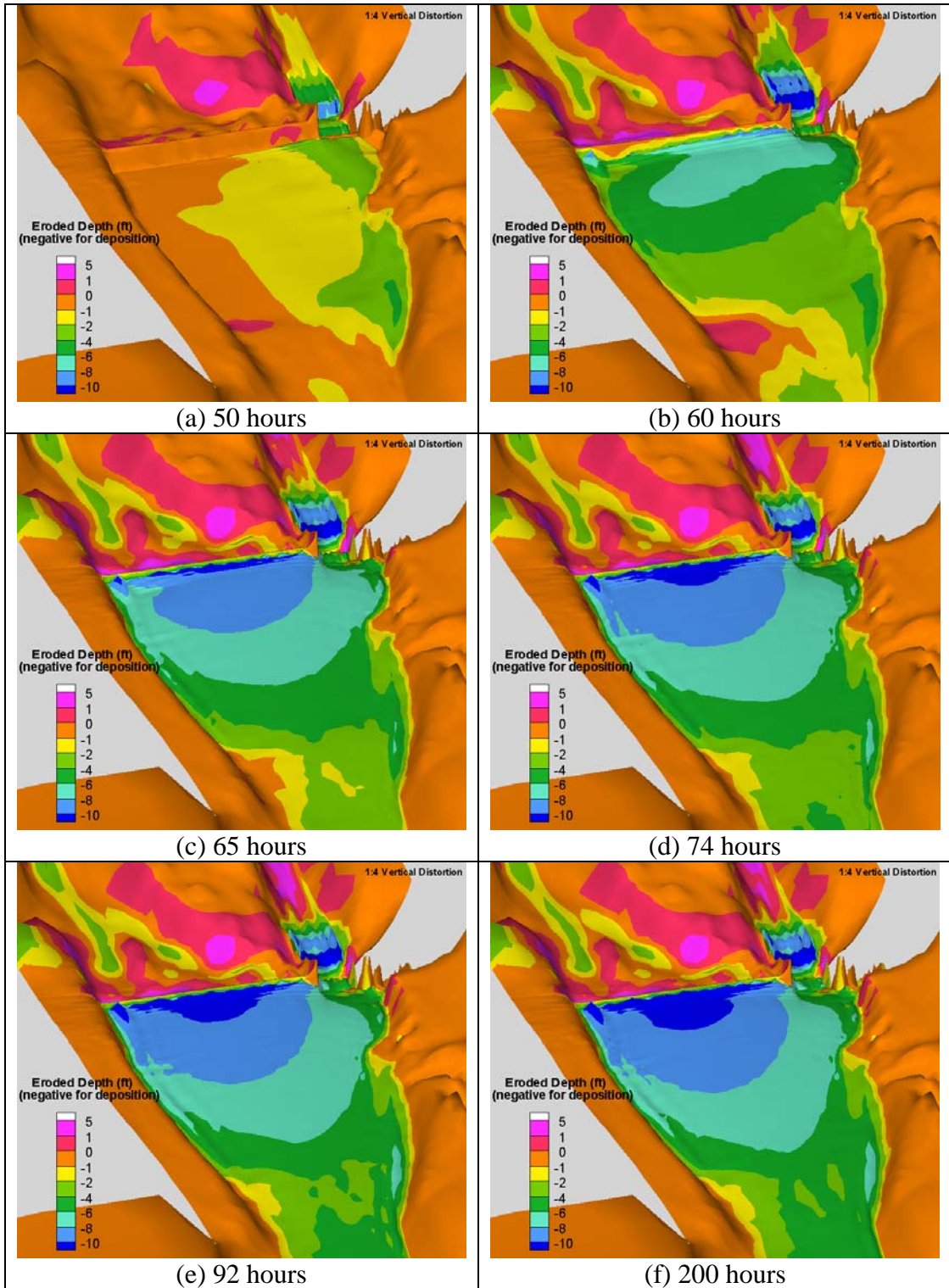


Figure 63. Simulated bed elevation and deposited depth for the existing condition with the 1998 hydrograph and after-dam removal sediment input

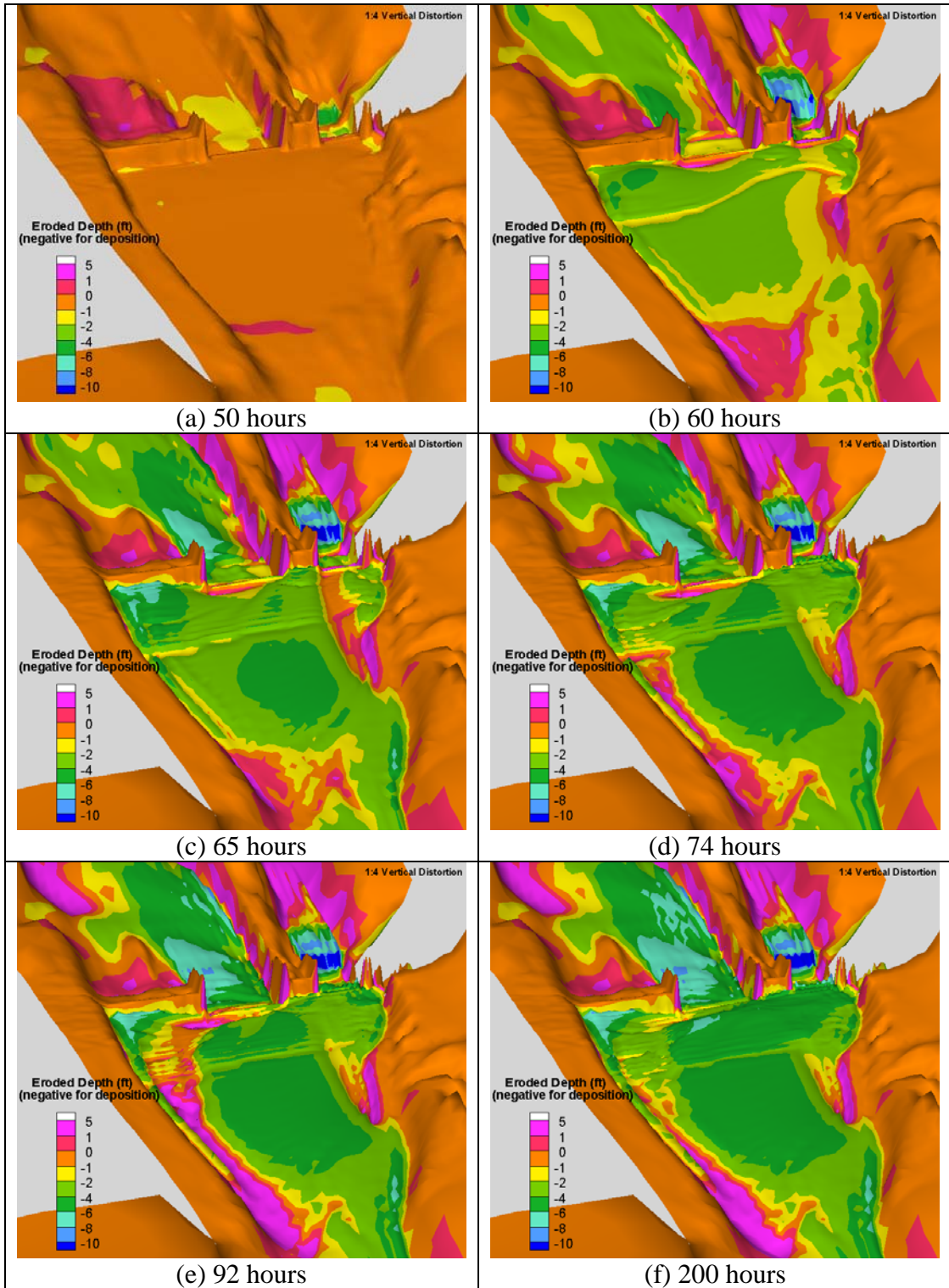


Figure 64. Simulated bed elevation and deposited depth for the RHFBS scenario with the 1998 hydrograph and after-dam removal sediment input

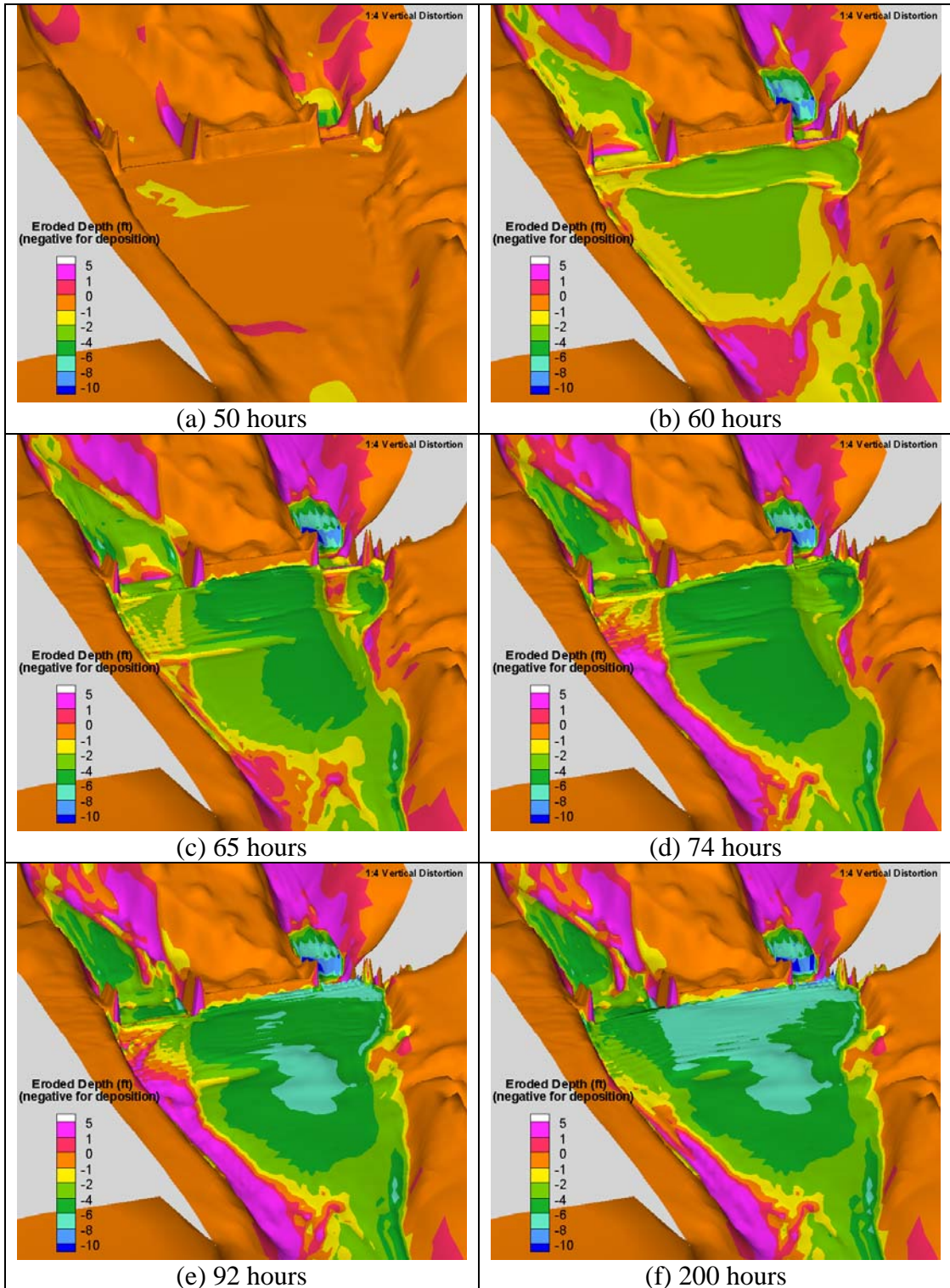


Figure 65. Simulated bed elevation and deposited depth for the LHFB scenario with the 1998 hydrograph and after-dam removal sediment input

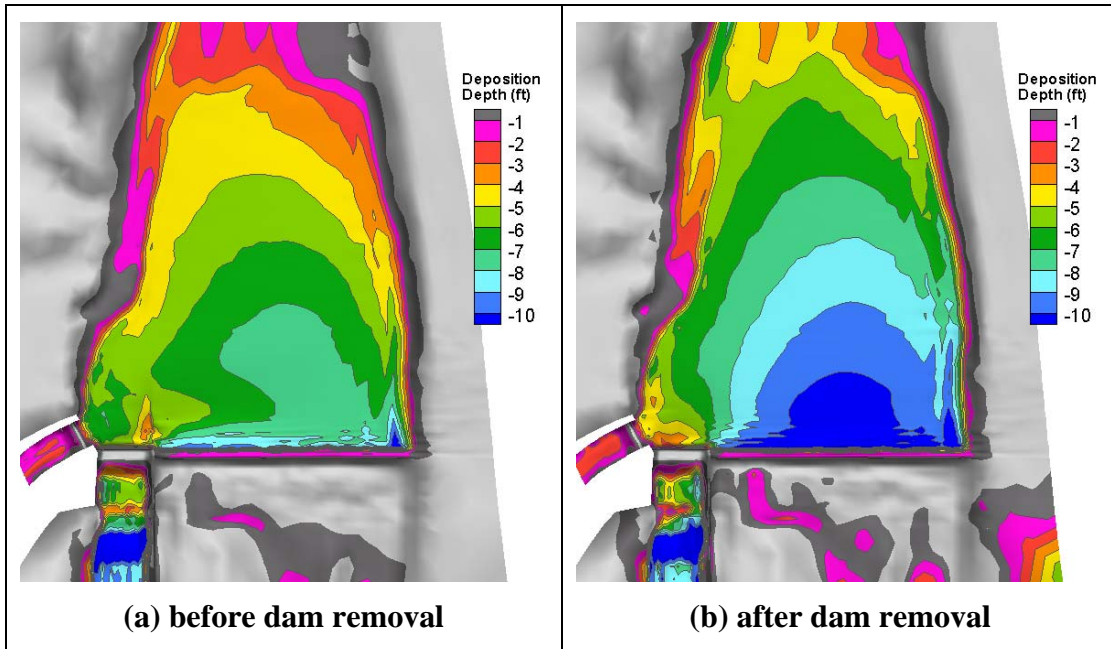


Figure 66. Comparison of deposited depth between before-dam and after-dam removal for the 1998 hydrograph and existing condition scenario

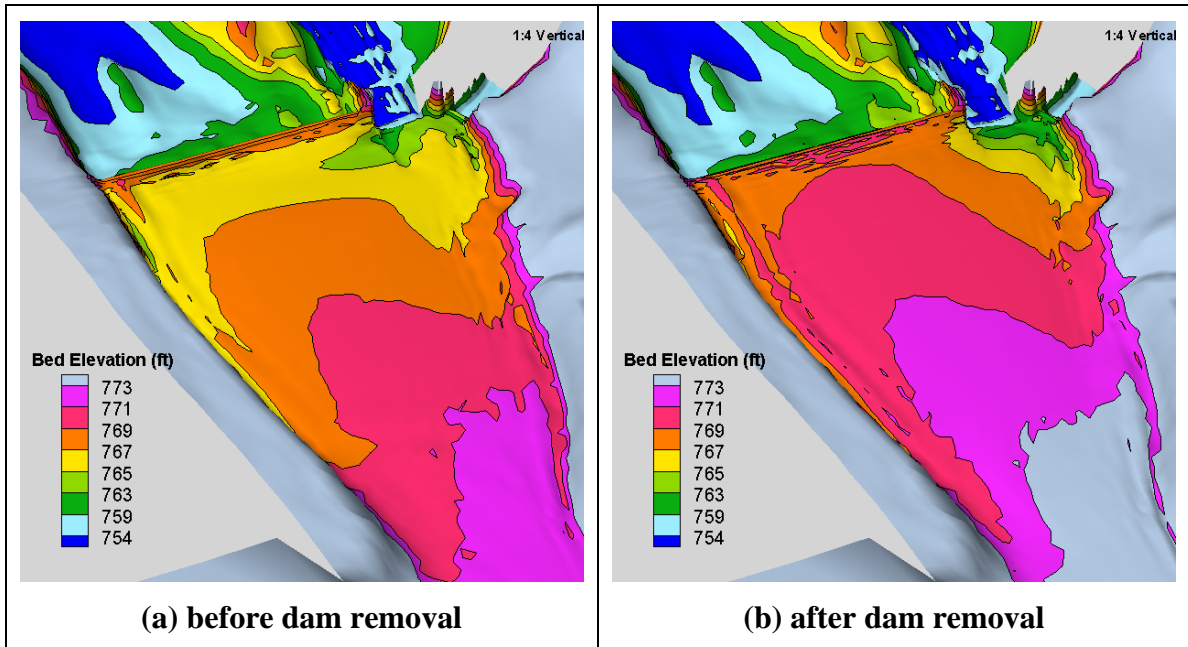


Figure 67. Comparison of bed elevation between before-dam and after-dam removal for the 1998 hydrograph and existing condition scenario

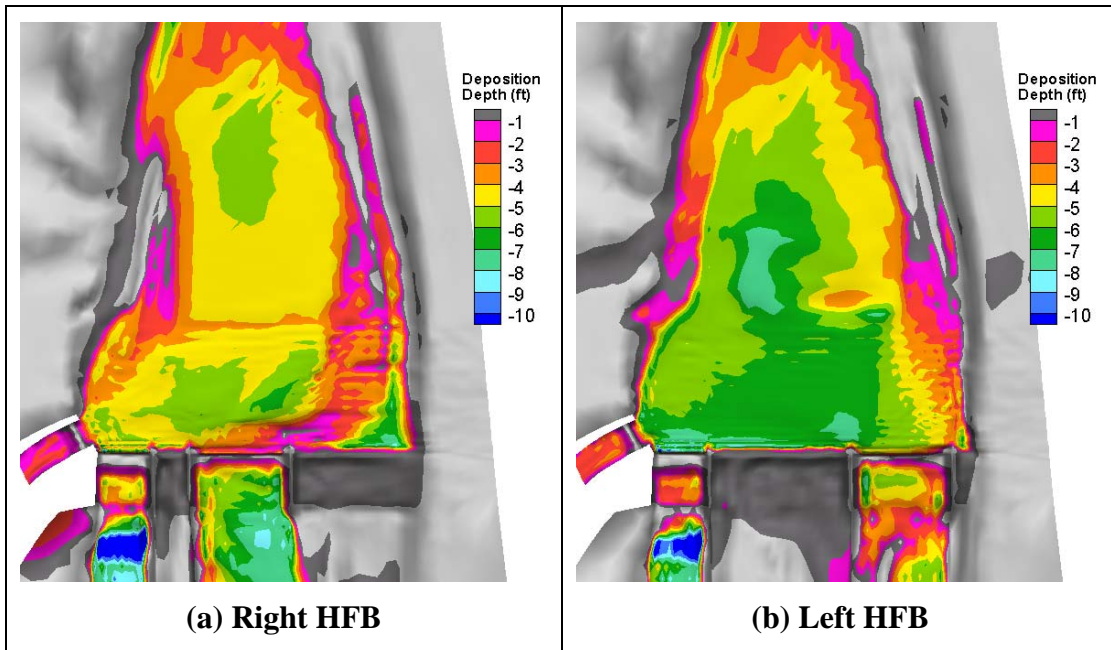


Figure 68. Comparison of deposited depth between the right and left HFB cases for the 1998 hydrograph and after dam removal

7.0 Discussion and Uncertainty

7.1. Discussion and Summary

Numerical modeling of physical model cases presented in Chapter 5.0 shows that the results from both the numerical and physical models are in agreement with each other. This provides confidence in the numerical model and points to the reliability of the results from both models. Major findings, based on the modeling of physical model cases, are:

- (1) With the existing radial gates, too much deposition would occur upstream of the Robles weir. Specifically, the sediment delta would reach the diversion canal gates under both the 6,000 cfs and 14,000 cfs hydrographs. The thickness of the delta is high enough that there is a high likelihood of bedload sediments being transported into the canal.
- (2) With the high flow bypass (HFB) gates added, the model results show that it is less likely that the bedload sediments would enter the diversion canal.
- (3) The total amount of sediment deposition upstream of the weir is tabulated in Table 10 for all simulated physical model cases. It shows that more than 85% of the incoming sediments would be trapped upstream of the weir under the 6,000 cfs hydrograph with or without the HFB gates. The benefit of the HFB gates shows up only for flows higher than 6,000 cfs. For example, with the 14,000 cfs hydrograph, about 70% of the input sediments are deposited upstream of the weir for the existing condition scenario while the percentage is reduced to about 53% if the HFB gates are operated. It is interesting to note that the delta deposition remains constant when the flow is increased from the 6,000 cfs hydrograph to the 14,000 cfs hydrograph.
- (4) No appreciable difference is observed between the left and right HFB options in terms of the ability to move the sediment.
- (5) The final bed topography near the existing and diversion canal gates may be altered through the sluicing ability of the existing radial gates. But not enough research has been carried out to derive a quantitative scheme for sluicing.

The physical model test cases are limited in several aspects. The 14,000 cfs hydrograph used in the lab is not the same as the 1998 hydrograph in the field which had a peak of more than 20,000 cfs. Also, the total sediments added for the 14,000 cfs hydrograph may not be high enough as the computed input based on the fact that transport capacity is more than 10 yd³. Coupled with the potential

effects of the limited size of the test box and the scalability, there is a need to model the field cases which would eliminate most of the limitations mentioned above.

Table 10. Cumulative volume (excluding voids) deposited upstream of the weir during the period of test hydrograph

Cases	Total Sediment Volume Input (yd ³)	Volume Deposited Upstream of Weir (yd ³)
PM-SED-EX-91	3.7	3.25
PM-SED-EX-98	5.85	4.03
PM-SED-RHFB-91	3.7	3.24
PM-SED-RHFB-98	5.85	3.08
PM-SED-LHFB-91	3.7	3.10
PM-SED-LHFB-98	5.85	3.22

The numerical model for the field study was calibrated first with the available flow data. Simulation of the 2005 flood allowed the comparison of the simulated water surface elevation with the high water mark survey. The comparison was tabulated in Table 6. The difference between the simulation and survey is 0.22 ft and 0.36 ft, respectively, for the two survey points.

The field model was then used to simulate the 100-year flood and results were compared with the previous inundation study results based on the 1D model. Close agreement was obtained between the two models as far as the water surface elevation is concerned.

The mobile-bed simulation was carried out to study the sediment transport and bed evolution. Qualitative comparison of the simulated results with the field observation under the existing condition scenario showed that the model results were reasonable. The total amount of predicted sediment deposition upstream of the weir was in agreement with the field observation; and the predicted bed form and flow pattern after a major flood were plausible. Simulation of the existing condition scenario and comparison of the model results with the available data and observations gave us confidence about the reliability of the numerical model.

Mobile-bed simulations for all three scenarios - the existing, the right HFB, and left HFB - were carried out with both flow hydrograph and results were examined and compared. Major conclusions may be summarized as follows:

- (1) The flow discharge of 1,000 cfs may be taken as the threshold below which no appreciable sediment movement and deposition would occur near the Robles Diversion Dam.
- (2) For all modeled scenarios, sediments would be accumulated behind the Robles Diversion Dam (Weir) quickly. The overall deposition pattern was largely determined during the rising limb of the hydrograph. Only minor

deposition and bed form adjustments would occur shortly after the flow peak.

- (3) After dam removal, more sediment depositions would be accumulated upstream of the Robles Diversion Dam for the existing condition scenario. The model estimated deposition depth (with voids) and volume (without voids) are tabulated in Table 11 under the existing condition scenario.

Table 11. Average deposition depth (with voids) and total deposition volume (without voids) under the existing condition scenario

Sediment Input Case	Before-Dam Removal 1991 Hydrograph	After-Dam removal 1991 Hydrograph	Before-Dam Removal 1998 Hydrograph	After-Dam Removal 1998 Hydrograph
Deposition Depth (ft)	2.0	3.5	7.5	10.5
Deposition Volume (yd ³)	4,130	8,770	21,900	26,500

- (4) Model results showed that the existing radial gates alone are not capable of efficiently moving the additional sediments added after dam removal. Sediment deposition in front of the canal gates would be so high that there is a high likelihood the bedload sediments would be transported into the diversion canal if a flood similar to 1998 (about 15-year flood) would occur.
- (5) If high flow bypass (HFB) radial gates are in place, the total sediment deposits between RM 14.1098 and Robles Diversion Dam would be reduced by approximately 50% and 40%, respectively, for the 1991 and 1998 hydrographs. HFB gates are capable of moving sediments efficiently once the dam is removed and there is less likelihood for the bedload sediments to move through the diversion canal.
- (6) Model results showed that the right HFB appeared to have an advantage over the left HFB. Firstly, the average total deposition depth near the weir was lower for the right HFB case: 2.5 ft for the right HFB versus 3.0 ft for the left HFB for the 1991 hydrograph and 5.0 ft versus 6.5 ft for the 1998 hydrograph. Secondly, the total sediment volume deposited between RM 14.1098 and Robles Diversion Dam is also lower for the right HFB. Finally, more deposition occurred in front of the canal diversion gates for the left HFB scenario.

7.2. Model Uncertainties and Limitations

The mobile bed modeling performed in this project represents the current state-of-the-art. However, even the most advanced modeling typically cannot exactly predict the complex three-dimensional geomorphic response. Uncertainty is inherent in any numerical modeling due to the assumptions used to develop the model. Assumptions are mostly related to the theoretical development (e.g., the sediment transport equation and bed dynamics) and the method and input data used. Key areas of modeling uncertainty and limitations for this project are listed below:

- 2D modeling was necessary for the present analysis due to lateral (across the river) variations and the local erosion. The 2D model represents a significant improvement over a 1D approach. However, 3D effects are expected near the radial gates. The current 2D model does not take the vertical variation into account, and blockage of the bedload movement by a vertical wall was not modeled. As a result, the model cannot predict the amount of sediments moving through the canal diversion gates accurately. The risk of sediments movement into the diversion canal can only be indirectly assessed by examining the delta location and thickness in front of the canal gates.
- The sediment model was not calibrated or verified with field-measured sediment transport rates due to lack of such data. However, the flow model is calibrated in Section 6.1, and limited qualitative comparisons are discussed in Section 6.4.
- Uncertainties due to the sediment transport mechanics, such as the capacity equation and bed dynamics equations, are well known. The best available information, however, has been used in this project. The Parker (1990) sediment transport equation was used based on our past experience in modeling similar rivers.
- Other uncertainties include the impact of hydraulic flows, the initial bed gradation, etc. But they are deemed less important.

Despite various uncertainties, the current analysis is based on the current state-of-the-art modeling approach. The model has been carefully calibrated and compared with the available data in the laboratory and field. The analysis method chosen is adequate for the estimation of the bed evolution and sediment deposition study.

8.0 References

- Greimann, B.P., (2004). *Hydrology, Hydraulics and Sediment Studies of Alternatives for the Matilija Dam Ecosystem Restoration Project, Ventura, CA – Final Report*, Technical Service Center, Bureau of Reclamation, Denver, CO 80225.
- Greimann, B. P., (2006). *Hydrology, Hydraulics, and Sediment Studies for the Matilija Dam Ecosystem Restoration Project, Ventura, CA – DRAFT Report*, Technical Service Center, Bureau of Reclamation, Denver, CO 80225.
- Greimann, B.P., Lai, Y.G., and Huang, J., (2007). “Two-Dimensional Total Sediment Load Model Equations,” to appear in: *J. Hydraulic Engineering, ASCE*.
- Lai, Y.G., Weber, L.J., and Patel, V.C. (2003). “Non-hydrostatic three-dimensional method for hydraulic flow simulation - Part I: formulation and verification.” *J. Hydraulic Engineering*, 129(3), 196-205.
- Lai, Y.G. (2006). *Theory and User Manual for SRH-W 1.1*, Technical Service Center, Bureau of Reclamation, Denver, CO 80225.
- Lai, Y.G., and Greimann, B.P. (2007). “Numerical modeling of alternate bar formation downstream of a dike,” World Environmental & Water Resources Congress, May 15-19, 2007, Tampa, Florida.
- Lai, Y.G., and Greimann, B.P. (2008a). “Predicting contraction scour with a 2D model,” World Environmental & Water Resources Congress, May 12-16, 2008, Honolulu, Hawaii.
- Lai, Y.G., and Greimann, B.P. (2008b). “Modeling of erosion and deposition at meandering channels,” World Environmental & Water Resources Congress, May 12-16, 2008, Honolulu, Hawaii.
- Mefford, B., Stowell, H., Heinje, C. (2008). *Robles Diversion Dam High Flow and Sediment Bypass Structure, Ventura, California, Physical Model Study*, Hydraulic Laboratory Report HL-2008-7, Technical Service Center, Bureau of Reclamation, Denver, CO.
- Parker, G., (1990). “Surface-Based Bedload Transport Relation for Gravel Rivers,” *J. Hydraulic Research*, 28(4):417-436.